UNIVERSITY OF DEBRECEN
FACULTY OF ENGINEERING
DEPARTMENT OF
MECHANICAL ENGINEERING

FINITE ELEMENT AND MANUFACTURING ANALYSIS OF A CAR BODY MODEL

THESIS

Hasan Md Rafid
Production Engineering Specialization

Debrecen
2026

Table of Contents

Table of Notations

T	$[\mathrm{s}]$	periodic time
v	$\left[\frac{\mathrm{m}}{\mathrm{s}}\right]$	velocity
ρ	$\left[\frac{\mathrm{kg}}{\mathrm{m}^3}\right]$	density
D_f	$\left[\frac{\mathrm{kg}\times\mathrm{m}}{\mathrm{s}^2}\right]$	aerodynamic drag force
C_d	$[-]$	co-efficient of drag
L_f	$\left[\frac{\mathrm{kg}\times\mathrm{m}}{\mathrm{s}^2}\right]$	aerodynamic lift force
C_l	$[-]$	co-efficient of lift
A	$[\mathrm{m}^2]$	reference area

Table of Glossary

FEM	Finite Element Method
FEA	Finite Element Analysis
CAD	Computer Aided Design
CFD	Computational Fluid Dynamics
CAM	Computer Aided Manufacturing
TIG	Tungsten Inert Gas
MIG	Metal Inert Gas
NURBS	Non-Uniform Rational B-Splines
CNC	Computer Numerical Control
GCI	Grid Convergence Index

Introduction

Automotive sector is an essential part of the field of advanced manufacturing and our modern life. Along with all the developments in vehicle aerodynamics, structural design, overall safety and fuel efficiency; it evolved by complex modelling and simulation methods. Among these methods, Finite Element Method is particularly outstanding as a pioneer computational tool that assists extensive simulation analyses throughout the dynamic design and manufacturing processes of diverse car models. FEM assists in assessing static and dynamic structural performances, simulating manufacturing techniques like sheet metal forming and assessing car crashworthiness, making it necessary in the field of automotive engineering and innovation.

Current trend towards multi-material and composite structures, the increasing application of digital twins and real-time simulations, along with the integration of Artificial Intelligence and Machine Learning into computational modelling, further enhancing the capabilities and expectations for Finite Element Analysis (FEA) in automotive. Nowadays, the growing need for vehicle speed, overall safety, initiatives for weight reduction to enhance fuel efficiency, sustainability and swift development necessitate, new car body models need to be designed such a way that would be much lighter, more rigid, featuring better management of speeding, crash energy and manufacturability.

In this era of advanced computational modelling, it is necessary to accomplish Finite Element Analysis; Computational Fluid Dynamics as well as Manufacturing Analysis by which it can be determined altogether how we can design & analyse such an efficient car body model that will be economical in every aspect for customers along with the manufacturers. For this reason, in this research; I will focus on designing a Computer Aided Design (CAD) model of a car body which will be analysed through different types of mesh sensitivity analysis, static structural and fluid flow analysis like CFD by utilising the ANSYS software. Then design the manufacturing technology for that car body model from metal through Computer Aided Manufacturing (CAM) analysis.

1. Literature Review

1.1 Aerodynamics in History of Automotive Design

The concept of aerodynamics in automobiles developed through four phases, determined by enhanced speed, crosswind sensitivity and the vital need to reduce dirt along with water deposition on lights and windows. In the 19th century testing methods, early drag coefficient tests relied on coast-down methods or maximum speed measurements but all of these were error-prone at that time. Aerodynamics in the history of automobiles, targeted mainly for two reasons. [1] They are followed by:

i. Advanced knowledge gain in aerodynamics of a vehicle and
ii. Implementation of gained learnings in automotive design. [1]

During the nineteenth century, all the efforts were taken to build cars focusing on the Streamlining Efforts which were inspired by naval and airship engineering. The aerodynamic drag was initially minimal due to lower engine power, low speeds and poor road conditions at that time. [2] From the historical principles of aerodynamics, the vintage motor car, which was built by Camille Jenatzy, was driven by electricity. That electric “torpedo-shaped” car exceeded 100 km/h speed at that time but suffered drag from uncovered wheels and driver. [1]

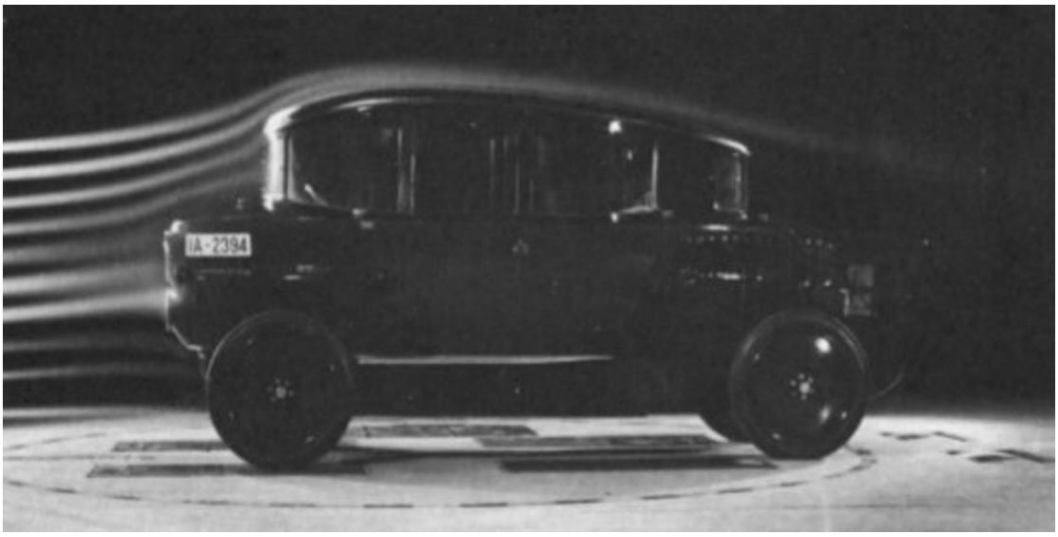

Figure 1.1 The Rumpler car in velocity streamline. [1]

Innovations after the world war I, the depicted 'Rumpler-Taube' automobile was engineered with a teardrop-shaped body. From a top view, its form resembled that of an aerofoil, while the roof was carefully streamlined to enhance aerodynamic efficiency. Rumpler’s vehicle body design featured exposed wheels which consequently contributed to an increase in aerodynamic drag. [2] Later Jaray, a

leader in vehicle aerodynamics, developed a car that formed the 'combination form' by utilizing half-body sections. [2] Through this approach the drag force was significantly reduced by stopping rear airflow separation using an extended slender tail. The design also featured a smoothly rounded front, what became famous as the “Lange car”. [1]

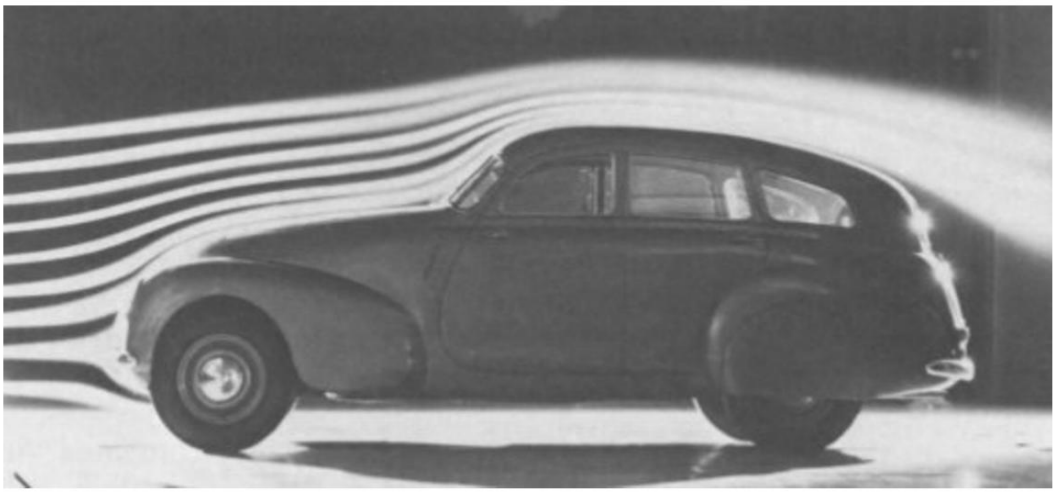

Figure 1.2 Velocity streamlines on the Kamm car. [1]

Scientiest, Lay refined the vehicle’s design by symmetrically modifying the front and rear sections, thereby isolating its aerodynamic characteristics. His investigations revealed a strong interdependence between the flow fields at the car’s front and rear. [2] While attached airflow along the front end contributed to reduced drag in long-tailed configurations, significant drag developed due to flow separation at the steep windshield. Consequently, the design proved impractical, as the increased drag rendered construction is not feasible. Lay’s findings indicated that a blunt rear end produced only a marginal rise in drag compared to a fully tapered tail. [3] Building upon Lay’s work, Kamm introduced the concept of ‘Kamm-back’ vehicles, characterized by blunt rear ends that maintained attached air flow. This tapering of the body increased rear-end pressure, thereby reducing overall drag and enhancing aerodynamic efficiency. [1]

After studying the above mentioned historical issues, it is proven that more research was needed by the time to develop the hidden knowledge of automobile aerodynamics concept and that is why considering the necessity of enhanced vehicle speed, crosswind sensitivity was streamlined through different channels and points to the vehicle to determine what is the cause of increasing or decreasing drag force that is need to be vastly studied by the time. [1] From then the researchers, engineers & automobile enthusiasts are working on this issue of downforce, lift and drag which became universal aerodynamic parameters that need to be controlled. To analyse these parameters, Finite Element Method is established to make it easier, compute more faster to understand and implement the complex concept of vehicle aerodynamics. [2]

1.2 Fundamental Parameters in Aerodynamics

The fundamental parameters in aerodynamics include downforce, drag, the drag coefficient, lift force and the lift coefficient. [1] By improving all of these aerodynamic parameters which are addressed below, we can achieve high performance desired outcomes in respect of weight to speed efficiency. [2]

1.2.1 Aerodynamic Downforce

Downforce refers to the vertical aerodynamic force generated when airflow passes over the vehicle's body components, pressing the car downward onto the road surface. [1] This increased downward load enhances tire grip, allowing drivers to negotiate winding roads and high-speed corners with greater stability and control. [2] [4]

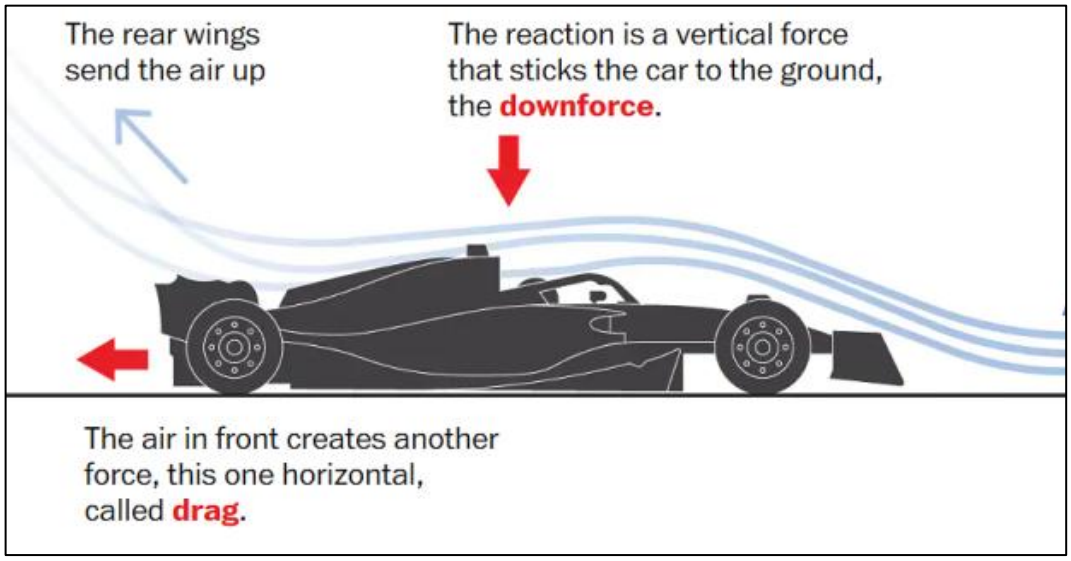

Figure 1.3 The illustration of downforce and drag on Formula One car. [4]

As mentioned by GPFANS web, Downforce represents a critical parameter in Formula One vehicles for ensuring adequate tire grip. Consequently, F1 cars are engineered with specialized aerodynamic elements such as the floor and wings that generate this force. Moreover, the magnitude of downforce can be tuned to accommodate varying track conditions and individual driving strategies. [4] [5]

This downforce concept is such vital that if it is ignored, it leaves very bad impacts on vehicle speed, drag, fuel efficiency and so on. [5] For manufacturing every high-speed vehicle, it must be considered while body kit designing. That is why we always see that the engine block is placed in various locations of the chassis of different car models to optimized the usage of this downforce. [2]

1.2.2 Aerodynamic Drag

Aerodynamic drag refers to the resistive force generated by air opposing the motion of a vehicle's body. This phenomenon is strongly influenced by the frontal geometry of the vehicle, with larger frontal areas producing greater pressure drag compared to streamlined designs. [2] In short, drag represents the reactive force of air resistance acting opposite to the vehicle's direction of travel. [6] The drag forces acting on automobiles are generally classified into four categories: [1]

i. Separation pressure,
ii. Interference,
iii. Induced and
iv. Viscous drag. [1]

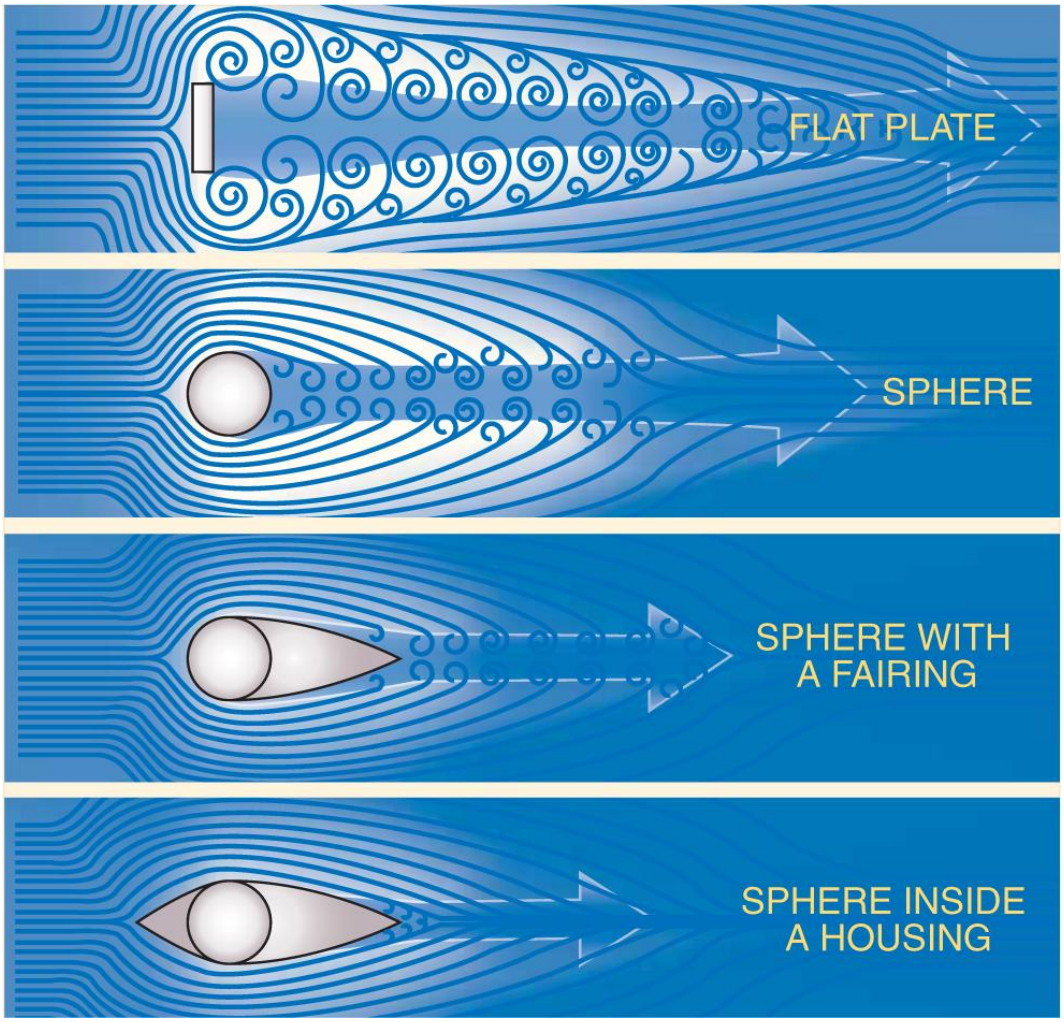

Figure 1.4 Illustration of Aerodynamic Drag on various shape of objects. [7]

In figure 1.4, it is shown that based on different objects shapes, the drag forces can be versatile. The flat plate causes the air to swirl around the edges until it rejoins the downstream, how swirling reduced drastically for changing shapes. [8]

The equation of drag force is:

$$D_f = \frac{C_d \,.\, \rho \,.\, v^2 \,.\, A}{2}; \quad (1)$$

The drag co-efficient is a dimensionless parameter. [1]

Equation of drag force co-efficient is:

$$C_d = \frac{2D_f}{\rho \,.\, v^2 \,.\, A}; \quad (2)$$

Here,

D_f = Drag,

C_d = Co-efficient of drag,

A = Front area of car,

v = Air Velocity,

ρ = Air Density.

1.2.3 Aerodynamic Lift

Aerodynamic lift is a upward force which is acting opposite to the weight of the vehicle. It's crucial mostly for high speed cars. [2] As the lift increases, the moving car behaves like a plane wing and reduces ground contact. [1] As the high velocity air is moving at the upper side of car body and low velocity air is passing from the bottom side of the car. According to the Bernouli's theorem, low pressure imposes at the speedy cars' top side and high pressure at the bottom. Then the speedy car body experiences aerodynamic lift. [9] This phenomena is well known for an aeroplane which getting the lift while taking off from ground.

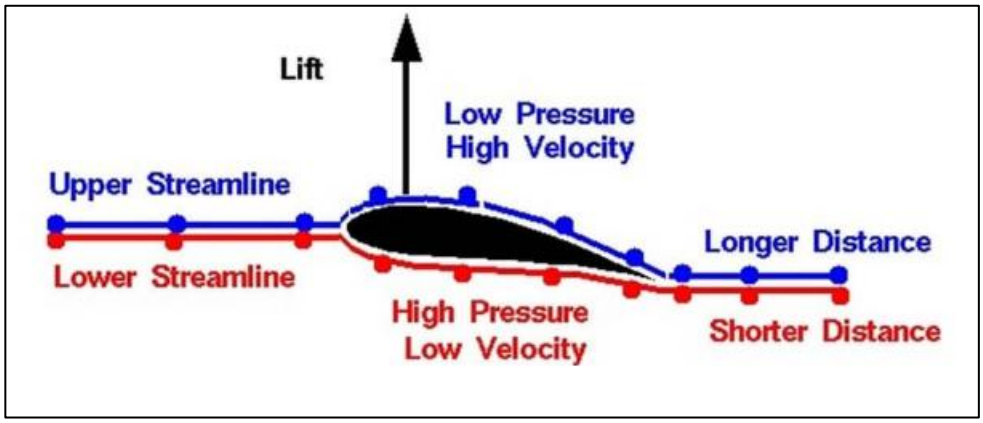

Figure 1.5 Illustration of aerodynamic lift force. [9]

This lift force reduces the amount of load on the wheels of the car which in turn reduces the traction of the wheels on to the road. [1] [2] It is very crucial that need to be balanced, otherwise speedy cars may lose control in stormy weathers.

The equation of aerodynamic lift force is:

$$L_f = \frac{C_l \,.\, \rho \,.\, v^2 \,.\, A}{2}; \tag{3}$$

The lift co-efficient is a dimensionless parameter that characterizes the lift generated as a function of air velocity, fluid density surrounding the vehicle body, and the effective frontal area of the lifting surface. [1] [10]

Equation of co-efficient of lifting force is:

$$C_l = \frac{2L_f}{\rho \,.\, v^2 \,.\, A}; \tag{4}$$

Here,

L_f = Lift,

C_l = Co-efficient of lifting force,

A = Front area of car,

v = Air Velocity,

ρ = Air Density.

1.3 Major Aerodynamic Components

Aerodynamic components such as splitter, canards, air dams, side skirts, diffusers, vortex generators, spoilers and inverted aerofoils which help to regulate airflow around the vehicle in order to achieve desired performance outcomes. [11]

1.3.1 Splitter

The splitter directs incoming airflow at the vehicle's front, where the blunt geometry induces a stagnation region of elevated pressure. By channeling this flow into differentiated high and low-pressure zones, the splitter promotes pressure imbalance that increases the aerodynamic downforce, improving tire grip and vehicle stability. [1] [11]

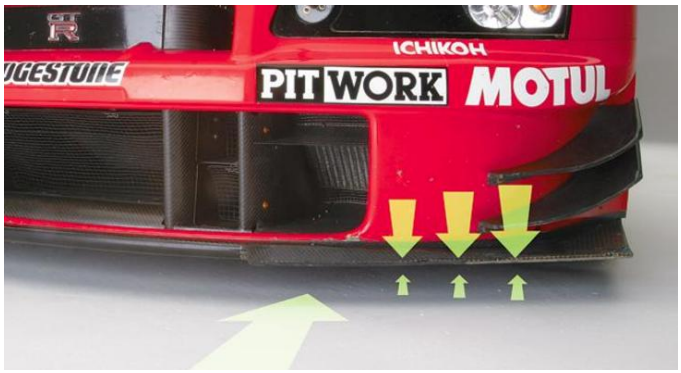

Figure 1.6 Airflow through the Splitter. [11]

1.3.2 Canards

Canards, also known as drive plates, are aerodynamic components which are designed to enhance downforce by directing the airflow in upward direction, which in turn pushes the vehicle downward. [2] They generate powerful vortices that travel along the both sides of the car, assisting to keep high-pressure airflow from disrupting low-pressure airflow beneath the vehicle. [1] [12]

Figure 1.7 Vortices created by the Canards. [11]

However, the main drawback of using canards is that they significantly increase drag force. [2] To minimize this added resistance, precise adjustments and fine-tuning of the car's aerodynamic setup are necessary. [1] [12]

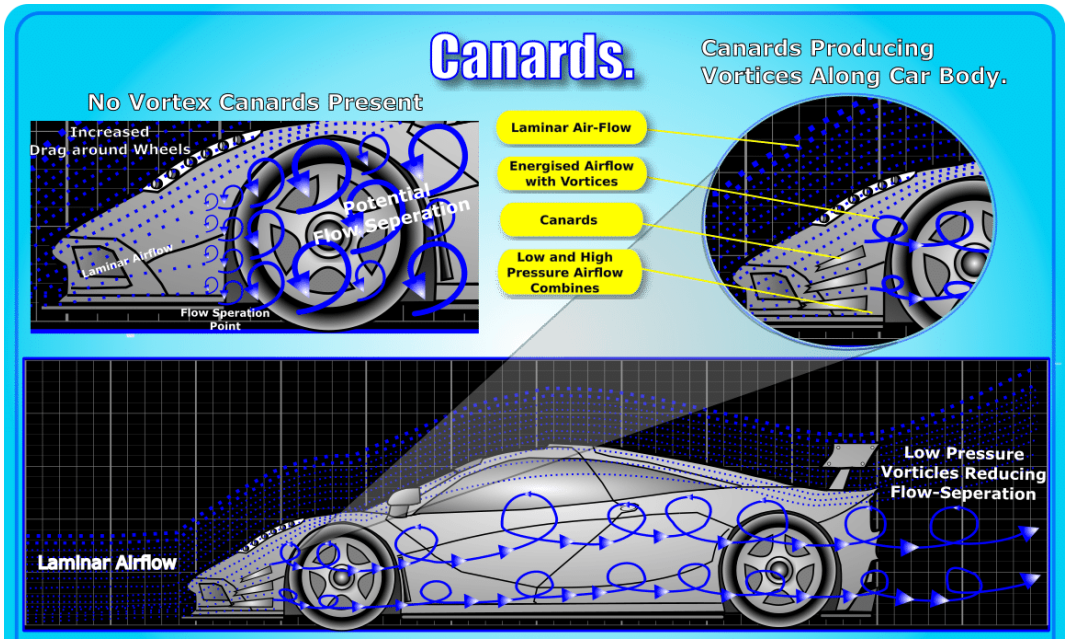

Figure 1.8 Flow-Separation with and without the Canards. [12]

1.3.3 Air dam

Air dam functions as an air flow-controlling device that restricts the airflow to go under the vehicle chassis. By deflecting the incoming airflow around and over the body, it creates a static pressure in that region. [1] [13]

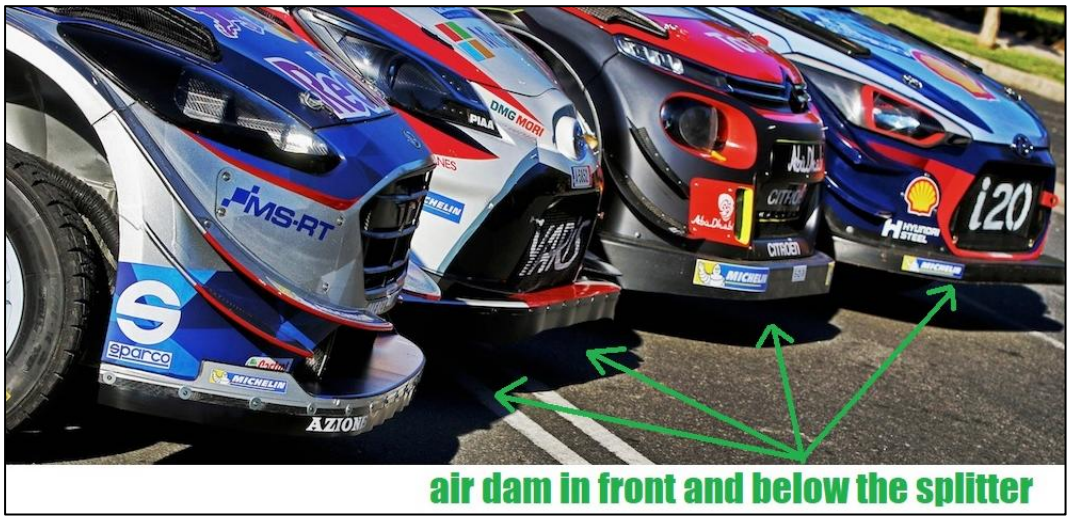

Figure 1.9 Air dams location. [13]

Moreover, the reduced mass flow rate underneath the car accelerates, by this way producing a low-pressure zone locally. This pressure difference causes a suction effect, hence contributing to aerodynamic downforce to the vehicle. [1] [13]

1.3.4 Side Skirts

Side Skirts are positioned along both sides of the vehicle body, through the front and rear wheels, in areas where sealing elements are typically located. Front-end aerodynamic elements such as splitters and air dams induce a localized low-pressure region that becomes significantly more effective when integrated with a flat underfloor and sealed lateral boundaries. This configuration promotes superior underbody flow management and substantially increases downforce generation. [12] [14]

Figure 1.10 Airflow pattern through the Side skirts channels. [11]

1.3.5 Diffuser

A diffuser is an aerodynamic component typically integrated into the lower section of a vehicle's body kit. It is most commonly positioned at the rear, referred to as a rear diffuser, though certain designs also incorporate front diffusers. Generally, it is made from carbon fibre to keep it light weight. [1] [12]

Figure 1.11 The Rear Diffuser. [12]

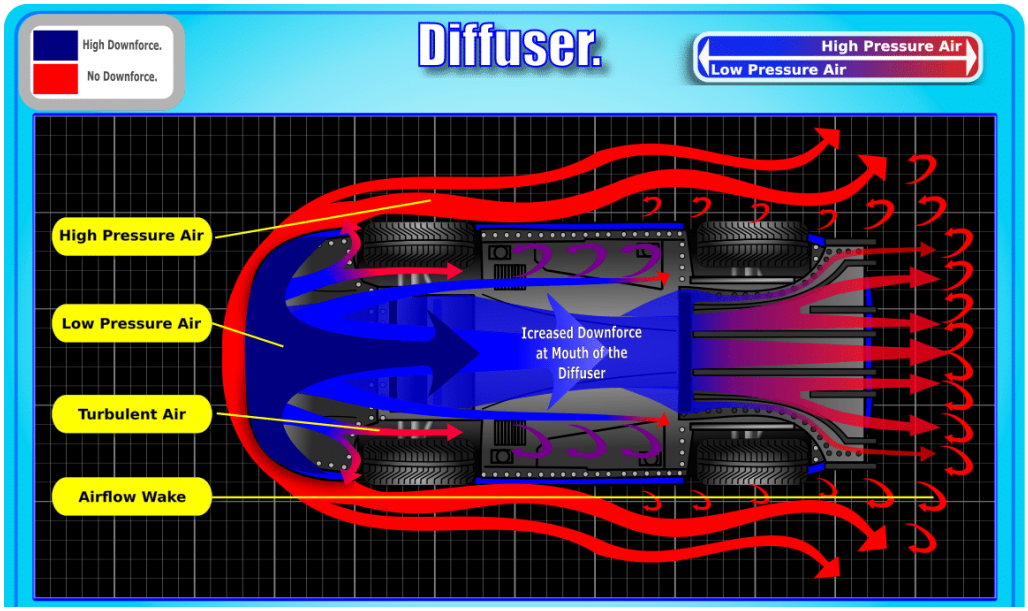

Figure 1.12 Airflow pattern through the rear diffuser. [12]

It is evident that diffusers perform multiple aerodynamic functions. Initially, they accelerate the incoming airflow, thereby reducing air pressure and subsequently decelerate the flow to restore pressure levels. [1] This mechanism operates through a Venturi-induced pressure reduction, which accelerates the flow and draws air through the aerodynamic channel. While doing this, it also has to make sure that flow separation does not occur, resulting to turbulent airflow in other words lots of drag. This can be achieved by having a gradual gradient and a volumetric increase along the body of the diffuser. [12]

1.3.6 Vortex Generators

Originally developed for aircraft applications, vortex generators have since been adopted in motorsport to enhance high-speed vehicle design. [1] Their main role is to maintain attached flow by postponing boundary-layer separation, since premature detachment over the vehicle surface increases pressure drag and turbulent wake formation, ultimately diminishing the performance of downstream aerodynamic elements. [12]

Figure 1.13 Vortex Generators. [12]

The Vortex generators are normally shaped like triangular fins, small and fit inside the boundary layer. It can be fabricated from composite materials like carbon fibre and even plastics. [12]

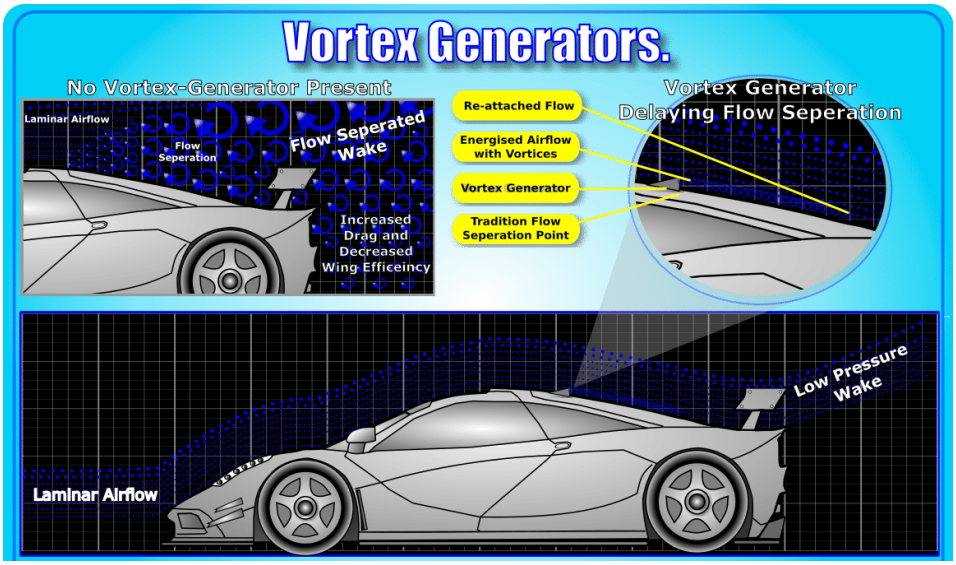

Figure 1.14 Flow Separation with and without Vortex Generators. [12]

1.3.7 Spoiler or Inverted Aerofoil

Spoiler assists rear tire performance during acceleration, braking and cornering while reducing oversteer. [1] Due to the rear side turbulent airflow, it is aerodynamically efficient while handling. [12]

Figure 1.15 Airflow off of the Spoiler and the rear diffuser. [11]

1.4 Overview of Finite Element Method

Finite Element Method is a mathematical tool that uses computational power to calculate approximate solutions approach to solving engineering problems involving complex geometries, loading conditions, and material behaviours, particularly where closed-form analytical solutions are unavailable. [2] In any complex design, FEM enables designers or engineers to decompose a problem into discretized finite elements (2D or 3D), facilitating stress, strain, and deformation analysis under multiple load cases. [15] [16]

1.4.1 Basic Finite Element Domains

In finite element analysis, geometry of the computational domain is determined through two essential inputs: [16]

i. the nodal points position that establishes the discretized framework and
ii. the domain interpolation functions which may overlay with those used for approximating the dependent field variables. [16]

1.4.2 Shapes of One-Dimensional (1D) Finite Elements

A one-dimensional finite element domain is represented by line sections which may be either straight or curved as shown below. [16]

Figure 1.16 One-dimensional finite element domains. [16]

1.4.3 Shapes of Two-Dimensional (2D) Finite Elements

Two-dimensional finite element domains are typically represented by triangular or quadrilateral shapes with either straight or curved boundaries, as illustrated in Figure 1.17. More complex geometrical elements are hardly ever exercised in standard engineering applications. [16]

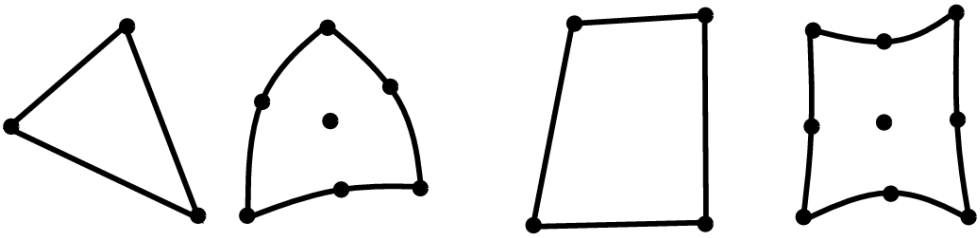

Figure 1.17 Two-dimensional finite element domains. [16]

1.4.4 Shapes of Three-Dimensional (3D) Finite Elements

The most commonly utilized three-dimensional finite element domains include tetrahedral (tets), pentahedral (prisms) and hexahedral (bricks), which may feature as straight or curved edges and either flat or non-flat faces, as illustrated in Figure 1.18. It should be emphasized that elements with more complex geometrical configurations are generally avoided in regular engineering practice. [16]

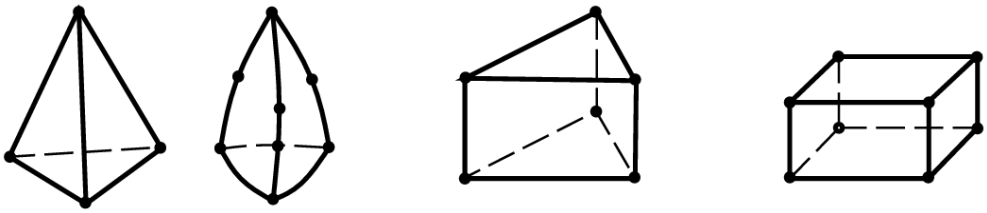

Figure 1.18 Three-dimensional finite element domains. [16]

1.4.5 Construction of A Finite Element Space

It is shown in the figure 1.19, how the finite element space is generally constructed from above mentioned 2D or 3D shapes and how it tries to adjust with the desired shape of the exact domain. As shown in figure 1.20, the discrepancies in boundary conditions arise from the mismatch between the exact domain and its finite element space representation. [16]

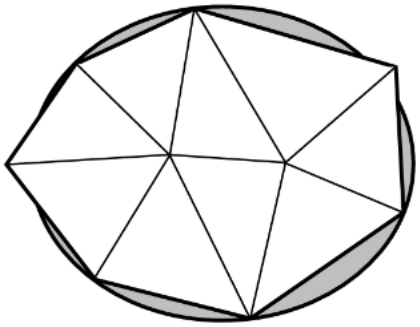

Figure 1.19 Finite element vs Exact domain [16]

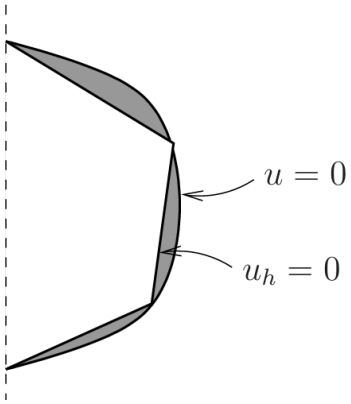

Figure 1.20 The discrepancies in Dirichlet boundary conditions. [16]

1.5 Overview of Finite Element Analysis

Finite Element Analysis is a computational modeling approach that discretizes complex geometries into interconnected finite elements-collectively forming a mesh to numerically evaluate structural and physical responses such as stress, thermal loading, vibration, and fluid interaction. This method enables engineers to identify critical failure regions and refine designs efficiently, reducing reliance on extensive physical prototyping. [17] [18]

1.5.1 Working Methodology

There is a specific working procedure involved in almost every FEA tool. Mostly four processes are followed by one after another. [17] They are as follows:

i. **Decomposition:** User given complex model is divided into millions of simple, interconnected domains or shapes which are called "finite elements" or meshing elements. [17] [18]

ii. **Mathematical Modeling:** The entire range of physical mathematical equations are applied to each element to model its behavior under multiple parameters. [17] [18]

iii. **Combined Results:** Computed results from the elements are combined to show the overall performance of the complex model given. [17] [18]

iv. **Simulation:** Program solves these complex calculations to predict outcomes like stress, strain, deformation, temperature distribution and simulates model based on given inputs to show the reactions. [17] [18]

1.5.2 Key Benefits and FEA Features

It’s possible to reduce the investment for the costly and time-consuming test rigs. [18] There is an opportunity to optimize design flaws in the early development stages. Complex scenarios like simulate in extreme conditions (e.g., automotive and aerospace crash, composite material testing etc.) that are dangerous or difficult to test physically. [17]

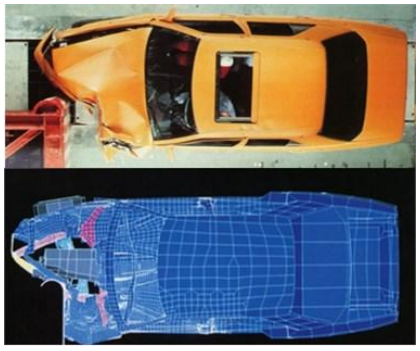

Figure 1.21 Collision model in real and FEA. [17]

Mostly available FEA features [17] are as follows:

i. Hydrodynamics,
ii. Thermal Analysis,
iii. Fluid-Structure Interaction,
iv. High Performance Computing,
v. Linear Dynamics and Non-linearities.

1.6 Overview of Computational Fluid Dynamics

Computational Fluid Dynamics uses computational and numerical methods to simulate and analyze fluid (-i.e., liquid and gas) flows, predicting patterns, temperatures, pressures and velocities around models or within systems which are crucial for optimizing the designs. [18] [19]

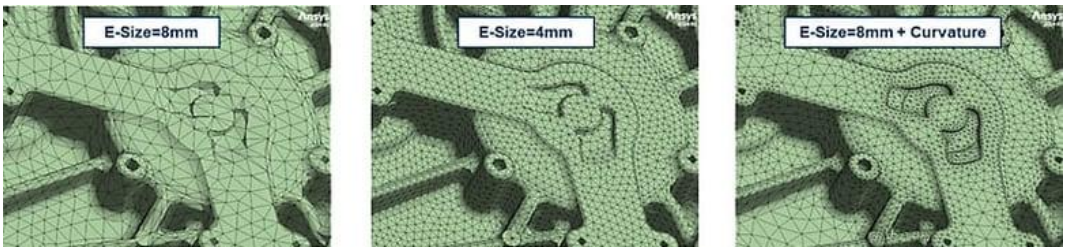

Figure 1.22 Left: coarse basic mesh, Center: fine basic mesh, Right: coarse basic mesh and curvature. [20]

1.6.1 Operational Methodology

Like FEA, a specific operational method included in CFD tools. Mostly three processes are pursued by one after another. [18] [19] They are as follows:

i. **Pre-processing:** Defining the geometry (-i.e., the model/domain) is the first task. Then creating a mesh cell (-i.e., divide the model volume into tiny computable 2D/3D elements) and finally, setting the boundary conditions (-i.e., fluid property, inlets/outlets, symmetry, slip walls). [18] [19]

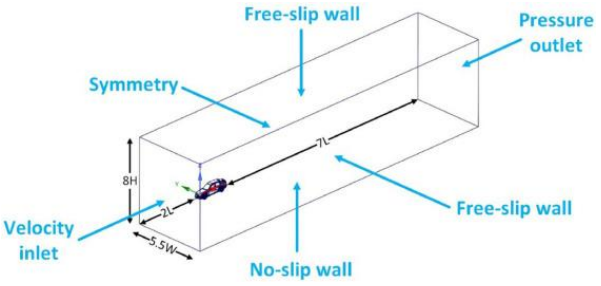

Figure 1.23 Computational domain and boundary conditions. [19]

ii. **Processing (Solving):** Computer solves various complex equations for mass, momentum, energy conservation for each mesh cell. [18] [19]

iii. **Post-processing:** Visualize results like flow lines, pressure contours and temperature diagrams to describe and analyze the performances. [18] [19]

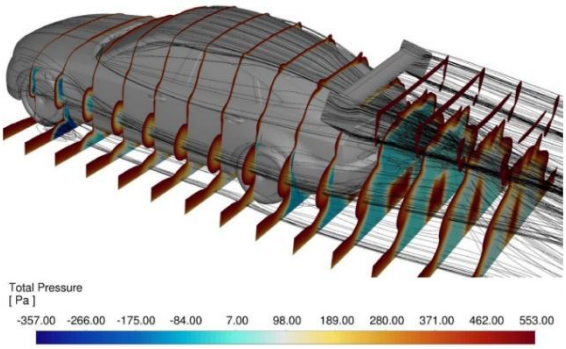

Figure 1.24 Pressure Contours. [19]

2. The Car Body CAD Model

For the geometric design of the car, "The Concept Car" is selected for Structural, CFD and CAM analysis for it's appealing aerodynamic design. The CAD model is downloaded from a open-source well known online site named as grabcad.com.

2.1 Illustration of The Concept Car

This concept car features a sophisticated geometric design that enhances the study of airflow and aerodynamics. Along with the developments of speedy vehicles, traditional components like grills and engine cooling air intakes are also necessary, allowing for greater flexibility in shaping and optimizing the vehicle's body panel. This results in improved efficiency and performance.

Different views of the concept car CAD model are presented below:

Figure 2.1 Front Side View of the concept car. [21]

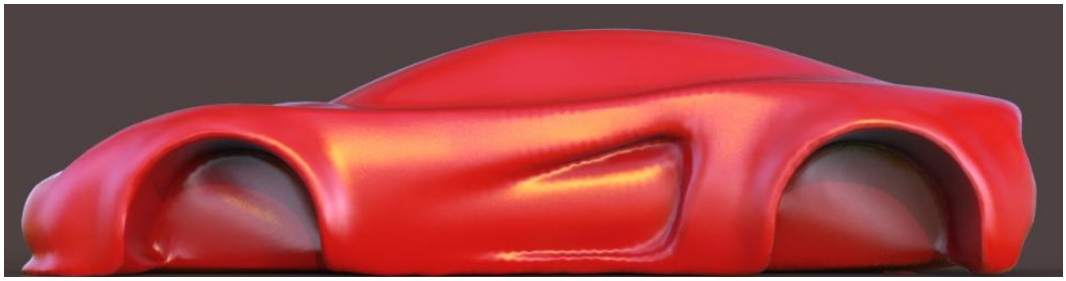

Figure 2.2 Right Side View of the concept car. [21]

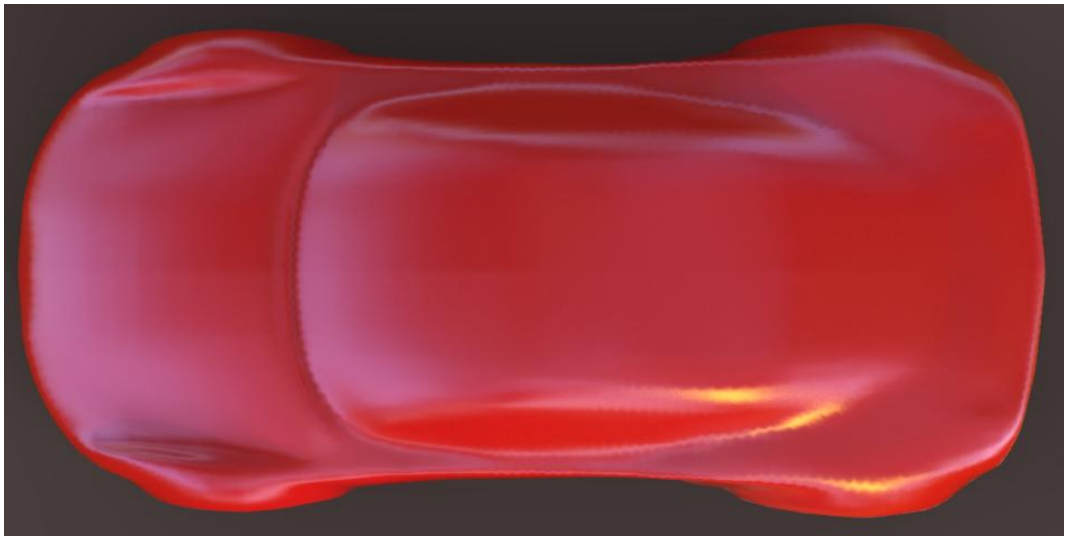

Figure 2.3 Top Side View of the concept car. [21]

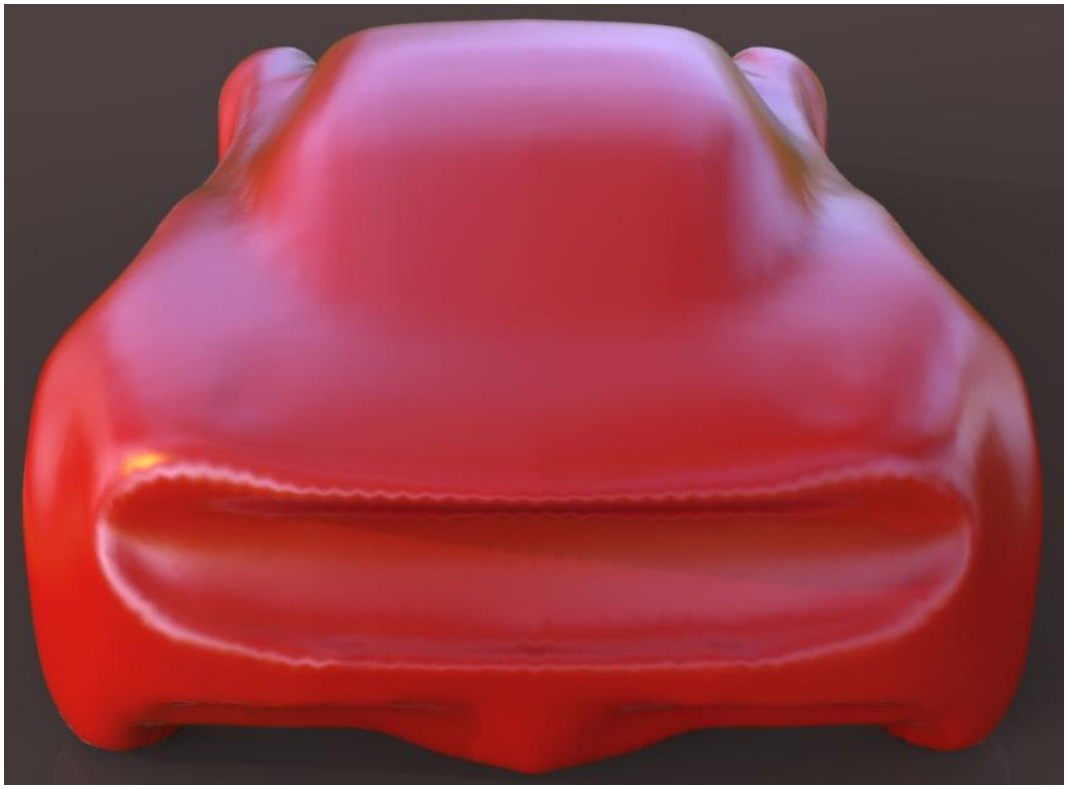

Figure 2.4 Rear Side View of the concept car. [21]

Figure 2.5 Front Isometric View of the concept car. [21]

Figure 2.6 Rear Isometric View of the concept car. [21]

2.2 Reasons behind choosing this car model

There are plenty of two-seated concept car models available for the FEA, CFD & CAM Analysis. Main reasons behind the chosen model are given below:

- ✓ Aerodynamic Hood & Roof
- ✓ Front & Rear Design
- ✓ Air Dam & Side Skirts

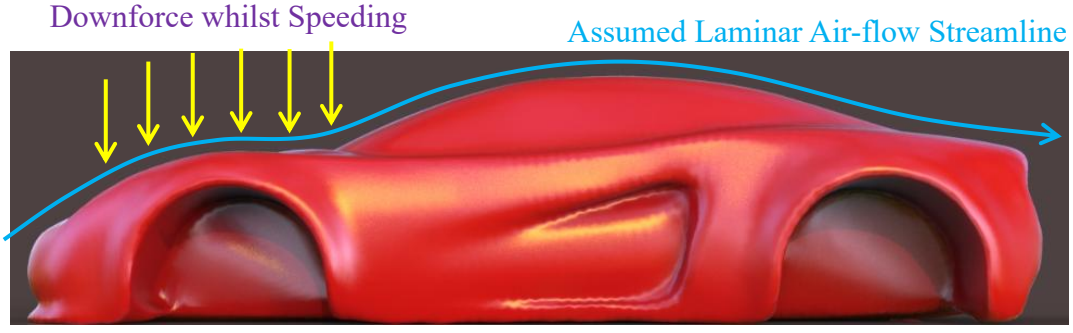

Figure 2.7 Aerodynamic design considerations of the concept car.

Downforce whilst Speeding due to the aerodynamic hood design

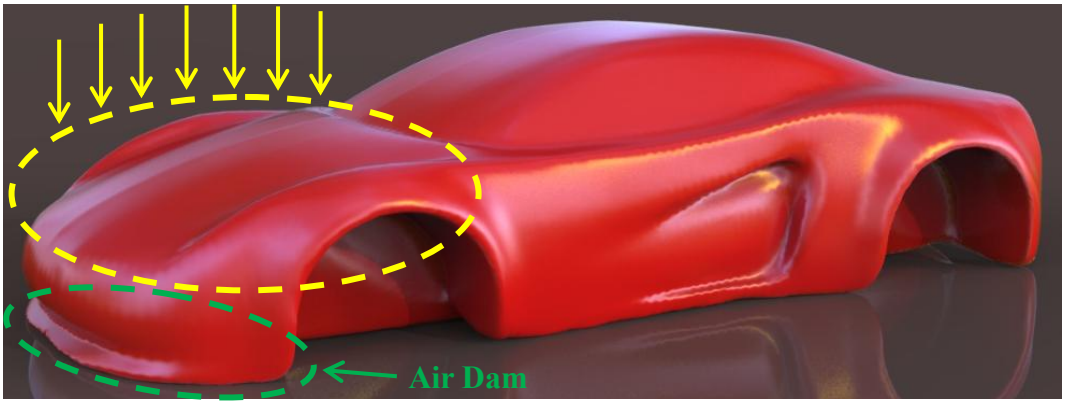

Figure 2.8 Front air dam and hood design of the concept car.

Figure 2.9 Air flow through the bottom and rear diffuser of the concept car.

Because of all the above mentioned fundamental parameters in aerodynamics, this car body model is selected for analysis to get the validity of the design. The small-scale model of the car serves as a useful tool for analysing airflow dynamics at a very high speed and understanding the impacts of velocity & generated pressure on the car body panel.

3. Research Methodology

The research methodology of this thesis is prepared by several fundamental foundational considerations that ensure the accuracy, relevance and reproducibility of the structural, aerodynamic and manufacturing analyses which will be performed on the selected concept car model.

3.1 Basic Considerations

Basic considerations define the assumptions, constraints, computational strategies which will be applied throughout the study.

3.1.1 Geometric and Modelling Considerations

- ✓ The concept car geometry imported from an open-source is treated as a non-parametric surface model, requiring defect corrections, surface healing and simplifications before meshing.
- ✓ Since the OBJ format imported as a triangulated mesh**,** the geometry is assumed to represent the external body shell only without internal structural materials.
- ✓ Small features that do not influence global stiffness or aerodynamic behavior (i.e. badges, tiny fillets, decorative grooves) will be removed to avoid unnecessary mesh refinements.
- ✓ Symmetry is not applied because the car body includes asymmetric features such as air dams, diffuser curvatures and hood contours.

3.1.2 Material and Structural Considerations

- ✓ The car body is assumed to be manufactured from Aluminum 6061-T6 / 6061-T651 which is selected for its balance of strength, stiffness, formability and manufacturability.
- ✓ The analysis considers the car body as a thin-wall shell structure where bending stiffness and local deformations behavior dominates.
- ✓ Linearly elastic, isotropic material behavior is assumed for static structural analysis as the loading conditions do not exceed the yield strengths of the alloy.
- ✓ Boundary conditions will be simplified to represent realistic constraints without modelling the full chassis or the suspension systems.

3.1.3 Meshing and Numerical Considerations

- ✓ Mesh sensitivity analysis is a core requirement; so multiple mesh densities such as coarse, medium and fine will be generated to evaluate convergence of stress, deformation and aerodynamic coefficients.
- ✓ Quad Dominant Tetrahedral elements will be used for complex curvature regions while inflation layers will be applied in CFD to resolve boundary layer effects.
- ✓ Mesh quality metrics such as skewness, orthogonality and aspect ratios will be monitored to ensure CFX Solver's stability and accuracy.
- ✓ Computational domain for CFD will be sized according to the best practices to avoid artificial pressure gradients.

3.1.4 Aerodynamic and Fluid Flow Considerations

- ✓ Air flow around the vehicle is assumed to be steady, incompressible and turbulent; consistent with high-speed automotive external aerodynamics.
- ✓ The CFD analysis will be done appropriate turbulence models such as k-ω SST model to capture flow separation, diffuser's behavior and vortex core regions formations.
- ✓ Boundary conditions will be included as a uniform inlet velocity, pressure outlet, no-slip walls on the car and ground surfaces.

3.1.5 Manufacturing and CAM Considerations

- ✓ The manufacturing analysis is planned, the car body panel will be produced from sheet metal forming processes compatible with 6061-T6/T651.
- ✓ Toolpath generation in CAM is based on simplified outer surface geometry, focusing on manufacturability rather than aesthetic detailing.
- ✓ Formability limits, minimum bend radius and spring back tendencies of 6061-T6 are considered when evaluating the feasibility.
- ✓ CAM workflow is designed to reflect realistic industrial constraints such as tool accessibility, any machining allowances and all the surface finishing requirements.

3.1.6 Computational and Practical Constraints

- ✓ All simulations are performed within the computational limits of ANSYS Workbench, as per the mesh refinement and fluid flow CFX solver time.
- ✓ The study focuses on global behavior (overall stiffness, drag, lift and manufacturability) rather than micro-scale phenomena such as fatigue crack propagation or any type of thermal cycling.
- ✓ Since the model is conceptual, validation relies on literature benchmarks, aerodynamic theory and mesh convergence rather than physical testing.

3.1.7 Assumptions and Limitations

- ✓ The car body is analyzed without internal reinforcements, windows or other required complex chassis components.
- ✓ Environmental factors such as crosswinds, road roughness and transient aerodynamic effects are excluded.
- ✓ Manufacturing analysis is not included full die design or cost modelling only feasibility studies and process planning.

3.2 Ansys Workbench Geometry Preparation

Main purposes of this research are to analyse the car body model for structural, fluid flow analysis through CFX solver and finally CAM analysis. That's why Ansys Workbench software supported common CAD file type "OBJ" is selected which is a widely used for exchanging 3D model but is not native to most parametric CAD software, often importing as mesh rather than editable NURBS (Non-Uniform Rational B-Splines) establish a mathematical framework for representing complex 3D geometry, enabling CAD and computer-graphics systems to construct highly accurate, smoothly varying curves and surfaces.

3.2.1 Pre-processing for Car Panel Structural Analysis

Flow Chart 3.1 Exact steps which are followed while pre-processing.

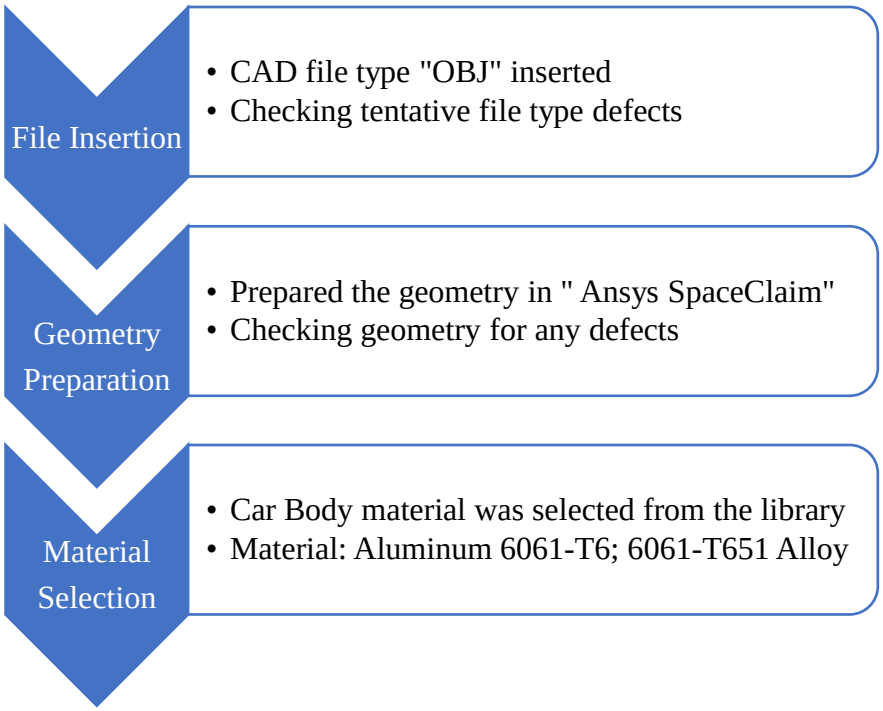

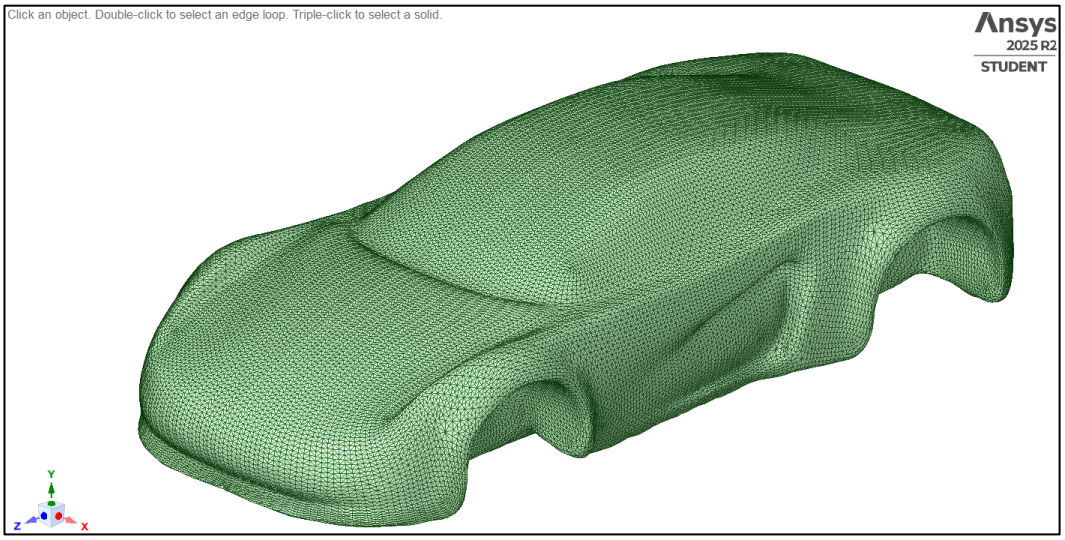

Figure 3.1 Pre-processed Geometric model of Car for Structural Analysis.

Aluminum alloy, wrought, 6061, T6

Aluminum, 6061, T6, wrought

Data compiled by **Ansys Granta**, incorporating various sources including JAHM and MagWeb.

ANSYS, Inc. provides no warranty for this data.

Density	2.713e-06 kg/mm³

Structural	
Isotropic Elasticity	
Derive from	Young's Modulus and Poisson's Ratio
Young's Modulus	69040 MPa
Poisson's Ratio	0.33
Bulk Modulus	67686 MPa
Shear Modulus	25955 MPa
Isotropic Secant Coefficient of Thermal Expansion	2.278e-05 1/°C
Tensile Ultimate Strength	313.1 MPa
Tensile Yield Strength	259.2 MPa

Figure 3.2 Material properties of the "Aluminum 6061-T6; 6061-T651".

Key reasons selected material "Aluminum 6061-T6; 6061-T651" is good for a sports car body panel:

- ✓ **Low weight with decent strength:** Material density is about 2.7 g/cm^3, roughly one-third of steel while ultimate tensile strength is around 313 MPa and yield strength is about 240-275 MPa in T6/T651. As per the requirements for a light sports car, this gives a good stiffness-to-weight and strength-to-weight ratio for outer panels.

- ✓ **Good stiffness for car panels:** Modulus of elasticity is about 69 GPa which is lower than steel but enough high with proper section design like beads, folds, curvatures to avoid "oil-canning" and give a solid quality feel.

- ✓ **Corrosion resistance for exposed bodywork:** It is a Mg-Si alloy with a good natural corrosion resistance, especially when painted or coated. That's important for a sports car that may see outdoor storage, rain and road salt.

- ✓ **Weldability and joinability:** It is readily weldable for (MIG/TIG) and also works well with mechanical fastening and adhesive bonding. That's useful for mixed-processes body construction like the spaceframe, subframes, brackets and car body other panel's attachments.

- ✓ **Formability for relatively simple sports car panels:** It doesn't match deep-draw 5XXX alloys for extreme forming but for many sports-car panels like doors, hood, fenders with moderate draw and curvature, these sheets can be formed with proper tooling and temper selection.

- ✓ **Fatigue and durability:** Fatigue strength around 95-100 MPa which is fully reversed and high cycle is adequate for non-primary crash structures and body panels, especially when combined with good design against stress concentrations.

- ✓ **Availability and cost:** These are one of the most common structural aluminum alloys available as sheet, plate etc. along with well-known data, standards and supply chains. That reduces cost and risk for a low-volume sports car.

- ✓ **Aesthetic and customization:** Aluminum 6061-T6; 6061-T651 takes coatings, paint well, and can be machined or extruded into visually expressive parts (-i.e., hood vents, aero pieces, brackets) that match a sporty designed car body panel just like the selected model.

In short, **Aluminum 6061-T6; 6061-T651** is popular for sports car body panels due to its excellent balance of properties. It has a low density, high strengths and good stiffness, making it lightweight yet durable. It's corrosion-resistant, formable and weldable which is crucial for manufacturing. It's also widely available and cost-effective.

Key limitations of "Aluminum 6061-T6; 6061-T651":

- ✓ **Formability vs 5XXX series:** For very deep or complex drawing processes, 5XXX (e.g., 5182 and 5754) is often preferred; 6061 may require more careful process designs while very complex deep drawing.

- ✓ **Strength vs 7XXX series:** 7XXX alloys (e.g., 7075) can be much stronger but they're highly expensive, less weldable and more sensitive to corrosion, so Alloy 6061 is a more balanced, practical choice for body panels rather than primary crash structures.

However, the selected material has some limitations compared to 5XXX/7XXX alloys, especially in complex deep draw formability and dent resistance. It's also less fatigue-resistant than some alternatives. Still, its overall performance makes it a solid choice. That is why "Aluminum 6061-T6; 6061-T651" was selected for car body external panel structural analysis.

3.2.2 Pre-processing for Fluid Flow Analysis

Inserting the CAD file into the Ansys Workbench software, first task is to prepare the geometry within the enclosure along with maintaining appropriate spacing in the enclosure where meshing analysis will be taken place.

Flow Chart 3.2 Exact steps which are followed while preparing the geometry.

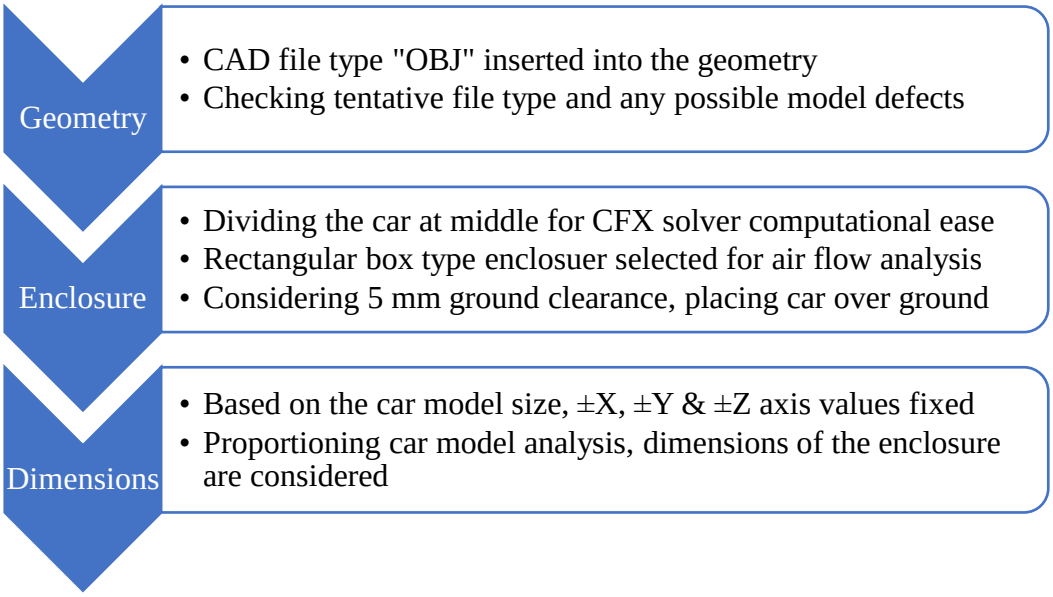

Here, the box type enclosure is selected for getting proper velocity streamlines and pressure as the car is considered as a wall and air flow movement through the meshed air properties. Considered dimensions of the enclosure are mentioned in the table 3.1 below.

Table 3.1 Dimension of the box type enclosure of the CFD model.

Direction	Size [mm]	Position According to Car
Cushion -X	0	Left Side
Cushion +X	150	Right Side
Cushion -Y	5	Bottom Side/Ground Clearance
Cushion +Y	100	Top Side
Cushion -Z	500	Rear/Back Side
Cushion +Z	100	Front Side

Before the enclosure preparation, a plane was taken and the car model was divided at the middle as shown in the picture below:

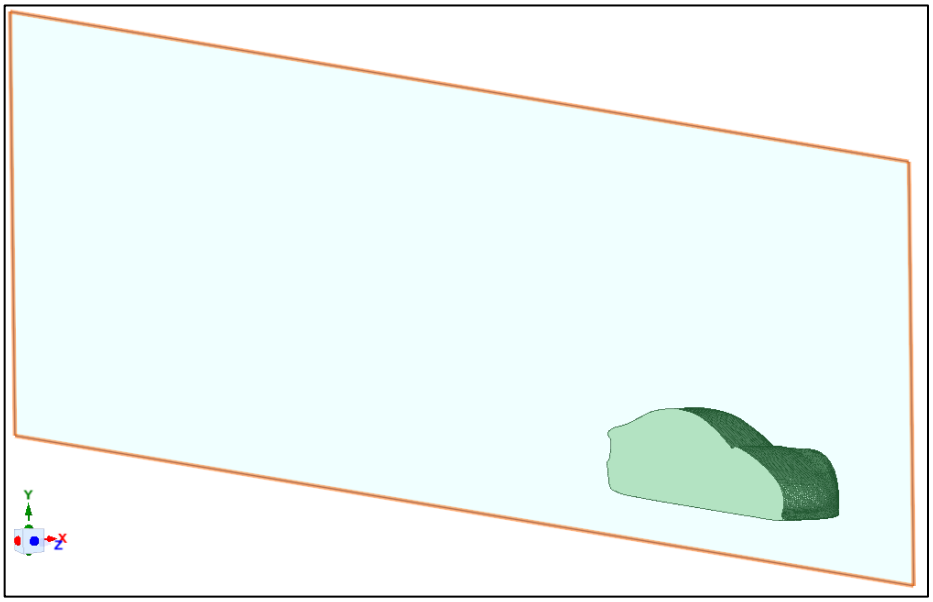

Figure 3.3 Dividing the concept car for enclosure of fluid flow Analysis.

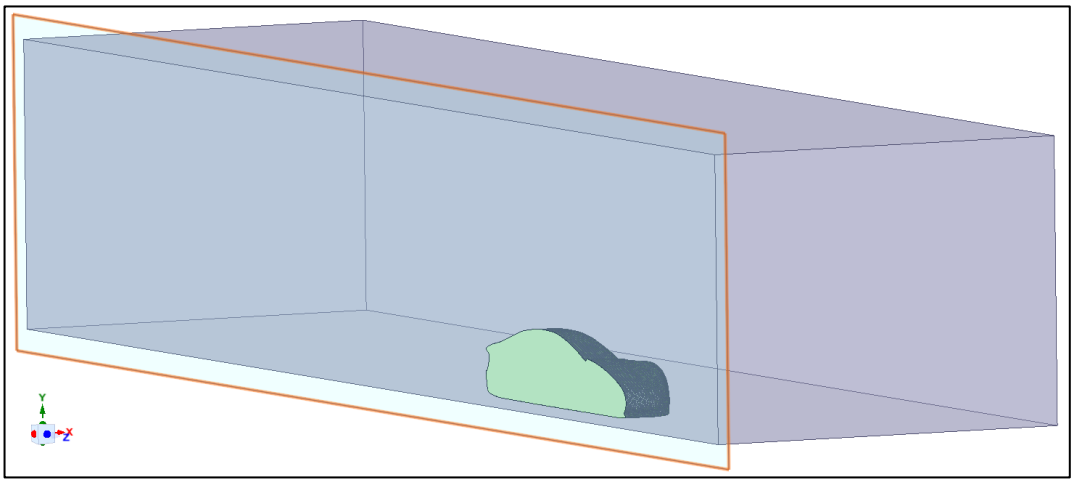

Figure 3.4 The box enclosure was placed on the right side of plane.

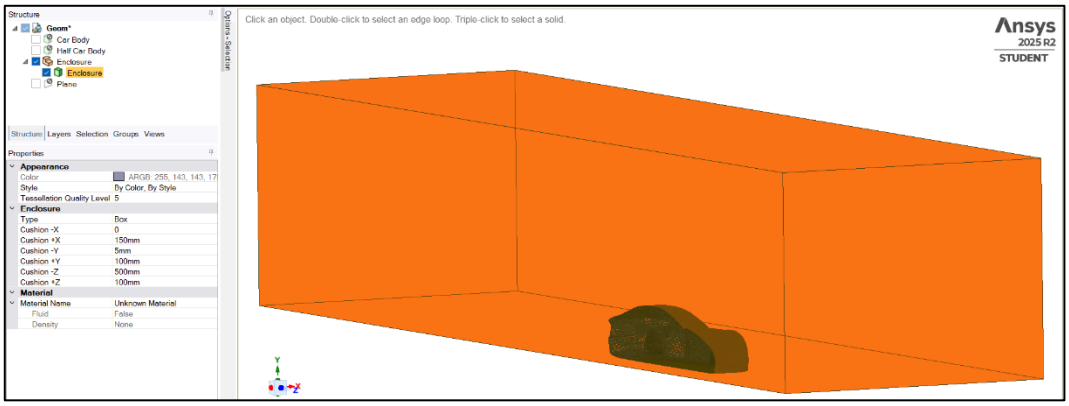

Figure 3.5 The car model inside the box enclosure along with the dimensions.

Except the box enclosure; the car, half car bodies and 2-D planes are suppressed for physics as shown in Figure 3.5 because the only the enclosure inside void spaces will be considered as air properties which will be taken into computation.

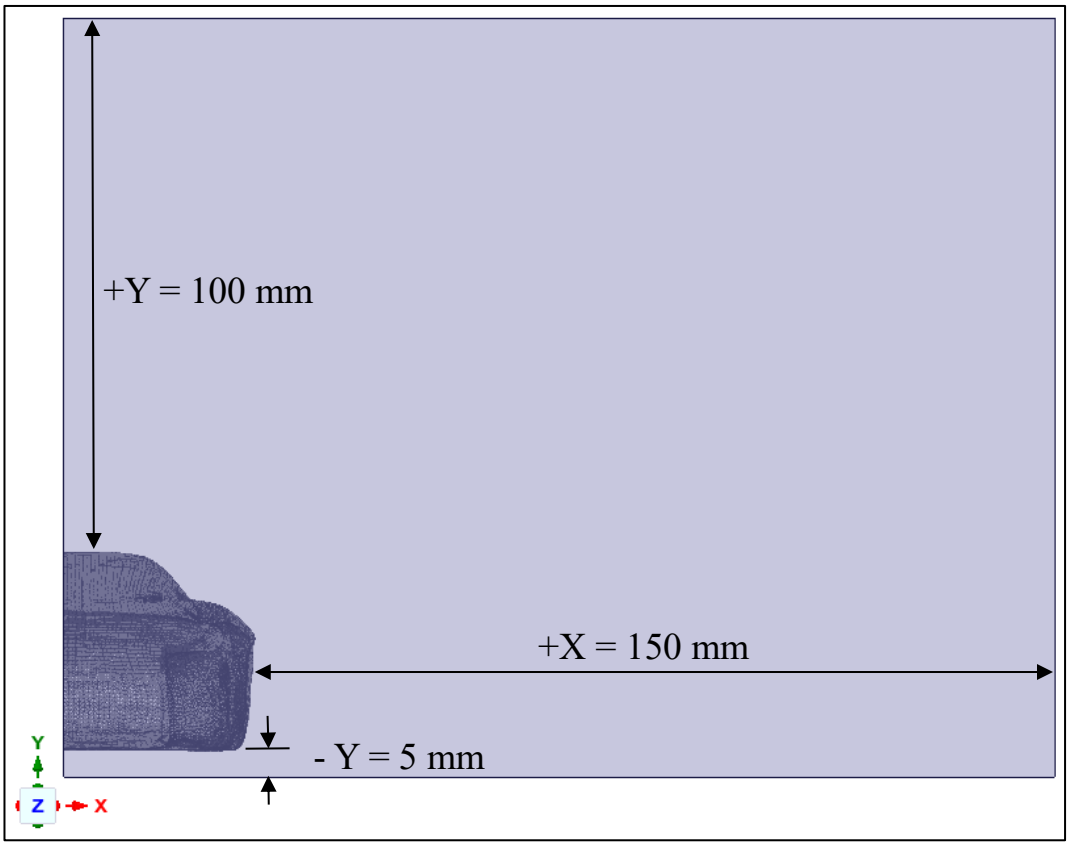

Figure 3.6 X-Y Plane front side view of the enclosure in Ansys Workbench.

Here, in this fluid flow simulation, we'll mesh and simulate only the air, which is the empty space of the enclosure other than the car body surfaces, will be physically computed in Ansys Workbench CFX solver as the surrounding air flowing inside the enclosure. Considering the wheel positioning spaces, car body is placed 5mm above the ground.

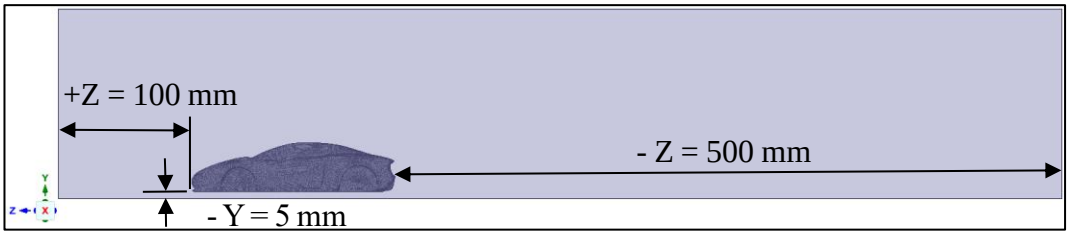

Figure 3.7 Z-Y Plane right side view of the enclosure in Ansys Geometry.

The half cut car body surfaces and ground will be considered as fixed walls so that we can evaluate and analyze the velocity, pressure & drag forces relative to the cunceptual car body model. That is why the enclosure void spaces kept so huge to get more accurate results. Now, the model is ready for further simulations.

3.3 Meshing Strategy and Analysis

Meshing is a decisive step in both structural and fluid flow simulations. To ensure the accuracy and convergence, a systematic meshing strategy was applied:

3.3.1 Structural Mesh

- ✓ **Element Type and Size:** Quad dominant elements were selected due to the complex curvature of the car body panel.
- ✓ **Default Element Size:** 1 mm element size was selected for meshing.
- ✓ **Mesh Refinement Zones:**
  - High curvature regions (hood, fenders, diffuser)
  - Stress concentration areas (mounting points, edges)

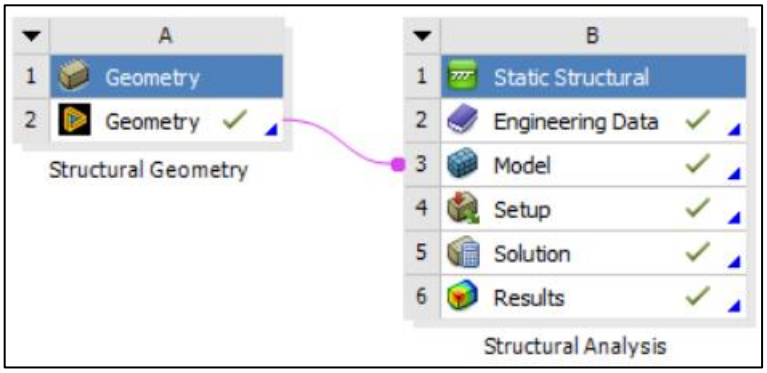

Figure 3.8 Structural Geometry was inserted into the model for meshing.

Details of "Mesh"

Display	
Display Style	Use Geometry Setting
Defaults	
Physics Preference	Mechanical
Element Order	Program Controlled
Element Size	1.0 mm
Sizing	
Use Adaptive Sizing	Yes
Resolution	Default (2)
Mesh Defeaturing	Yes
Defeature Size	Default
Transition	Fast
Span Angle Center	Coarse
Initial Size Seed	Assembly
Bounding Box Diagonal	172.44 mm
Average Surface Area	0.27085 mm²
Minimum Edge Length	0.20723 mm

Figure 3.9 Element Size and Mesh Sizing Details.

Details of "Mesh"

Sizing	
Quality	
Check Mesh Quality	Yes, Errors
Error Limits	Aggressive Mechanical
Target Element Quality	Default (5.e-002)
Smoothing	Medium
Mesh Metric	None
Inflation	
Use Automatic Inflation	None
Inflation Option	Smooth Transition
Transition Ratio	0.272
Maximum Layers	10
Growth Rate	1.2
Inflation Algorithm	Pre
Inflation Element Type	Wedges
View Advanced Options	No
Advanced	
Automatic Methods	
Statistics	
Nodes	1021069
Elements	609232
Show Detailed Statistics	No

Figure 3.10 Generated Mesh Nodes 1,021,069 and Elements 609,232.

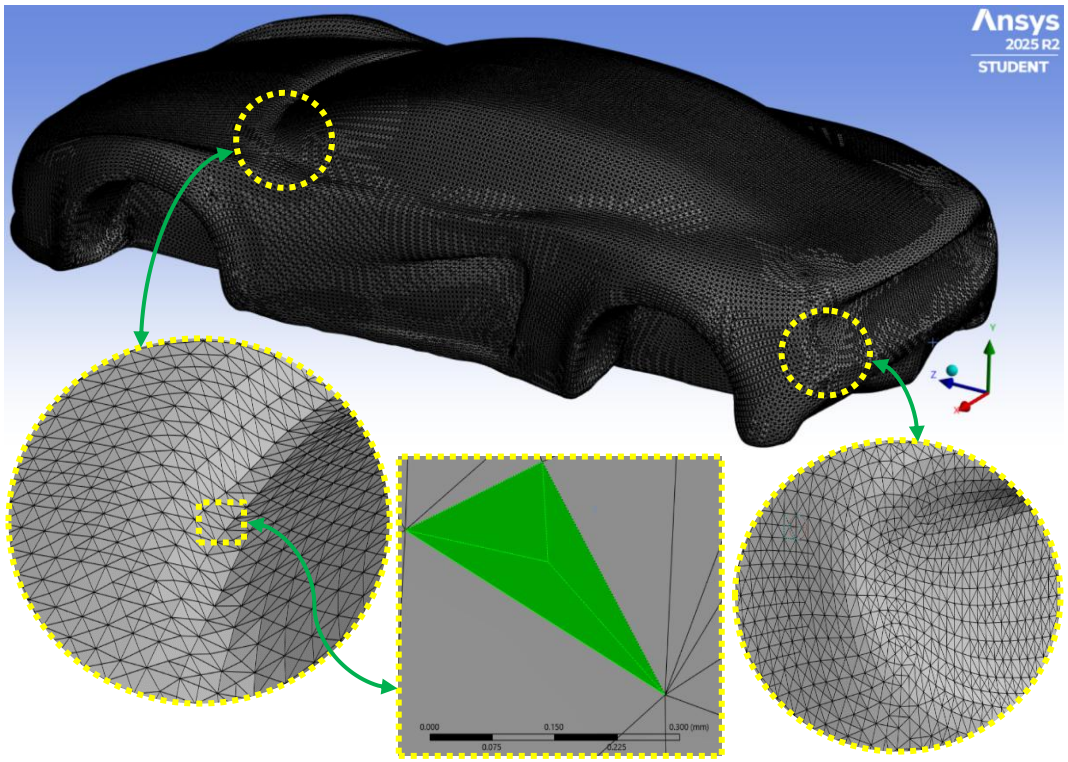

Figure 3.11 Rear isometric view of car body fine meshing element size of 1 mm.

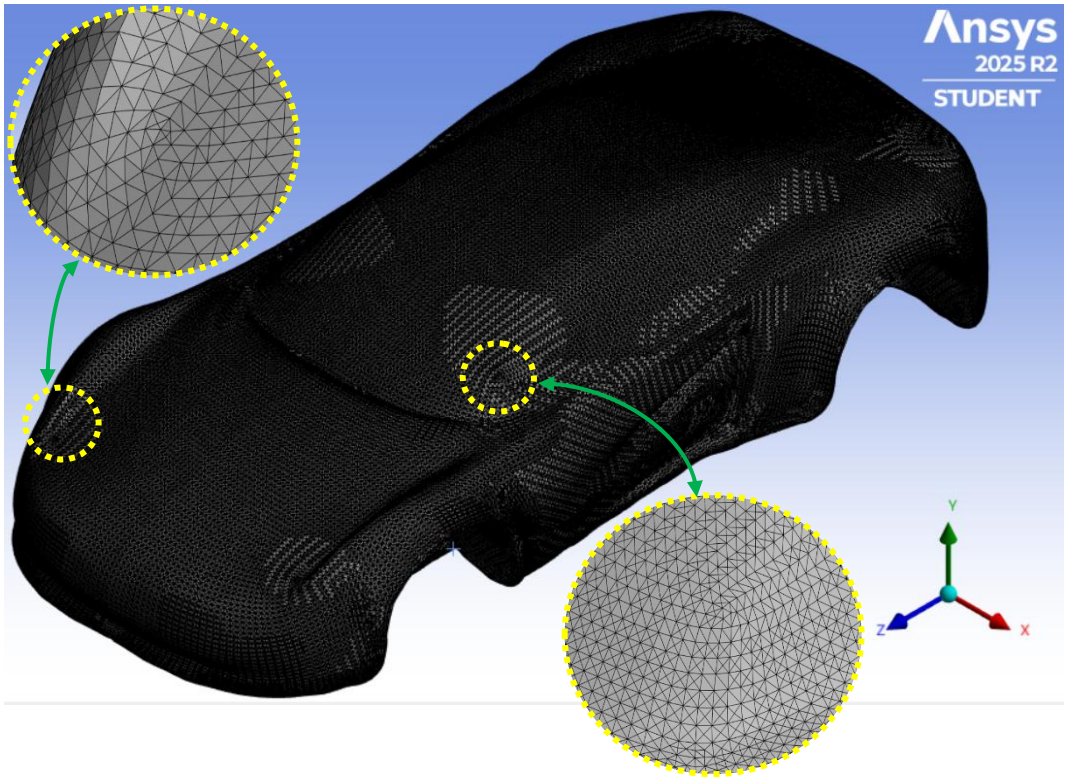

Figure 3.12 Front isometric view of the car body fine meshing size of 1 mm.

3.3.2 Computational Fluid Dynamics (CFD) Mesh

For the analysis of CFD meshing, three different types of mesh elements sizes were applied to prepare fine, medium and coarse meshes for meshing analysis.

All other applied strategies are as follows:

- ✓ **Boundary Layer Resolution:** Multiple inflation layers were applied to capture the near-wall velocity gradients and shear stresses.
- ✓ **Body Sizing:** To reduce the element sizes so that the meshing & simulation can be done effectively to get appropriate results.
- ✓ **Mesh Sensitivity:** Mesh sensitivity analysis was performed using coarse, medium and fine meshes to ensure that deformation and stress results were independent of mesh density.

Previously prepared geometry of the box enclosure was used for preparing all the three types of meshing by inserting it into Fluid Flow (CFX) Solver blocks as shown in the following Figure 3.13.

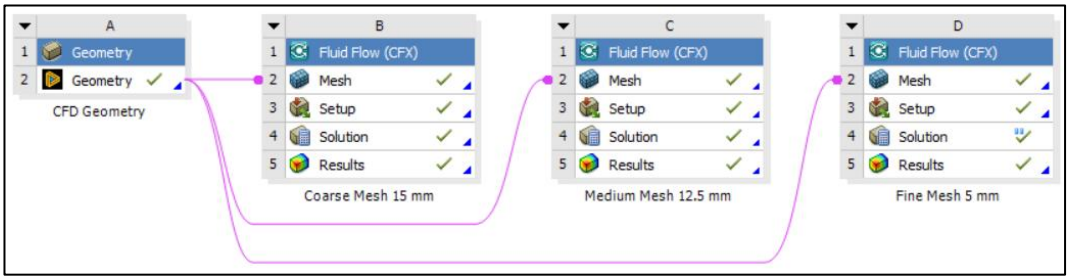

Figure 3.13 CFD Geometry enclosure was inserted into Mesh for solving in CFX.

I. Coarse Mesh Analysis:

Flow Chart 3.3 All the steps followed for coarse meshing are mentioned below:

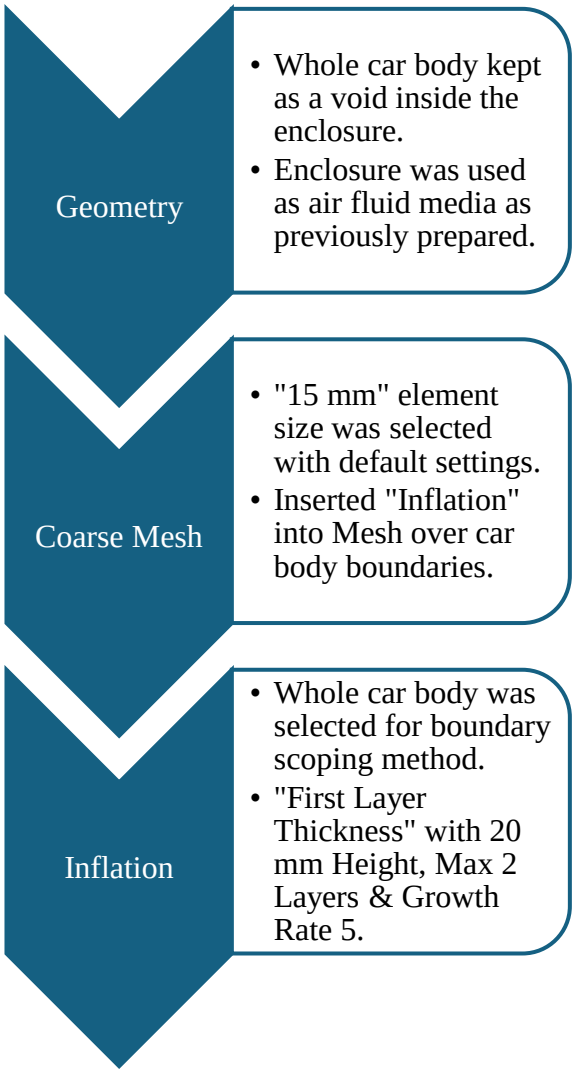

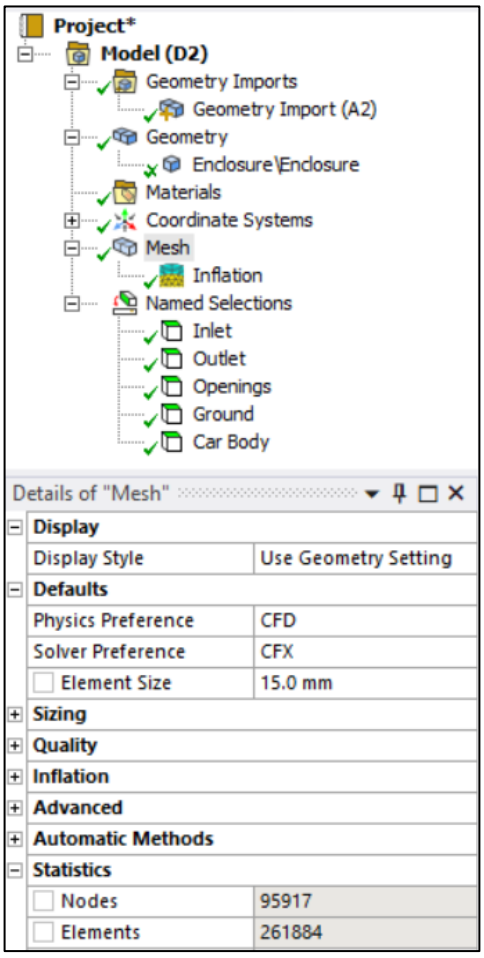

Figure 3.14 Coarse Mesh Setup.

After creating the coarse mesh, the result was generated with a total number of 95,917 nodes and 261,884 elements.

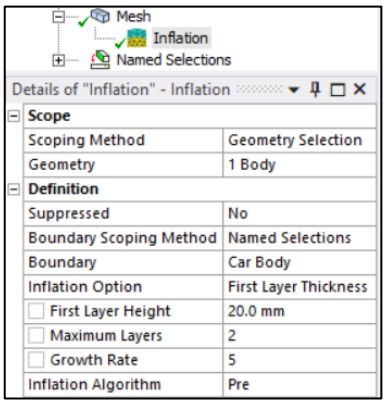

Scope	
Scoping Method	Geometry Selection
Geometry	1 Body
Definition	
Suppressed	No
Boundary Scoping Method	Named Selections
Boundary	Car Body
Inflation Option	First Layer Thickness
First Layer Height	20.0 mm
Maximum Layers	2
Growth Rate	5
Inflation Algorithm	Pre

Figure 3.15 Coarse mesh inflation layer setup.

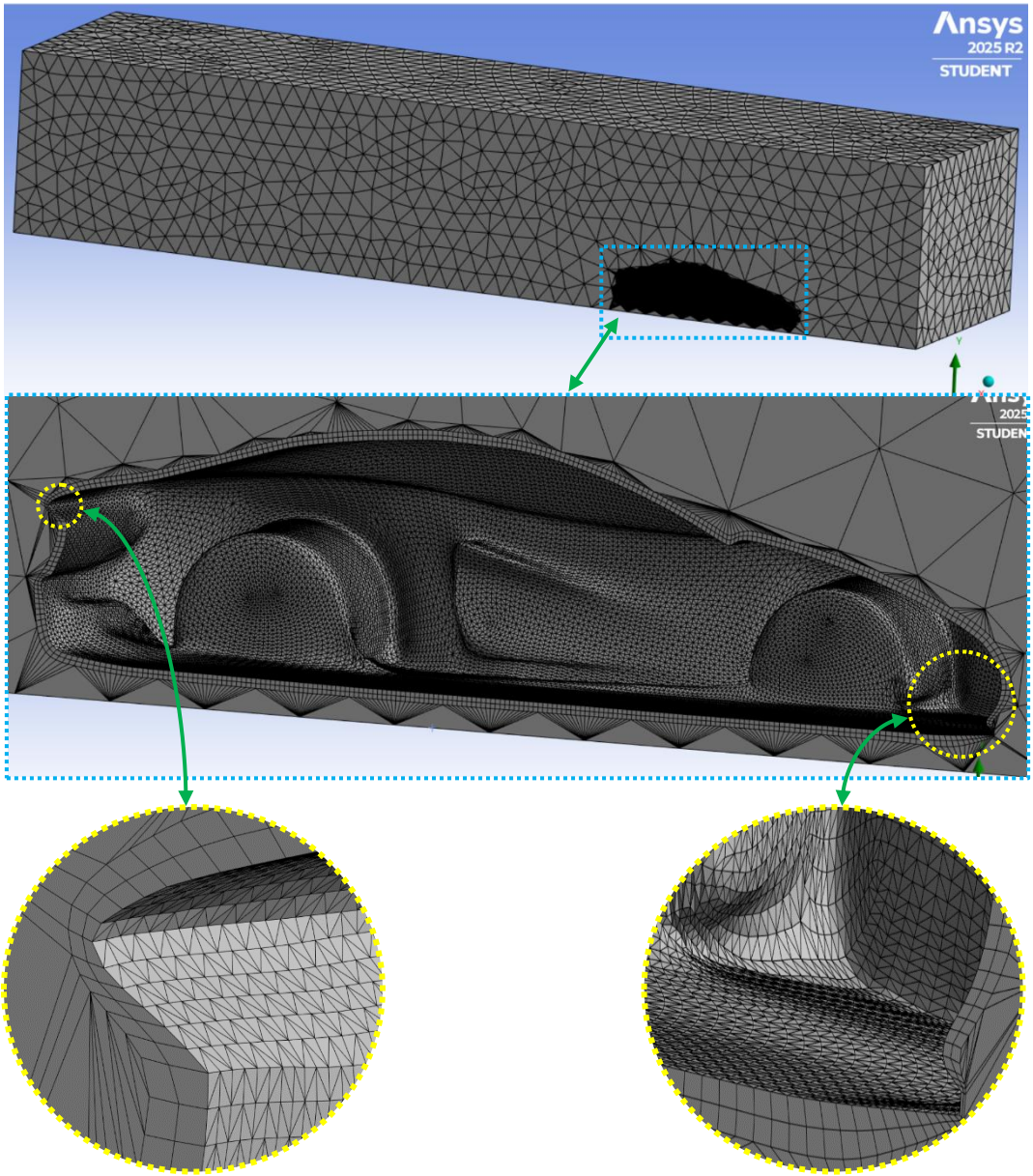

Figure 3.16 Element size 15 mm, coarse mesh with 2 inflation layers around car.

II. Medium Mesh Analysis:

Flow Chart 3.4 All the steps followed for medium meshing are mentioned below:

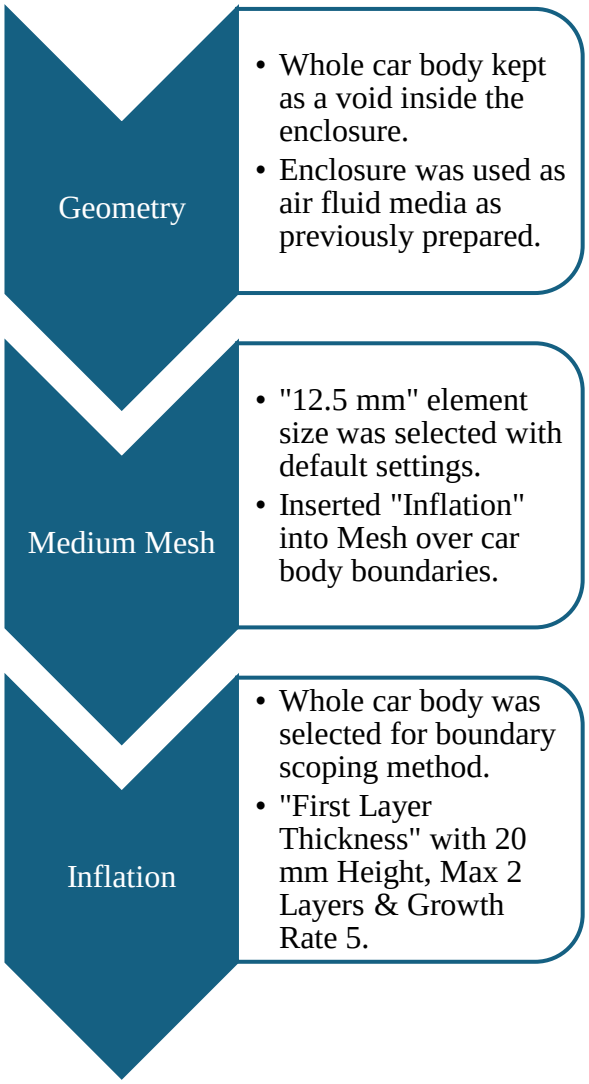

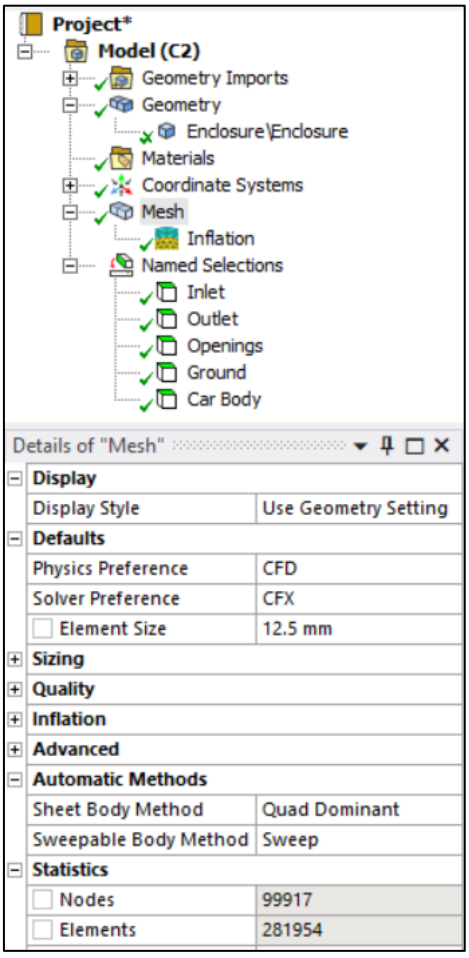

Figure 3.17 Medium Mesh Setup.

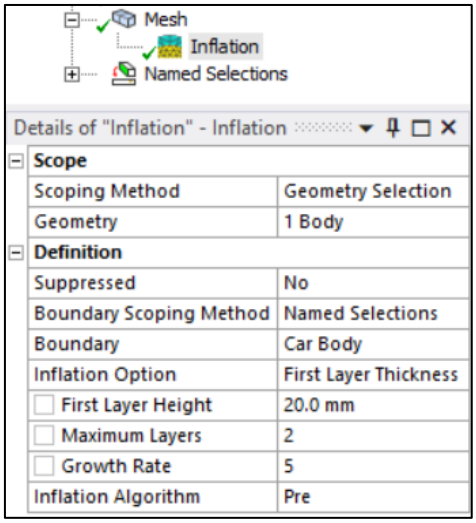

Figure 3.18 Medium mesh inflation layer setup.

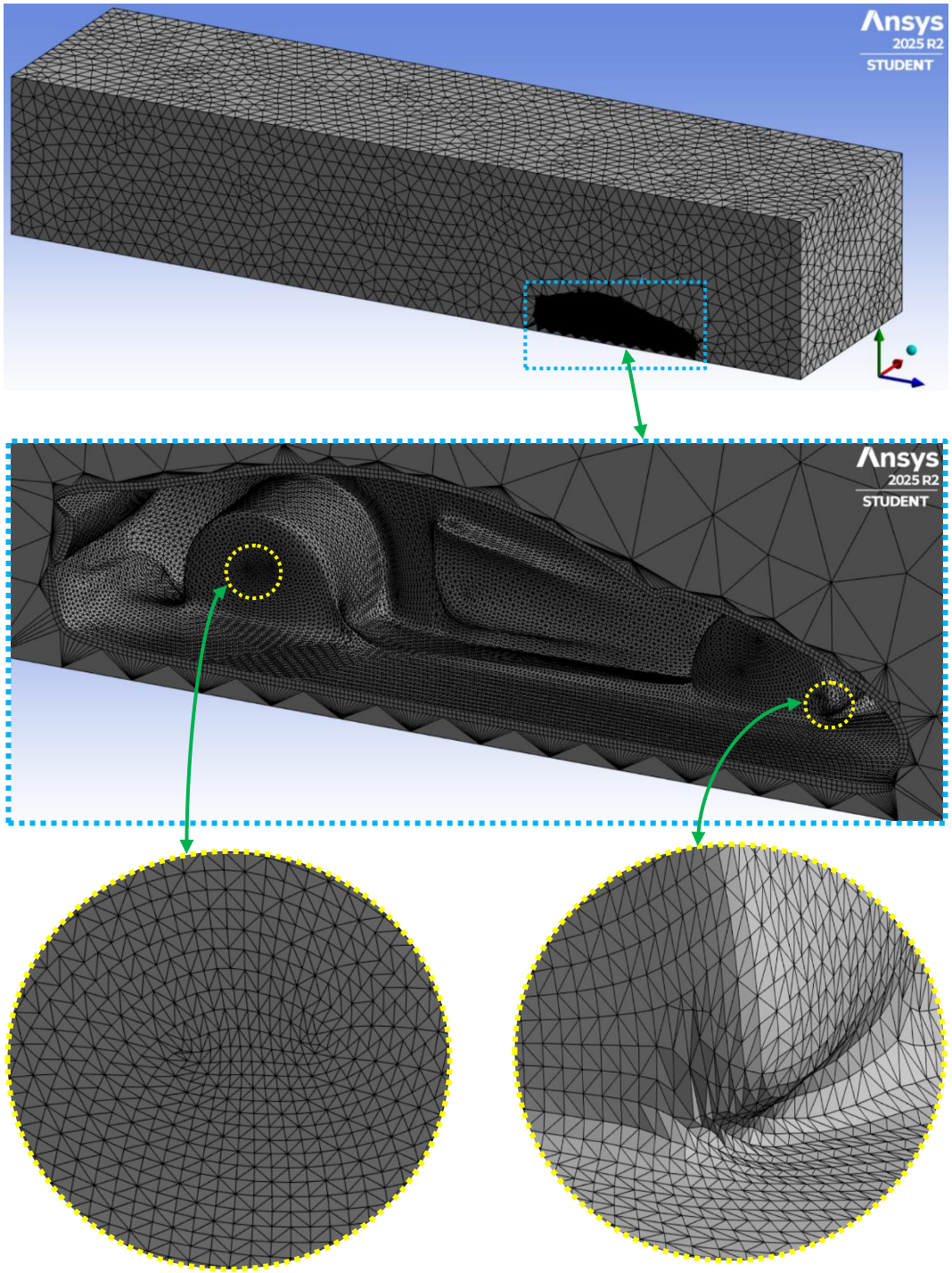

Figure 3.19 Element size 12.5 mm, medium mesh of enclosure around car.

After creating the medium mesh of enclosure around the car void space, the result was generated with a total number of 99,917 nodes and 281,954 elements.

III. Fine Mesh Analysis:

Flow Chart 3.5 All the steps followed for fine meshing are mentioned below:

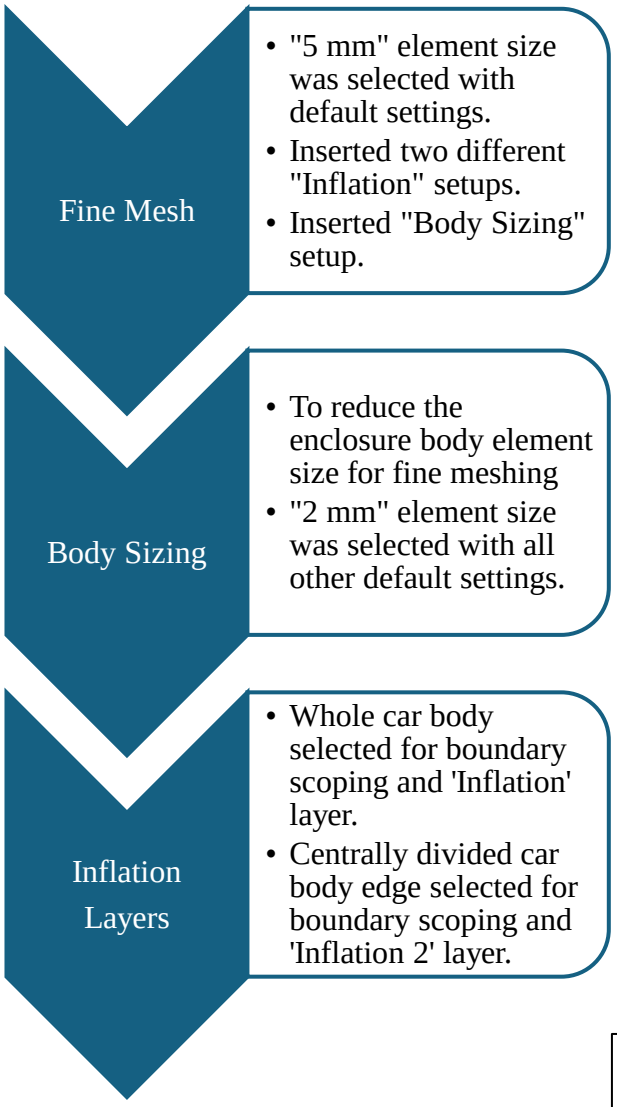

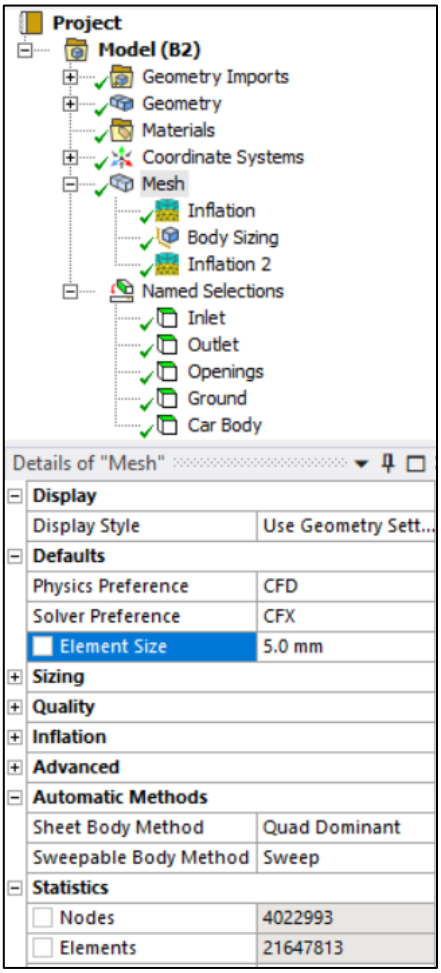

Figure 3.20 Fine Mesh Setup.

"First Layer Thickness" of Inflation was setup with 5 mm first layer height, max 100 layers & 1.2 growth rate as shown in the Figure 3.21.

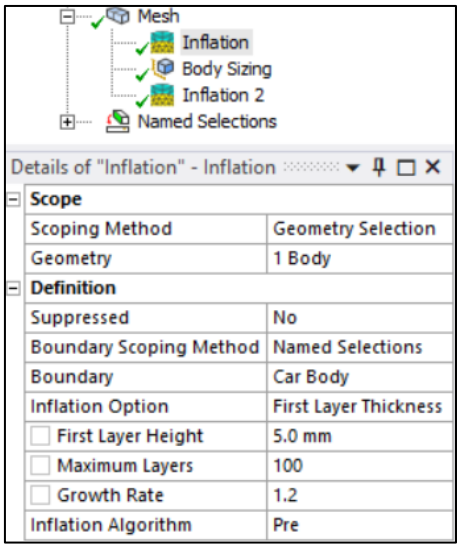

Figure 3.21 Fine mesh Inflation layer setup.

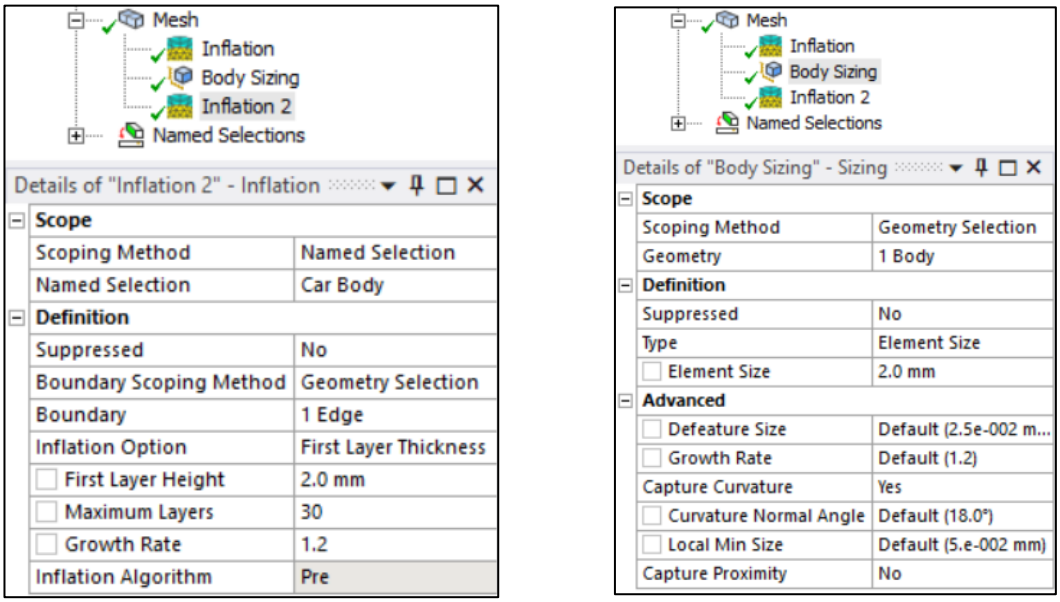

Figure 3.22 Fine mesh ‘Inflation 2’ & Body Sizing setup at the enclosure body.

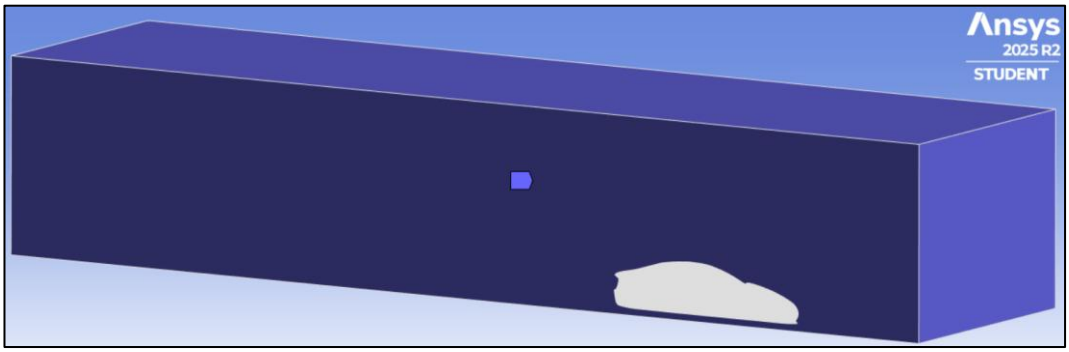

Figure 3.23 Inflation & Body Sizing setup at the enclosure body.

Main purpose is to set multiple inflation layers to capture the near-wall velocity gradients, pressure contour and shear stresses.

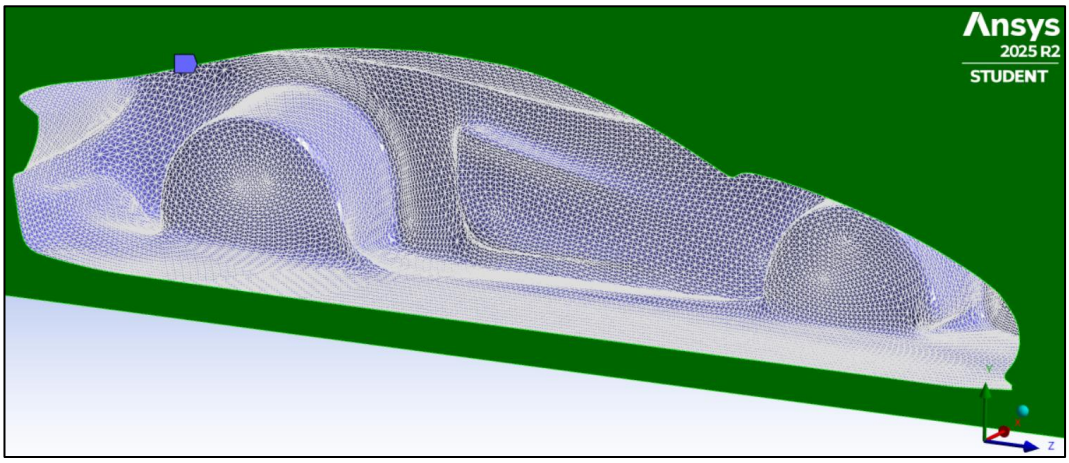

Figure 3.24 ‘Inflation 2’ applied at the centrally divided car body edge only.

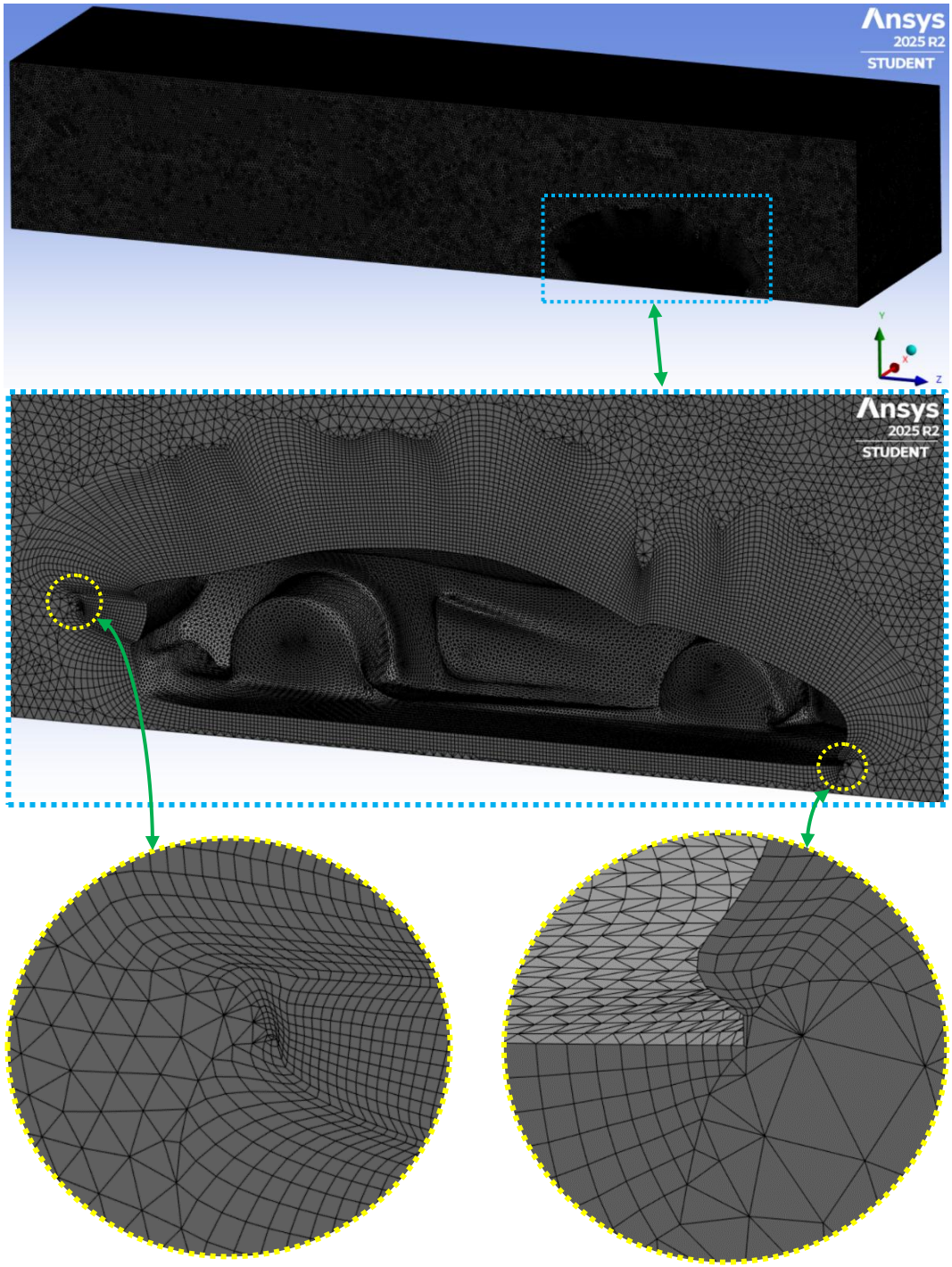

Figure 3.25 Element size 5 mm, fine mesh along with inflation layers at enclosure.

After creating the fine mesh of enclosure around the car void space, the result was generated with a total number of 4,022,993 nodes and 21,647,813 elements. Expecting that these multiple inflation layers will assist to compute and capture the near-wall velocity gradients, pressure contour and shear stresses very precisely.

3.4 Structural Analysis Method

The structural analysis designed to evaluate the stiffness, deformation behaviour and stress distribution of the car body under simplified loading conditions.

3.4.1 Boundary Conditions

- ✓ The car body was constrained at illustrative mounting points to simulate attachment to a chassis.
- ✓ Loads were applied to represent pressure, self-weight and localized forces.

3.4.2 Material Assignment

Aluminum 6061-T6 / 6061-T651 was assigned based on its mechanical properties, manufacturability and suitability for sports car body panels.

3.4.3 Solver Settings

- ✓ Linear static analysis was performed.
- ✓ Large deflection effects were ignored due to low expected deformations.

3.4.4 Output Parameters

- ✓ Total deformations
- ✓ Equivalent (von-Mises) stress
- ✓ Safety factors

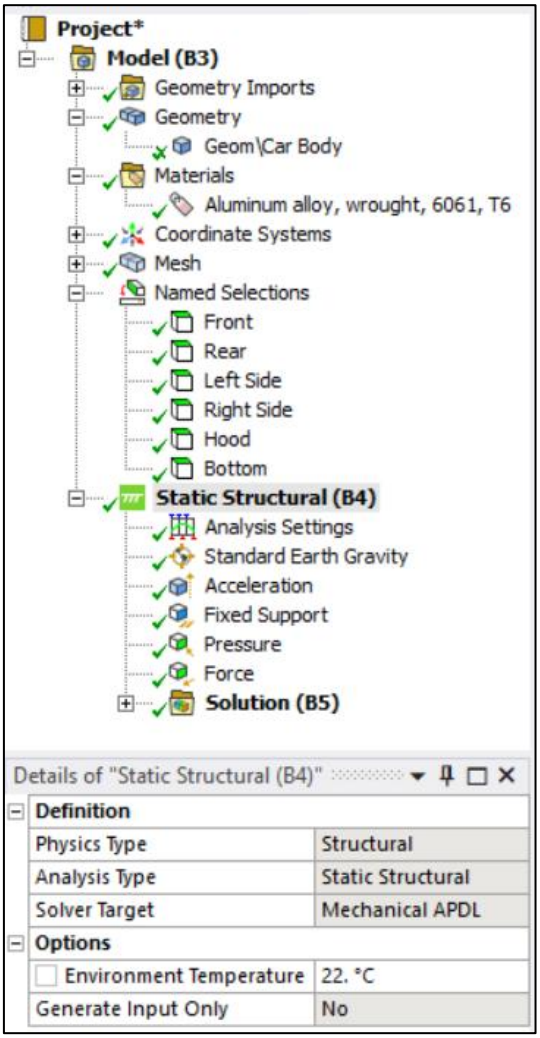

Figure 3.26 Static Structural Setup.

All the provided results will share the insight into the structural suitability of the concept car body panel.

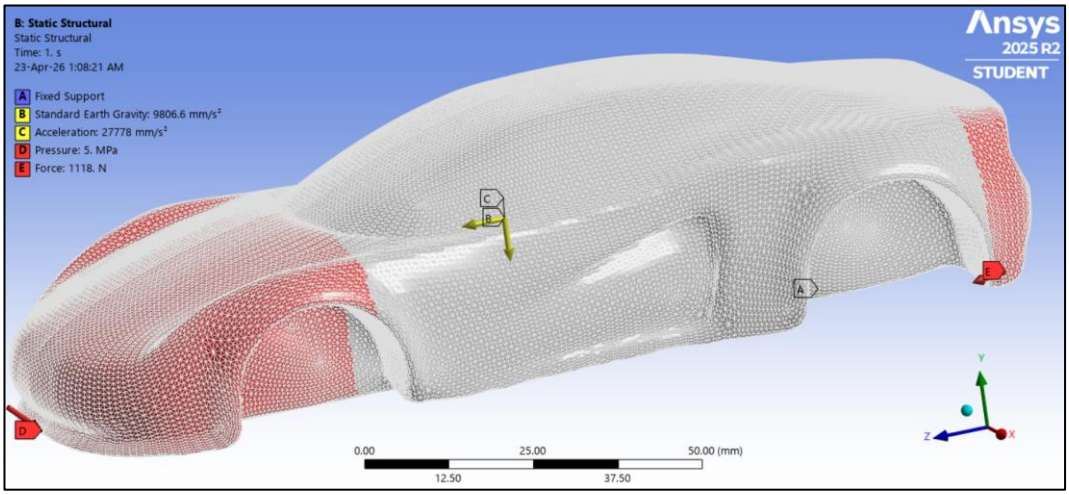

Figure 3.27 Applied Boundary Conditions Setup at Static Structural.

3.4.5 Static Structural Results

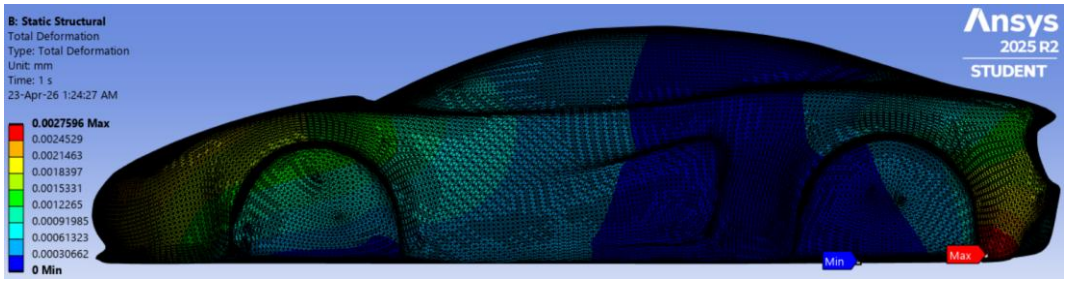

Figure 3.28 Static Structural Result, Total Deformation at 1.0 (True Scale).

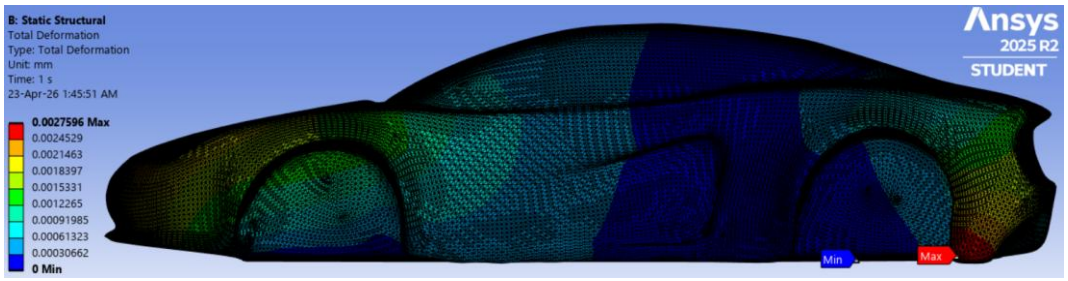

Figure 3.29 Static Structural Result, Total Deformation at 1.6e+003 (0.5x Auto).

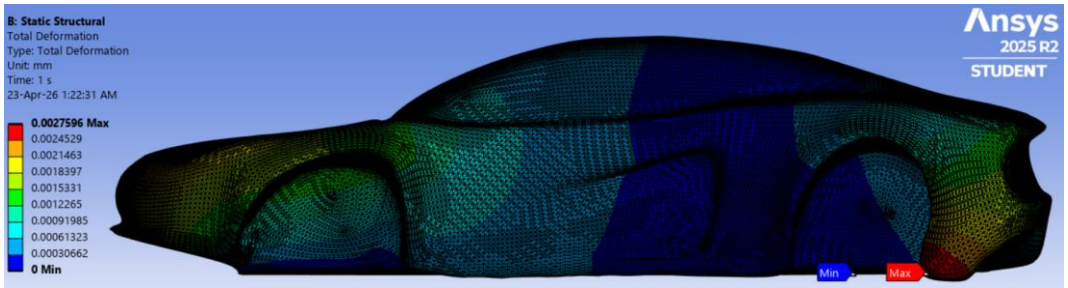

Figure 3.30 Static Structural Result, Total Deformation at 3.2e+003 (Auto Scale).

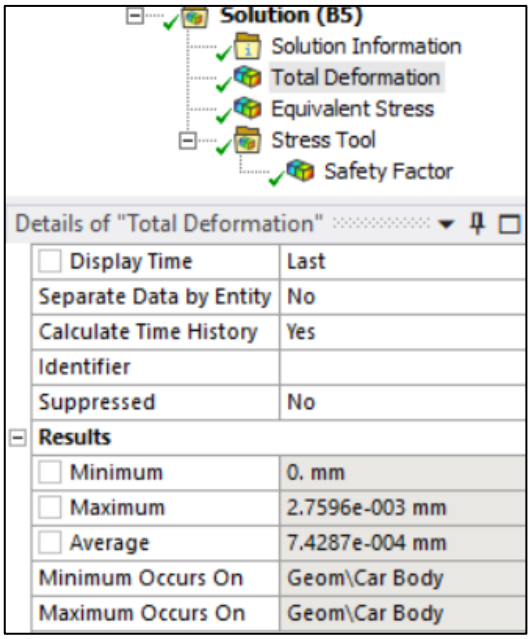

Figure 3.31 Static Structural, Acceptable Avg. and Max. Total Deformations.

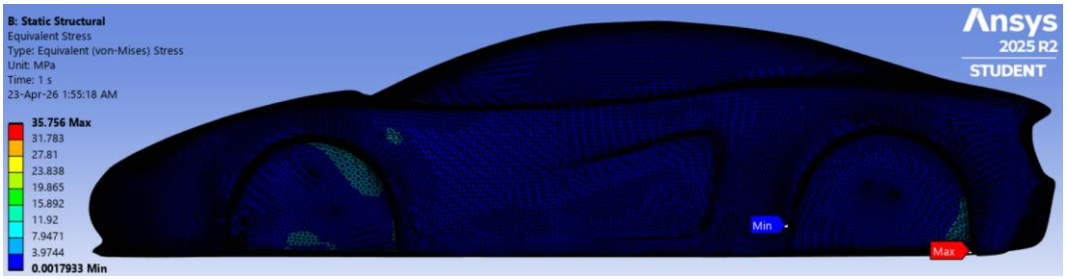

Figure 3.32 Equivalent (von-Mises) Stress Result at 1.0 (True Scale).

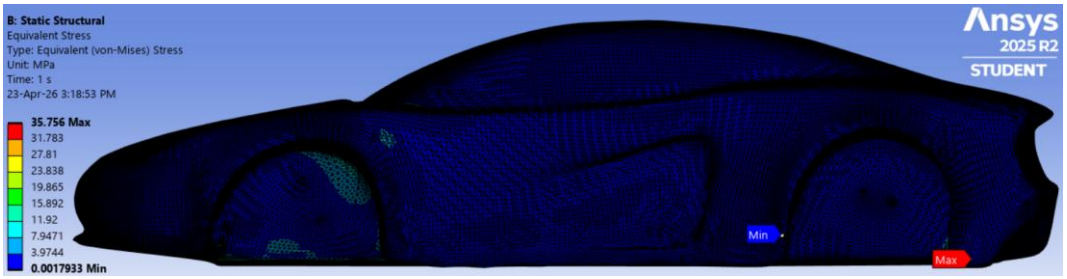

Figure 3.33 Equivalent (von-Mises) Stress Result at 1.6e+003 (0.5x Auto).

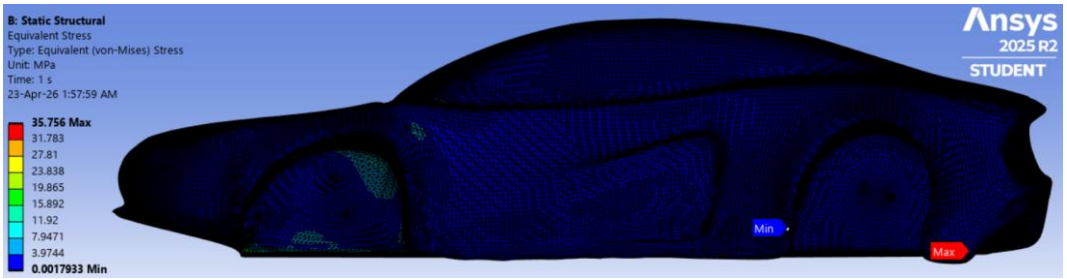

Figure 3.34 Equivalent (von-Mises) Stress Result at 3.2e+003 (Auto Scale).

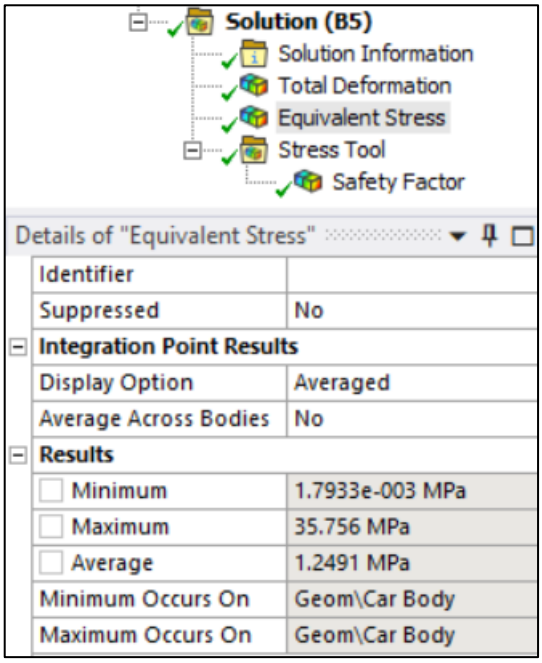

Identifier	
Suppressed	No
Integration Point Results	
Display Option	Averaged
Average Across Bodies	No
Results	
Minimum	1.7933e-003 MPa
Maximum	35.756 MPa
Average	1.2491 MPa
Minimum Occurs On	Geom\Car Body
Maximum Occurs On	Geom\Car Body

Figure 3.35 Acceptable Avg. and Max. Equivalent (von-Mises) Stresses.

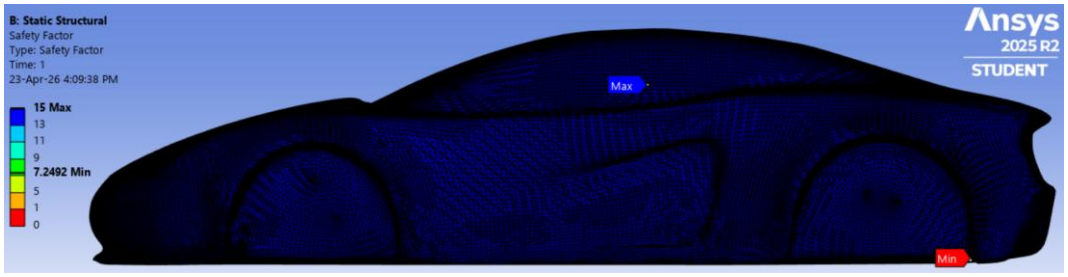

Figure 3.36 Safety Factor, Tensile Yield Per Material at 1.0 (True Scale).

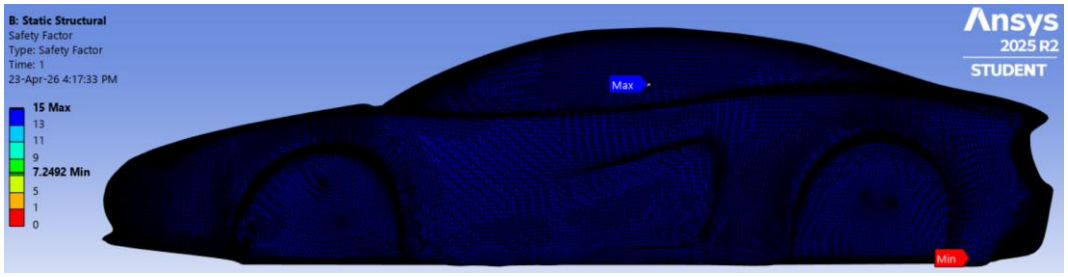

Figure 3.37 Safety Factor, Tensile Yield Per Material at 1.6e+003 (0.5x Auto).

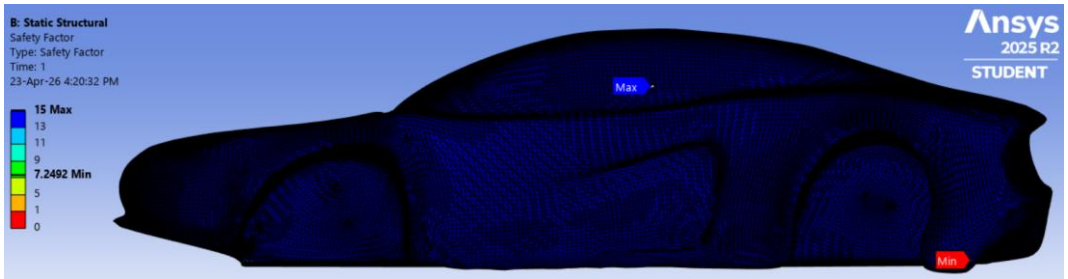

Figure 3.38 Safety Factor, Tensile Yield Per Material at 3.2e+003 (Auto Scale).

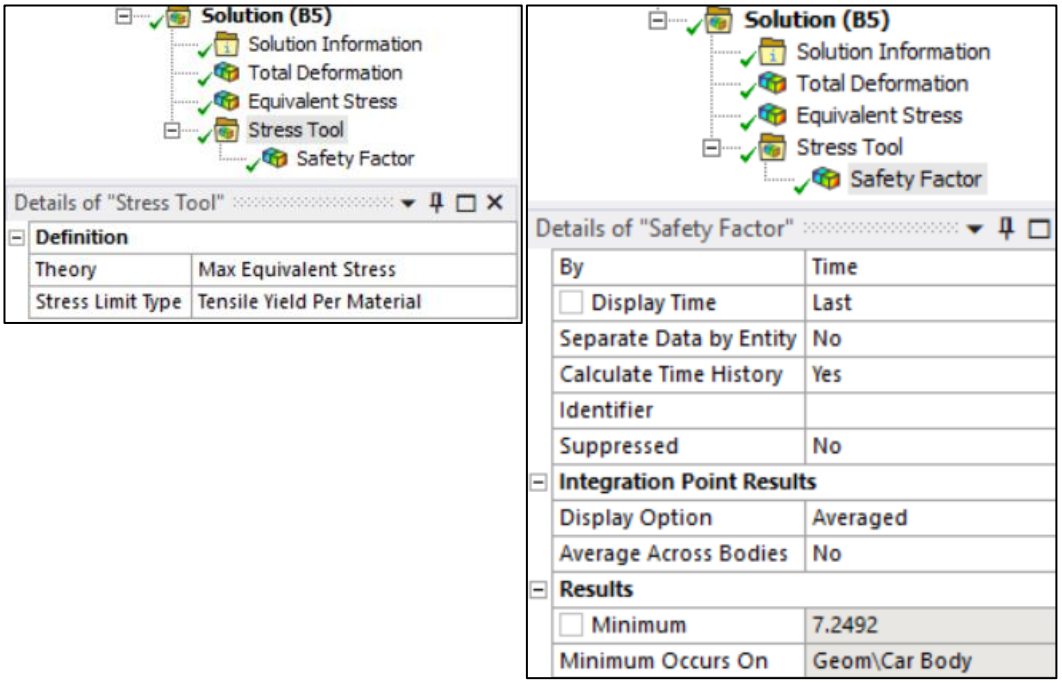

Figure 3.39 Stress Limit as per Tensile Yield of Aluminum 6061 T6 / 6061 T651.

3.5 Computational Fluid Dynamics (CFD) Method

The CFD analysis was conducted using ANSYS fluid flow CFX solver to evaluate aerodynamic performance, including drag, lift, pressure distribution and flow behaviours.

3.5.1 Fluid Domain and Boundary Conditions

The domain was designed to define four key boundary conditions like Inlet, Outlet, Openings and stationary objects such as walls. Air at 25°C temperature was chosen as the material to accurately simulate airflow behaviour.

- ✓ **Inlet:** Uniform velocity corresponding to high-speed driving conditions, assigned to a velocity of 100 km/h.
- ✓ **Outlet:** Maintained a static pressure of 0 Pa (equivalent to 1 atm).
- ✓ **Opening:** Identical conditions were applied to the three walls on top and both sides to create an opening that allowed force to move in any directions without restriction.
- ✓ **Walls:** The car and ground surfaces were given no slip wall parameters to effectively simulate the airflow dynamics surrounding them.

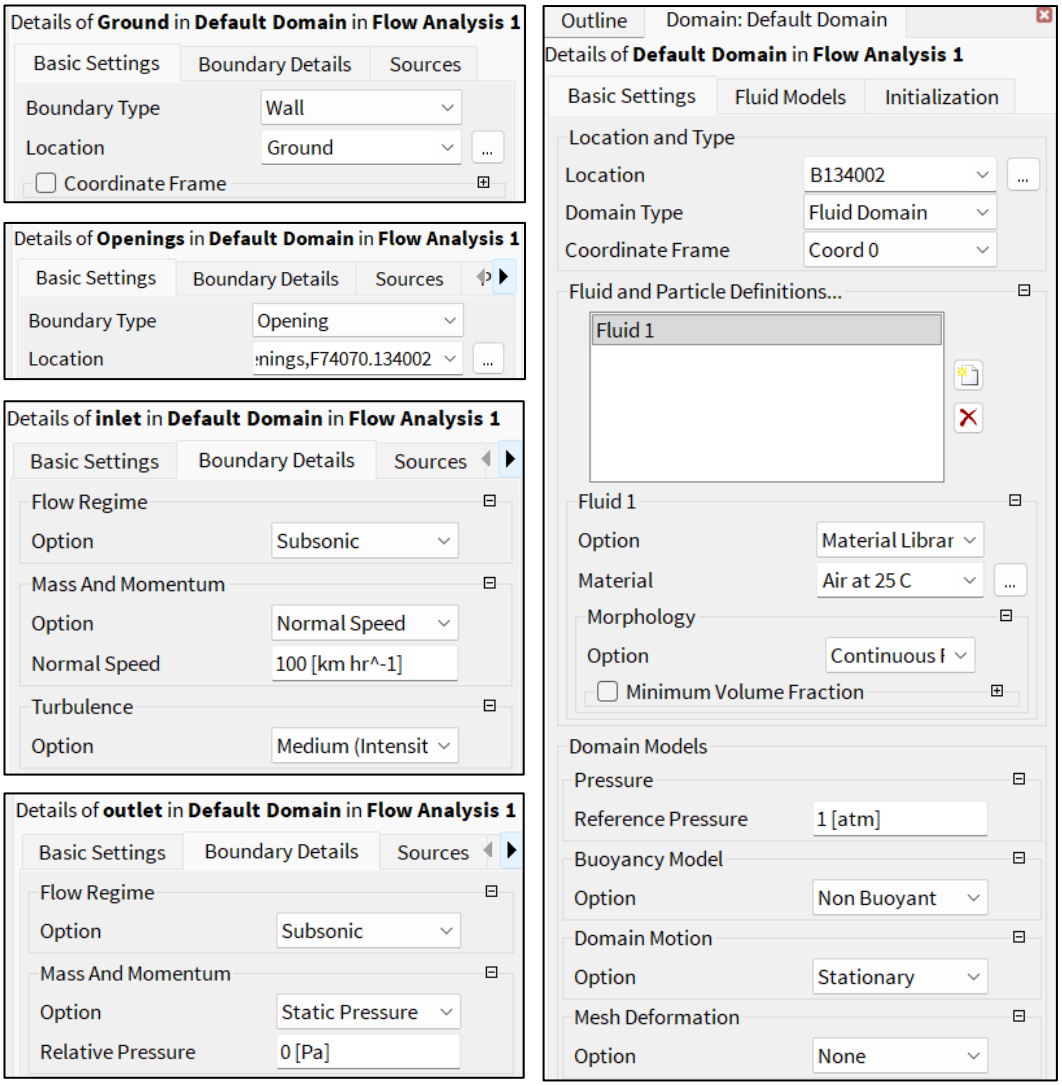

Figure 3.40 Fluid Domain as Air and Boundary Conditions Setup in Domain.

3.5.2 Turbulence Model Selection

k–ω SST (Shear Stress Transport) model selected due to its accuracy in predicting flow separation, diffuser performance and near-wall behavior while speeding.

However, generated turbulence at the rear of the vehicle can be further minimized by modifying the surfaces of the diffusers, air-channeling ducts and other possible aerodynamic enhancements. Main target is to maximize laminar flow while strategically managing turbulence.

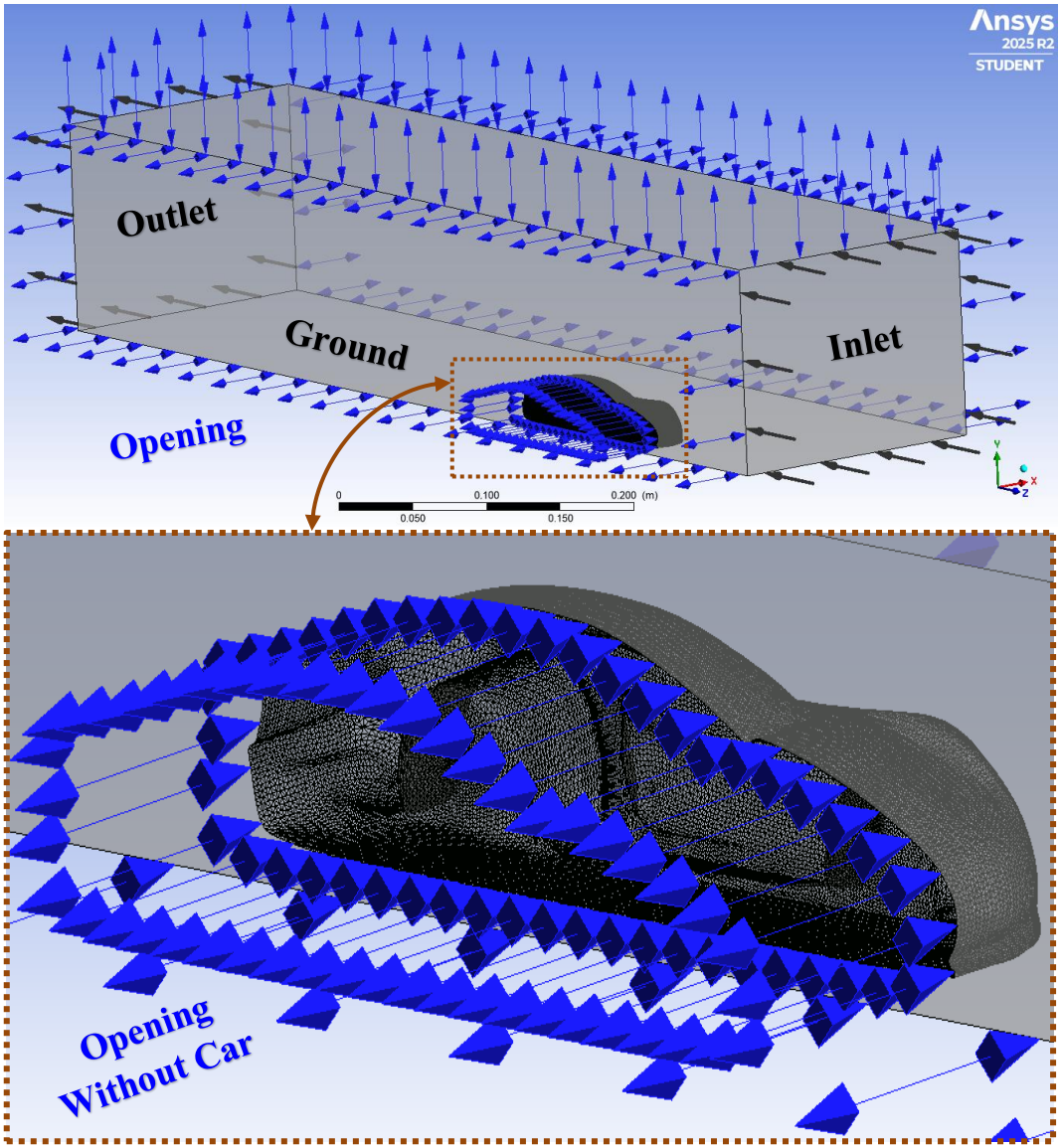

Figure 3.41 Applied Key Boundary Conditions in Fluid Domain.

3.5.3 Output Parameters

- ✓ Drag force and coefficient
- ✓ Lift force and coefficient
- ✓ Velocity streamlines
- ✓ Pressure and Y^+ contours
- ✓ Vortex formation regions
- ✓ Diffuser and underbody flow behaviors

3.5.4 CFX Solver Solutions Analysis

The prepared geometry was pre-processed by multiple mesh densities like coarse, medium and fine. The graphs of each meshing will be analysed one by one.

I. Course Mesh Solution Analysis:

The convergence info obtained from the 15 mm coarse mesh simulation provides an initial assessment of numerical stability and solver behaviour during the CFD analysis. The residual plot displays the evolution of the governing equation imbalances such as mass conservation RMS (P-Mass, U-Mom, V-Mom, W-Mom) and turbulence conservation (RMS K-Turbulence Kinetic Energy, RMS O-Turbulence Eddy Frequency) as a function of accumulated time steps.

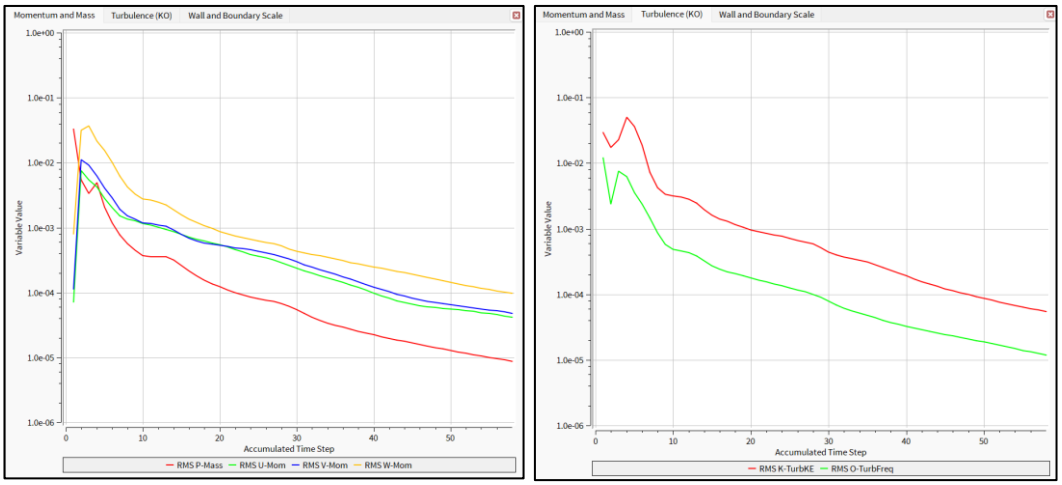

Figure 3.42 Coarse Mesh Solution of Mass-Momentum and Turbulence (KO).

Residual Behavior of Mass-Momentum and Turbulence

- ✓ The residual curves show a monotonic decrease over the course of the simulation, indicating that the solver progressively reduced the imbalance in the continuity and momentum equations.
- ✓ Although the coarse mesh does not achieve very low residual values, the downward trend validates that the solution is numerically stable and approaching a steady state condition.
- ✓ The mass residual (RMS P-Mass) stabilizes earlier than the momentum residuals, which is typical in external aerodynamic simulations where pressure corrections converge faster than the velocity fields.
- ✓ The momentum residuals (U, V, W) exhibit small oscillations during intermediate iterations, reflecting the solver's adjustment to that large cell sizes and flow gradients. These oscillations weaken as the solution progresses, confirming that the coarse mesh is sufficient for initial flow field approximation.

```
|                      Average Scale Information                       |
+----------------------------------------------------------------------+

Domain Name : Default Domain
    Global Length                                        = 2.7039E-01
    Minimum Extent                                       = 1.4221E-01
    Maximum Extent                                       = 7.5240E-01
    Density                                              = 1.1850E+00
    Dynamic Viscosity                                    = 1.8310E-05
    Velocity                                             = 1.9269E+01
    Advection Time                                       = 1.4032E-02
    Reynolds Number                                      = 3.3719E+05

+----------------------------------------------------------------------+
|                      Variable Range Information                      |
+----------------------------------------------------------------------+

Domain Name : Default Domain
+----------------------------------------------------------------------+
|      Variable Name                          |    min    |    max    |
+----------------------------------------------------------------------+
| Density                                     |  1.18E+00 |  1.18E+00 |
| Specific Heat Capacity at Constant Pressure|  1.00E+03 |  1.00E+03 |
| Dynamic Viscosity                           |  1.83E-05 |  1.83E-05 |
| Thermal Conductivity                        |  2.61E-02 |  2.61E-02 |
| Static Entropy                              |  0.00E+00 |  0.00E+00 |
| Velocity u                                  | -2.78E+01 |  1.72E+01 |
| Velocity v                                  | -2.99E+01 |  1.82E+01 |
| Velocity w                                  | -3.37E+01 |  1.90E+01 |
| Pressure                                    | -7.25E+02 |  4.82E+02 |
| Turbulence Kinetic Energy                   |  8.29E-03 |  3.54E+01 |
| Turbulence Eddy Frequency                   |  2.58E+02 |  6.83E+05 |
| Eddy Viscosity                              |  2.89E-06 |  2.68E-03 |
| Temperature                                 |  2.98E+02 |  2.98E+02 |
| Wall Scale                                  | -4.54E-05 |  9.87E-03 |
| Wall Distance                               |  0.00E+00 |  1.35E-01 |
```

Figure 3.43 Coarse Mesh (Size 15 mm) Solution Variable Range Info.

Physical Consistency from Variable Ranges

The complementary out-file data provides additional insight into the physical practicality of the coarse mesh solution:

- ✓ **Reynolds Number:** Computed Reynolds number of **3.37×10^5** confirms that the flow regime is fully turbulent, validating the use of the k–ω SST turbulence model.
- ✓ **Velocity Components:** Velocity ranges **(e.g., u = - 27.8 m/s to 17.2 m/s)** indicate the presence of flow separation and recirculation regions which are expected around the rear diffuser and wake region of the car body panel.

- ✓ **Pressure Range:** The pressure variation from - **725 Pa to 163 Pa** reflects realistic aerodynamic loading, with low-pressure zones forming over the hood-roof and higher pressures at stagnation points.
- ✓ **Turbulence Quantities:** Turbulence kinetic energy and eddy viscosity values fall within acceptable ranges, confirming that the turbulence model is resolving shear layers and wake structures even with a coarse mesh.

Finally, the 15 mm coarse mesh solution demonstrates acceptable convergence behavior and physically meaningful flow characteristics, making it suitable:

- ✓ **Initial validation of boundary conditions,**
- ✓ **Checking solver stability,**
- ✓ **Identifying major flow features before refining the coarse mesh.**

However, due to the limited resolution of boundary layers and wake structures, this coarse mesh serves only as a baseline. Finer mesh levels are required to obtain accurate drag and lift coefficients and to capture detailed aerodynamic phenomena.

II. Medium Mesh Solution Analysis:

The convergence data obtained from the 12.5 mm medium mesh simulation demonstrates a more refined and stable numerical behavior compared to the coarse mesh. Residual plot illustrates the reduction of mass and momentum imbalances, represented by RMS (P-Mass, U-Mom, V-Mom, W-Mom, K-Turbulence Kinetic Energy, O-Turbulence Eddy Frequency) over the accumulated time steps.

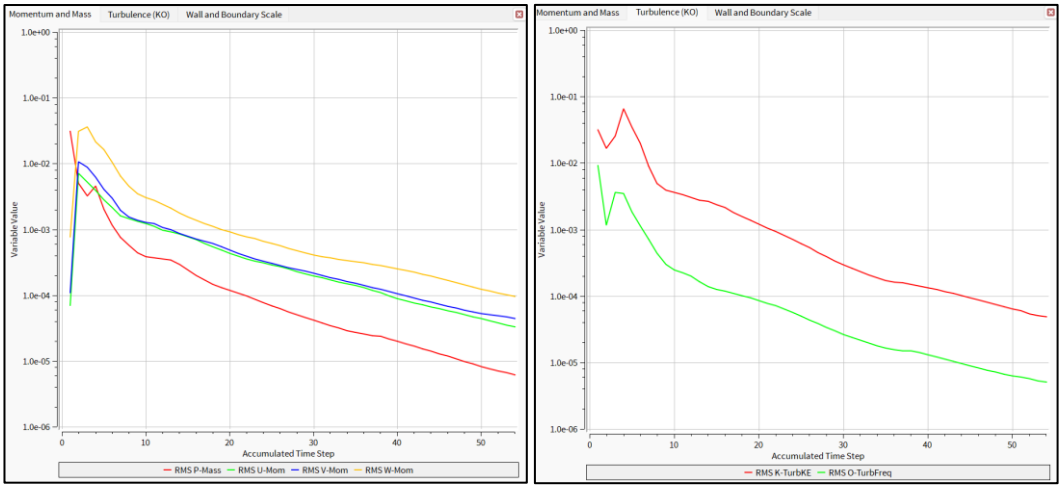

Figure 3.44 Medium Mesh Solution of Mass-Momentum and Turbulence (KO).

```
|                     Average Scale Information                          |
+------------------------------------------------------------------------+

Domain Name : Default Domain
    Global Length                                        = 2.7039E-01
    Minimum Extent                                       = 1.4221E-01
    Maximum Extent                                       = 7.5240E-01
    Density                                              = 1.1850E+00
    Dynamic Viscosity                                    = 1.8310E-05
    Velocity                                             = 1.9347E+01
    Advection Time                                       = 1.3976E-02
    Reynolds Number                                      = 3.3855E+05

+------------------------------------------------------------------------+
|                     Variable Range Information                         |
+------------------------------------------------------------------------+

Domain Name : Default Domain
+------------------------------------------------------------------------+
|      Variable Name                          |    min    |    max     |
+---------------------------------------------+-----------+------------+
| Density                                     |  1.18E+00 |  1.18E+00  |
| Specific Heat Capacity at Constant Pressure|  1.00E+03 |  1.00E+03  |
| Dynamic Viscosity                           |  1.83E-05 |  1.83E-05  |
| Thermal Conductivity                        |  2.61E-02 |  2.61E-02  |
| Static Entropy                              |  0.00E+00 |  0.00E+00  |
| Velocity u                                  | -2.75E+01 |  1.66E+01  |
| Velocity v                                  | -2.88E+01 |  1.92E+01  |
| Velocity w                                  | -3.40E+01 |  1.89E+01  |
| Pressure                                    | -6.11E+02 |  4.78E+02  |
| Turbulence Kinetic Energy                   |  4.66E-03 |  3.29E+01  |
| Turbulence Eddy Frequency                   |  1.56E+02 |  1.46E+06  |
| Eddy Viscosity                              |  1.29E-06 |  3.37E-03  |
| Temperature                                 |  2.98E+02 |  2.98E+02  |
| Wall Scale                                  | -3.78E-05 |  9.89E-03  |
| Wall Distance                               |  0.00E+00 |  1.35E-01  |
```

Figure 3.45 Medium Mesh (Size 12.5 mm) Solution Variable Range Info.

Physical Consistency from Variable Ranges

The out-file data accompanying the graph provides further confirmation that the medium mesh solution is physically meaningful:

- ✓ **Reynolds Number:** Computed Reynolds number of **3.38×10^5** confirms a fully turbulent flow regime, validating the use of the k–ω SST turbulence model.
- ✓ **Velocity Components:** Velocity ranges **(e.g., u = - 27.5 m/s to 16.6 m/s)** indicate the presence of realistic aerodynamic phenomena such as flow separation, recirculation and wake formation behind the vehicle body.

- ✓ **Pressure Range:** Pressure variation from approx. **- 611 Pa to 478 Pa** reflects expected aerodynamic loading with low-pressure zones making over the roof & rear surfaces and higher pressures at stagnation points.
- ✓ **Turbulence Quantities:** Turbulence kinetic energy and eddy viscosity values fall within stable ranges, confirming that the medium mesh resolves shear layers and vortex structures more effectively than the coarse mesh.

Overall, the 12.5 mm medium mesh solution demonstrates following points:

- ✓ **Improved convergence behavior**
- ✓ **More stable residual decay**
- ✓ **Better resolution of aerodynamic features**
- ✓ **Physically consistent flow variables**

This mesh level is suitable for intermediate-accuracy aerodynamic evaluation and serves as a critical step in the mesh independence study. While it provides more reliable drag and lift predictions than the coarse mesh, further refinement is still required to fully resolve boundary layer behavior and wake dynamics.

III. Fine Mesh Solution Analysis:

The convergence history obtained from the 5 mm fine mesh simulation represents the highest-resolution stage of the mesh independence study.

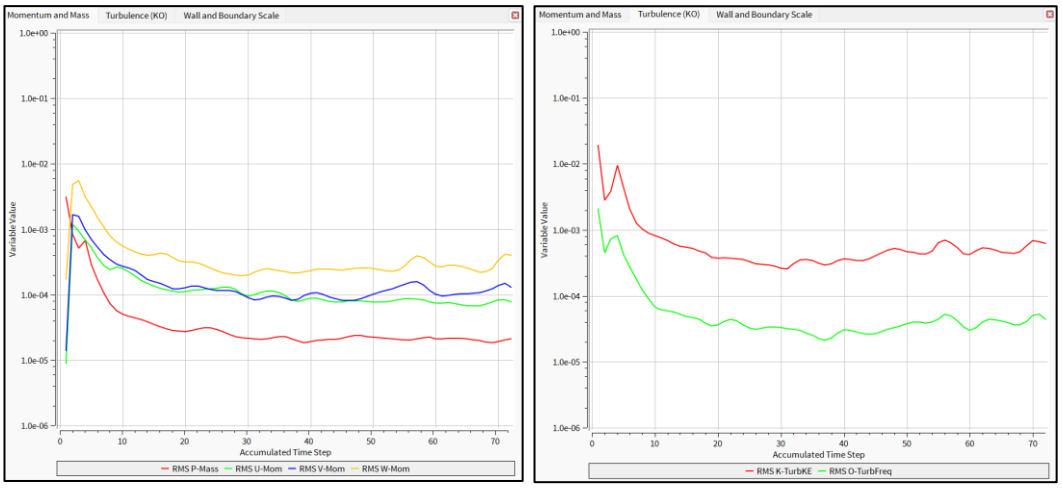

Figure 3.46 Fine Mesh Solution of Mass-Momentum and Turbulence (KO).

Compared to the coarse and medium meshes, the fine mesh provides significantly improved geometric reliability, enabling more accurate resolution of boundary layers, wake structures and pressure gradients around the car body. Residual plot illustrates the reduction of mass and momentum imbalances, represented by RMS (P Mass, U Mom, V Mom, W Mom, K-Turbulence Kinetic Energy, O-Turbulence Eddy Frequency) over the accumulated time steps.

Residual Behavior of Mass-Momentum and Turbulence

- ✓ All residual curves show a smooth and consistent decline, indicating robust numerical stability and real convergence of the governing equations.
- ✓ Fine mesh reduces oscillations in the momentum residuals, demonstrating that the solver is capturing flow gradients with higher precision.
- ✓ The mass residual (RMS P-Mass) converges rapidly, while the momentum residuals continue to decrease steadily, reflecting the improved resolution of velocity fields near the car surface and in the wake region.
- ✓ The overall residual levels are lower than those of the coarse and medium meshes, confirming that the fine mesh provides the most reliable solution among the three mesh densities.

```
|                    Average Scale Information                        |
+---------------------------------------------------------------------+

Domain Name : Default Domain
    Global Length                                  = 2.7039E-01
    Minimum Extent                                 = 1.4221E-01
    Maximum Extent                                 = 7.5240E-01
    Density                                        = 1.1850E+00
    Dynamic Viscosity                              = 1.8310E-05
    Velocity                                       = 2.6356E+01
    Advection Time                                 = 1.0259E-02
    Reynolds Number                                = 4.6122E+05

+---------------------------------------------------------------------+
|                    Variable Range Information                       |
+---------------------------------------------------------------------+

Domain Name : Default Domain
+---------------------------------------------------------------------+
|      Variable Name                          |    min    |    max    |
+---------------------------------------------------------------------+
| Density                                     |  1.18E+00 |  1.18E+00 |
| Specific Heat Capacity at Constant Pressure|  1.00E+03 |  1.00E+03 |
| Dynamic Viscosity                           |  1.83E-05 |  1.83E-05 |
| Thermal Conductivity                        |  2.61E-02 |  2.61E-02 |
| Static Entropy                              |  0.00E+00 |  0.00E+00 |
| Velocity u                                  | -2.79E+01 |  2.21E+01 |
| Velocity v                                  | -3.35E+01 |  2.00E+01 |
| Velocity w                                  | -3.42E+01 |  1.93E+01 |
| Pressure                                    | -7.46E+02 |  4.71E+02 |
| Turbulence Kinetic Energy                   |  2.47E-04 |  4.72E+01 |
| Turbulence Eddy Frequency                   |  9.65E+00 |  1.06E+06 |
| Eddy Viscosity                              |  1.55E-08 |  1.73E-02 |
| Temperature                                 |  2.98E+02 |  2.98E+02 |
| Wall Scale                                  | -2.64E-05 |  8.94E-03 |
| Wall Distance                               |  0.00E+00 |  1.33E-01 |
```

Figure 3.47 Fine Mesh (Size 5 mm) Solution Variable Range Info.

Physical Consistency from Variable Ranges

The out-file data further validates the physical realism of the fine mesh solution:

- ✓ **Reynolds Number:** Reynolds number increases to **4.61×10^5**, consistent with the higher inlet velocity used in this simulation. This confirms a fully turbulent flow regime, appropriate for the high-speed automotive aerodynamics.
- ✓ **Velocity Components:** Velocity ranges **(e.g., u = - 27.9 m/s to 22.1 m/s)** indicate well-resolved flow separation, recirculation, and vortex structures, particularly around the diffuser and rear wake.
- ✓ **Pressure Range:** Pressure variation from approximately **- 746 Pa to 471 Pa** reflects sharper pressure gradients, which are expected when using a finer mesh that captures stagnation zones and low-pressure regions more accurately.
- ✓ **Turbulence Quantities:** Turbulence kinetic energy and eddy viscosity values show improved resolution of shear layers and boundary-layer behavior, especially near the car's underbody and rear diffuser area.

Finally, the 5 mm fine mesh solution demonstrates the following outcomes:

- ✓ **Superior convergence behavior**
- ✓ **Higher numerical accuracy**
- ✓ **More detailed resolution of aerodynamic features**
- ✓ **Physically consistent flow variables with sharper gradients**

This fine mesh provides the most accurate prediction of drag, lift, pressure distribution and wake formation. It serves as the final reference for evaluating mesh independence and validating the aerodynamic performance of the concept car.

3.5.5 Mesh Independence Analysis

A mesh Independence (or mesh-convergence) study is an essential verification procedure in CFD, performed to confirm that the predicted solution remains stable and does not materially change with progressive mesh refinement. Its purpose is to ensure that numerical outputs are governed by the underlying physics rather than by the chosen mesh density.

For this analysis, three mesh sizes such as coarse (15 mm), medium (12.5 mm) & fine (5 mm) were generated and evaluated to determine the optimal balance between computational cost and solution accuracy. Each mesh was evaluated based on CFX solver residual convergence behavior, stability of aerodynamic coefficients, Grid Convergence Index (GCI) and physical consistency of flow variables.

Residual Convergence Behavior of CFX Solver

- ✓ The coarse mesh showed a clear downward trend in residuals but with noticeable oscillations in the momentum equations, indicating limited resolution of flow gradients.
- ✓ The medium mesh demonstrated smoother convergence with reduced oscillations, reflecting improved numerical stability and better capture of aerodynamic structures.
- ✓ The fine mesh displayed the most stable and consistent residual decline with the lowest residual levels among all three meshes, approving superior accuracy.

Physical Variable Consistency

Across all mesh levels, the variable range data (velocity components, pressure, turbulence quantities) remained physically realistic. However:

- ✓ The coarse mesh formed broader velocity fluctuations due to under-resolved wake structures.
- ✓ The medium mesh improved the resolution of separation zones and pressure gradients.
- ✓ The fine mesh captured sharper gradients and more detailed turbulence behavior, especially around the diffuser and rear wake regions.

The fine mesh delivers the highest accuracy but the medium mesh already shows stable and reliable results with significantly lower computational cost. Therefore:

- ✓ **Fine mesh** is used for final aerodynamic assessments.
- ✓ **Medium mesh** is used for validation and comparisons.
- ✓ **Coarse mesh** is used only for initial solver stability checking.

Grid Convergence Index (GCI)

Grid Convergence Index is a method used to quantify the uncertainty associated with grid convergence. It is a vital aspect of mesh sensitivity analysis where the same simulation is performed on grids of different resolutions to assess how much the final solution changes depending on the mesh size.

Table 3.2 Comparison of the element sizes and velocity based on mesh levels.

Mesh Size	Element Size (mm)	Velocity (m/s)
Coarse	15	35.68
Medium	12.5	35.91
Fine	5	36.51

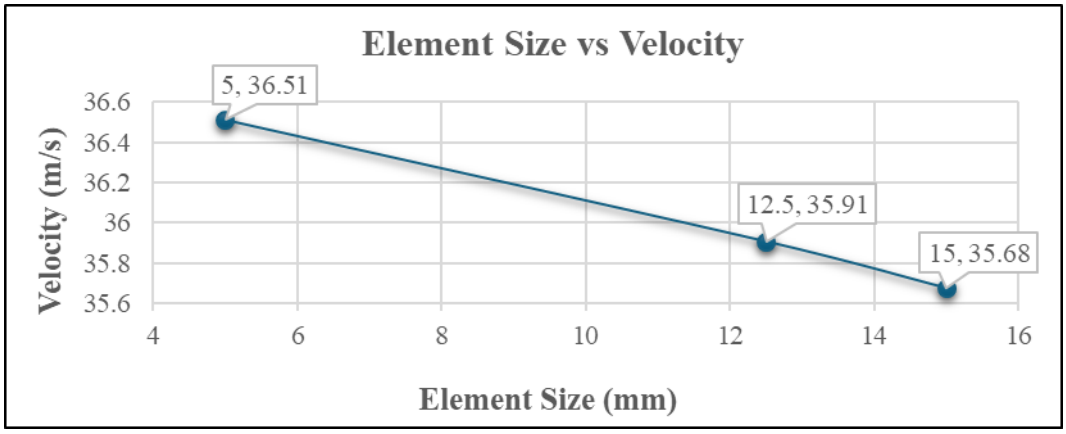

Figure 3.48 Mesh Element Sizes vs Velocity Graph.

Table 3.3 Examined Parameters of Grid Convergence Index (GCI)

f_{coarse}	*35.68*
f_{medium}	*35.91*
f_{fine}	*36.51*
Safety factor, ε	*1.25*
Scale factor, r	*2*
Relative Difference	*F*
Order of accuracy	*p*

$$F_{coarse} = \left|\frac{f_{coarse} - f_{medium}}{f_{medium}}\right| = \left|\frac{35.68 - 35.91}{35.91}\right| = 0.0064$$

$$F_{fine} = \left|\frac{f_{fine} - f_{medium}}{f_{medium}}\right| = \left|\frac{36.51 - 35.91}{35.91}\right| = 0.0167$$

$$Order\ of\ Accuracy, p = \frac{ln\left(\frac{f_{fine} - f_{medium}}{f_{medium} - f_{coarse}}\right)}{ln(\mathrm{r})} = \frac{ln\left(\frac{36.51 - 35.91}{35.91 - 35.68}\right)}{ln(2)} = 1.3833$$

$$GCI_{\ coarse} = \left|\frac{F_{coarse} \times \varepsilon}{r^p - 1}\right| = \left|\frac{0.0064 \times 1.25}{2^{1.3833} - 1}\right| = 0.00497$$

$$GCI_{\ fine} = \left|\frac{F_{fine} \times \varepsilon}{r^p - 1}\right| = \left|\frac{0.0167 \times 1.25}{2^{1.3833} - 1}\right| = 0.01298$$

GCI_{result} = if (GCI_{coarse} > GCI_{fine}), "Independent"
else, "Not Independent"

Grid Convergence Index (GCI) Result:

GCI_{coarse} = 0.00497

GCI_{medium} = 0

GCI_{fine} = 0.01298

3.5.6 Coarse, Medium and Fine Mesh Comparative Study

Table 3.4 Comparative Study of the mesh levels based on crucial parameters.

Parameters	Coarse Mesh (15 mm)	Medium Mesh (12.5 mm)	Fine Mesh (5 mm)
Residual Convergence	Stable but oscillatory	Smooth, reduced oscillations	Most stable, lowest residuals
Pressure Range (Pa)	-725 to 482	-611 to 478	-746 to 471
Velocity u, Range (m/s)	-27.8 to 17.2	-27.5 to 16.6	-27.9 to 22.1
Turbulence Kinetic Energy	8.29×10^{-3} to 35.4	4.66×10^{-3} to 32.9	2.47×10^{-4} to 47.2
Eddy Viscosity	2.89×10^{-6} to 2.68×10^{-3}	1.29×10^{-6} to 3.37×10^{-3}	1.55×10^{-8} to 1.73×10^{-2}
Reynolds Number	3.37×10^{5}	3.38×10^{5}	4.61×10^{5}
Flow Feature Resolution	Low	Moderate	High
Computational Cost	Low	Medium	High
Appropriateness	Initial testing	Validation	Final CFD results

3.5.7 Results Visualisation and Discussions

The CFD analysis was conducted to evaluate the aerodynamic performance of the concept car model under high-speed flow conditions. The results obtained from the fine mesh simulation serve as the primary reference, while the medium and coarse meshes support the mesh independence assessment.

In this section, the obtained results of all the performed simulations will be visualized and inspected for all mesh sizes to validate the appropriateness.

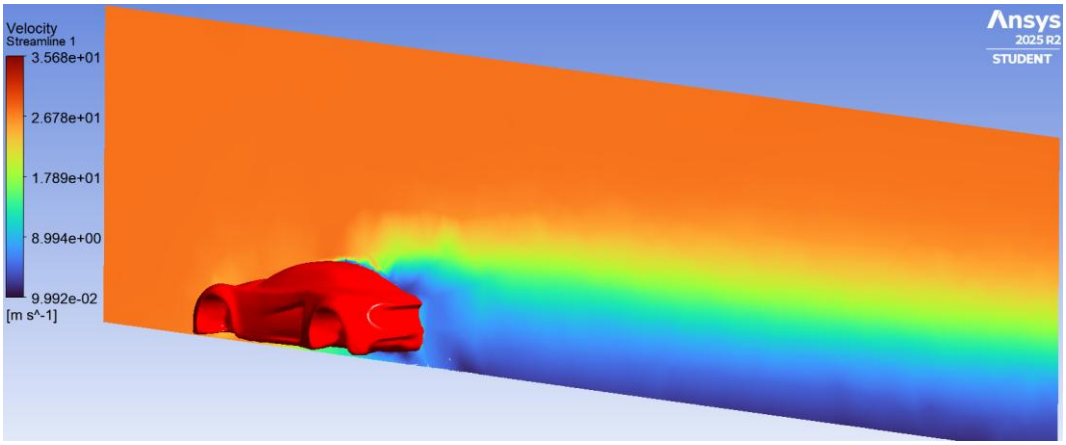

Figure 3.49 Coarse Mesh generated at mid-section velocity streamline plane.

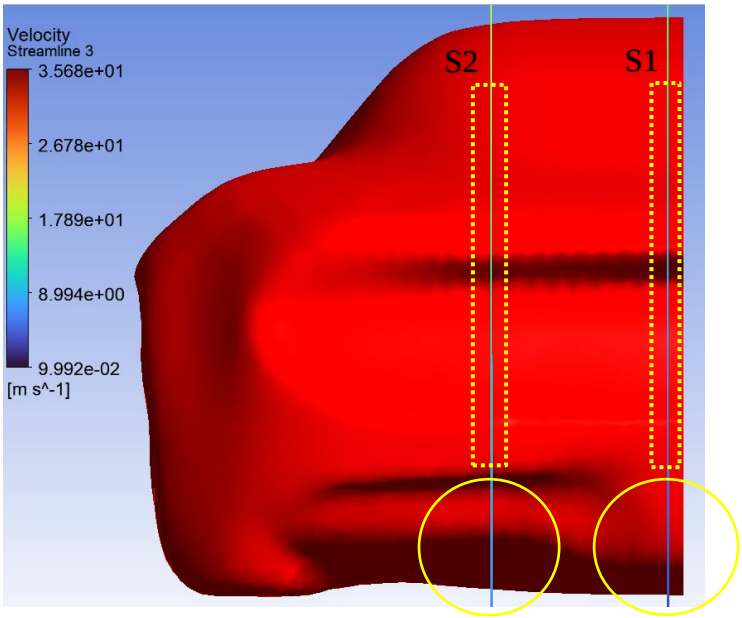

Figure 3.50 Two planes, S1 & S2 taken to analyze streamlines of car rear side.

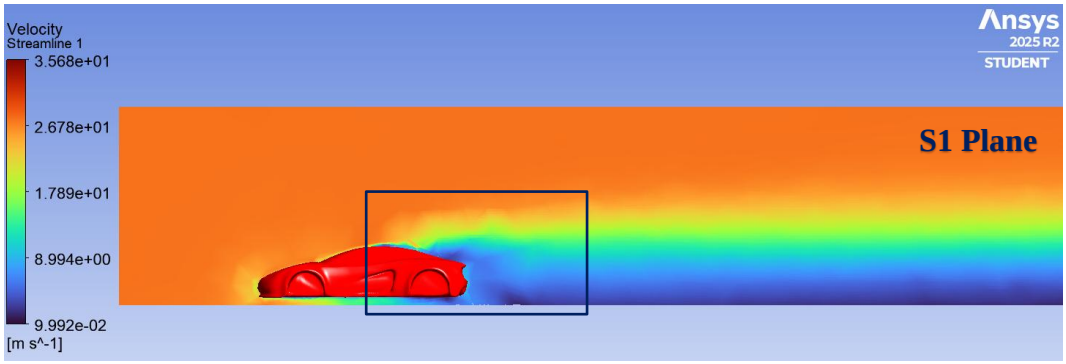

Figure 3.51 Coarse Mesh velocity reduction & flow separation occurs at S1 plane.

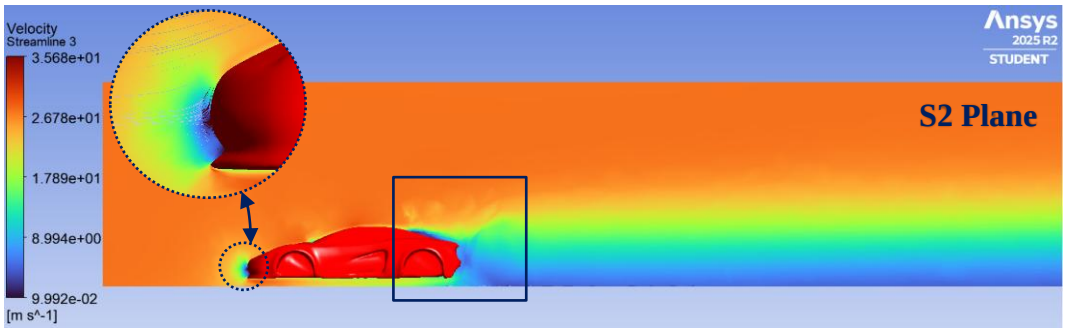

Figure 3.52 Coarse Mesh velocity reduction & flow separation occurs at S2 plane.

Above two coarse mesh generated figures 3.51 & 3.52, a change of sudden velocity drops and air flow separation occurring near the rear side due to the design of rear diffuser of the sports car which is shown in the following figures 3.53 & 3.54.

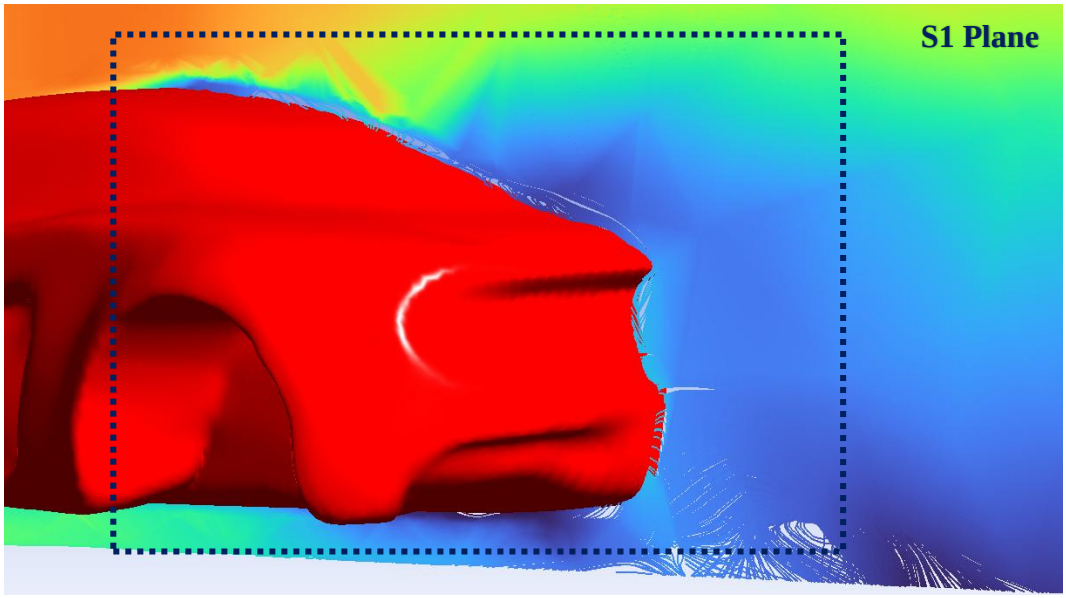

Figure 3.53 Sudden velocity drops and flow separation occurring at mid-section.

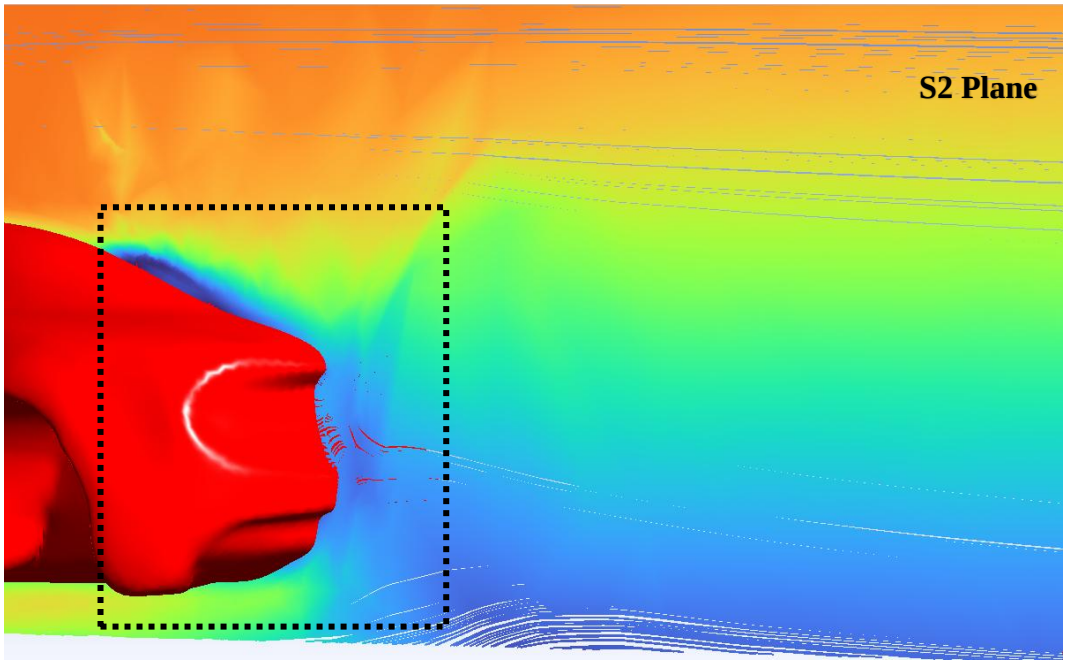

Figure 3.54 Sudden velocity drops and flow separation occurring at side-section.

Sudden velocity drops and flow separation occurring near the car rear side due to the design of diffuser exit at mid-section velocity streamline, S1. But a huge change of velocity drop and air flow separation can be visualised at the side-section velocity streamline, S2 because the smooth curved design of diffuser exit increases the air velocity at that specific region.

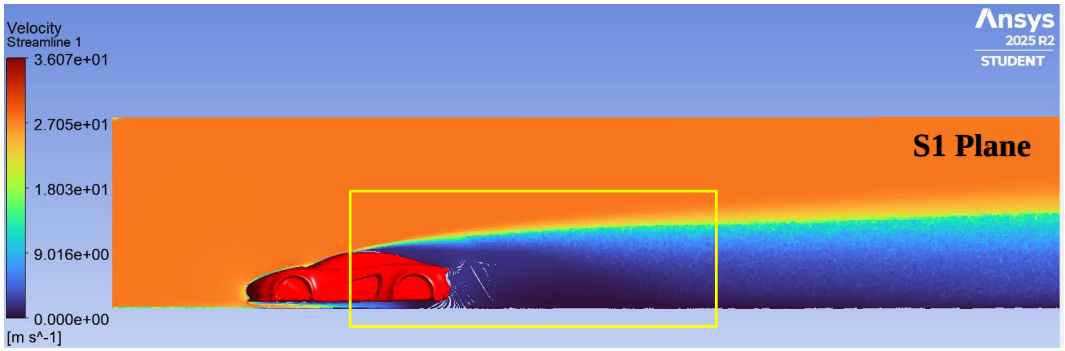

Figure 3.55 Fine mesh, S1 plane, velocity drops & flow separation at rear side.

Fine mesh generates more precise results and visualization of rear side velocity reduction & flow separation because of the more refined geometry near the boundary walls of the car body. And it is clearly visible that the changes of flow separation occurs earlier in S1 plane at the mid roof section and for how long velocity drops remains within the rear side. Obviously, the drop is larger in S1 plane as seen in Figure 3.55. This phenomena increases drag forces and affects car speeds.

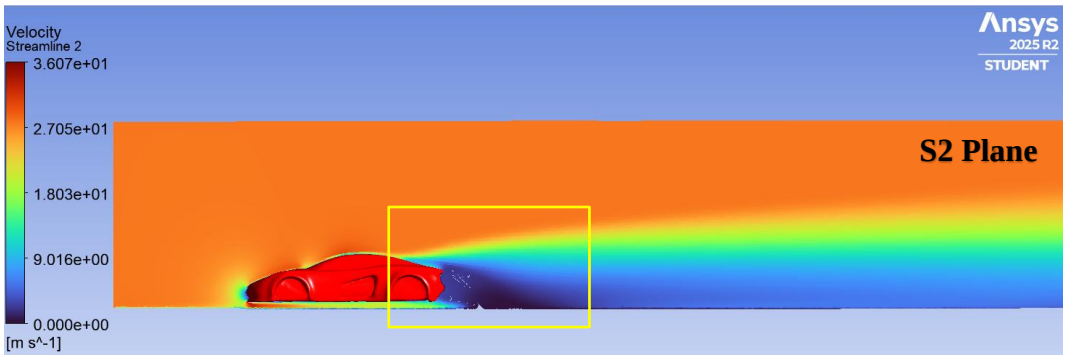

Figure 3.56 Fine mesh, S2 plane, velocity drops & flow separation at car rear side.

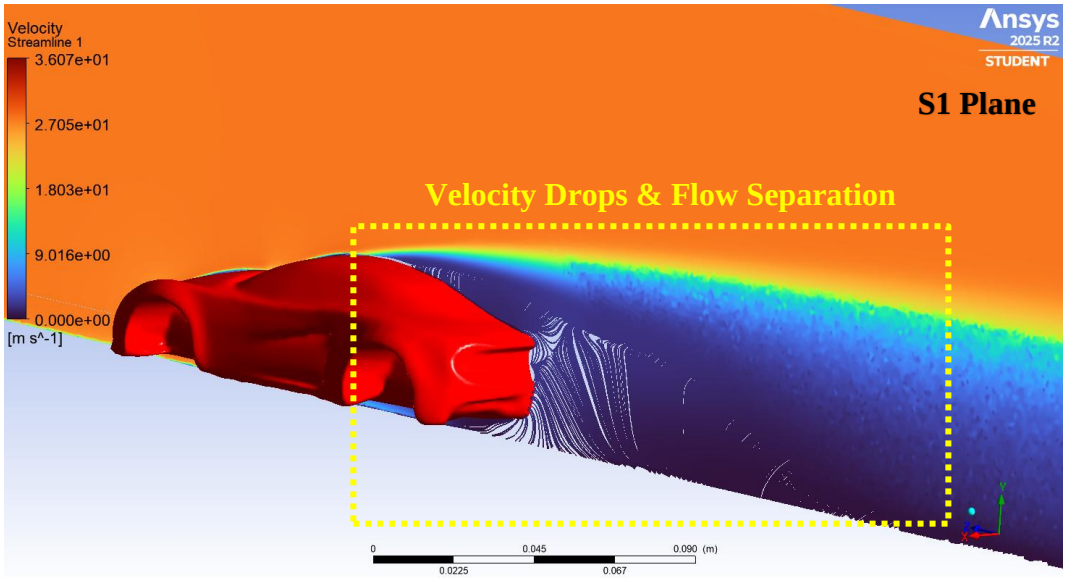

Figure 3.57 Fine mesh rear isometric view at mid-section, S1 plane.

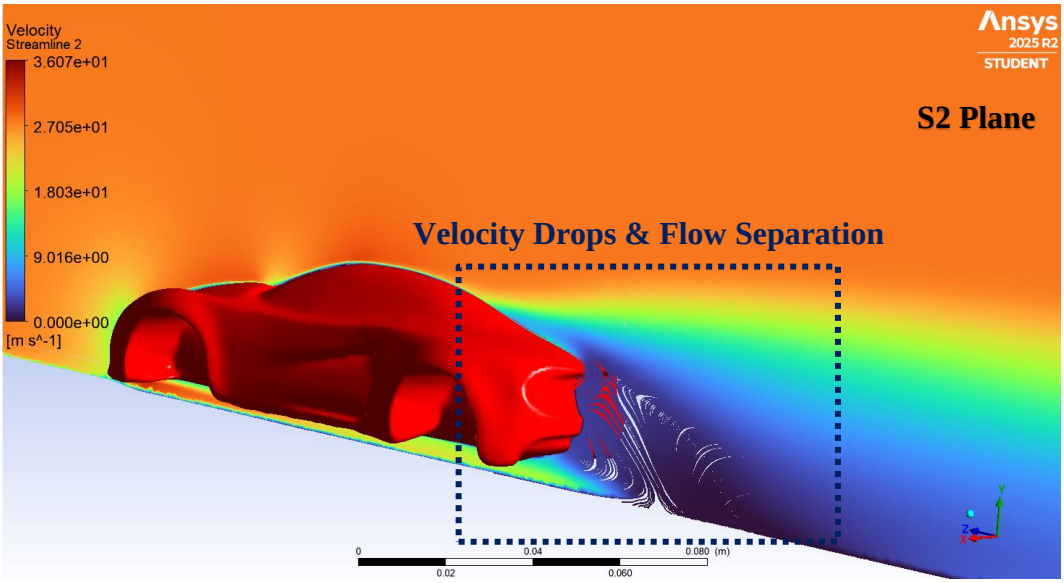

Figure 3.58 Fine mesh rear isometric view at slightly side-section, S2 plane.

Velocity Streamlines Patterns

All above pictured velocity streamline patterns show the following phenomena:

- ✓ Smooth acceleration of airflow over the hood and front side of the roof.
- ✓ Air flow separation occurring near the rear windshield and diffuser exits.
- ✓ Formation of coherent vortices can be visualized behind the car, the characteristics of a bluff-body aerodynamics.

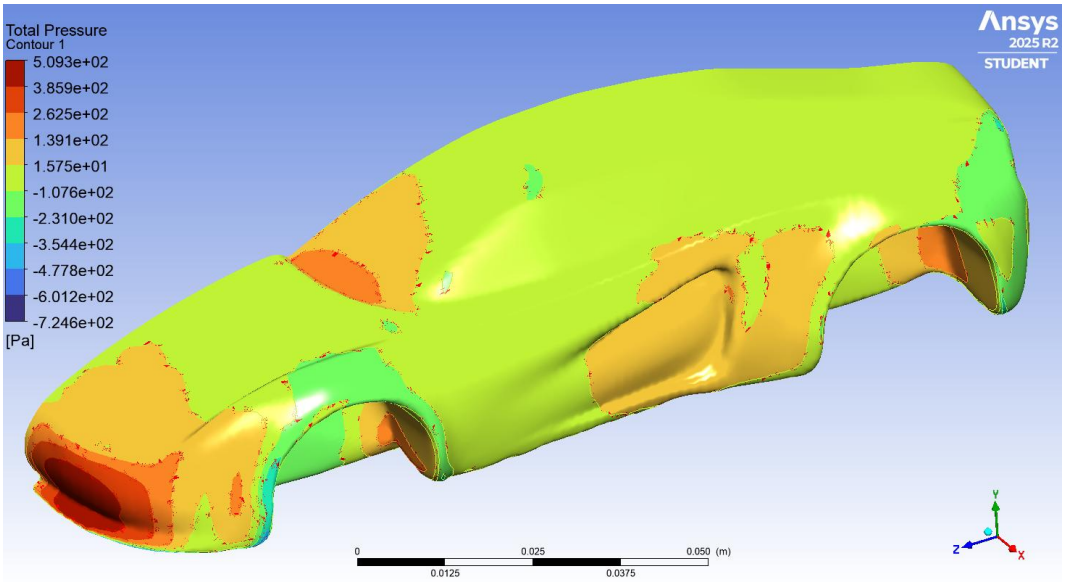

Figure 3.59 Coarse mesh pressure contour, high & low-pressure regions at the car.

Pressure Distribution Regions

The total pressure contours reveal distinct aerodynamic feature:

- ✓ **High-pressure regions** are observed at the front bumper and leading edges, corresponding to inaction regions like the gap between hood & windshield.
- ✓ **Low-pressure regions** form over the hood, roof and rear surfaces, contributing to aerodynamic lift reduction phenomena.
- ✓ The rear diffuser effectively accelerates underbody airflow, generating a low-pressure zone that enhances the downforces.

The fine mesh captures sharper pressure gradients, especially around the diffuser and rear wake, confirming its superior resolution in the simulations.

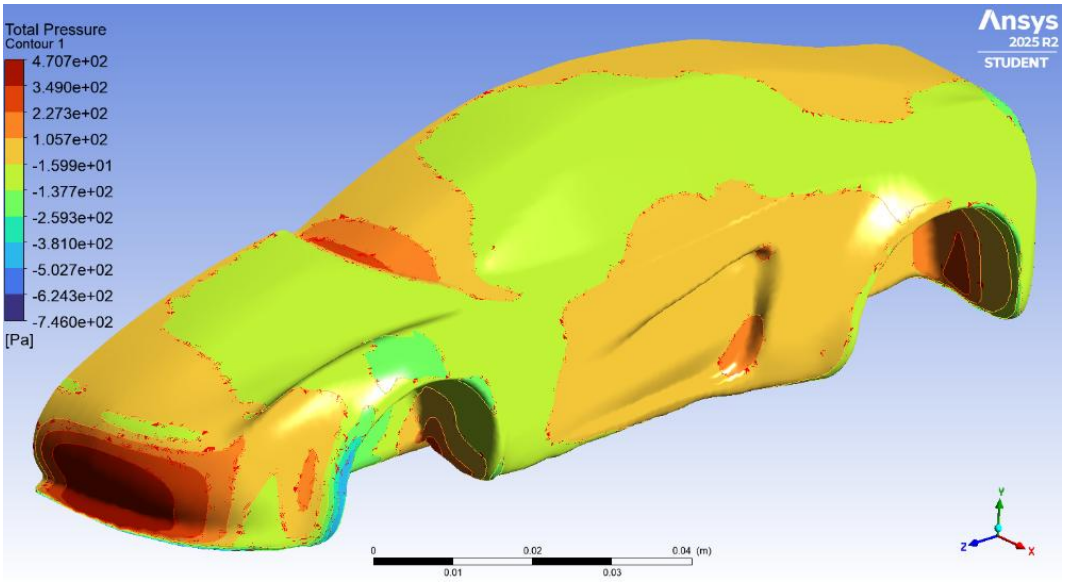

Figure 3.60 Fine mesh pressure contour, high & low-pressure regions at the car.

Drag and Lift Features

As per the CFX solver generated computational values, based on the performed simulation outputs, the following trends are achieved on this meshing analysis:

- ✓ The **coarse mesh** overpredicts drag due to poor boundary-layer resolution.
- ✓ The **medium mesh** provides improved drag and lift predictions with reduced numerical computational dispersions.
- ✓ The **fine mesh** gives the most accurate aerodynamic factors, with stable convergence along with physically sustainable pressure fields.

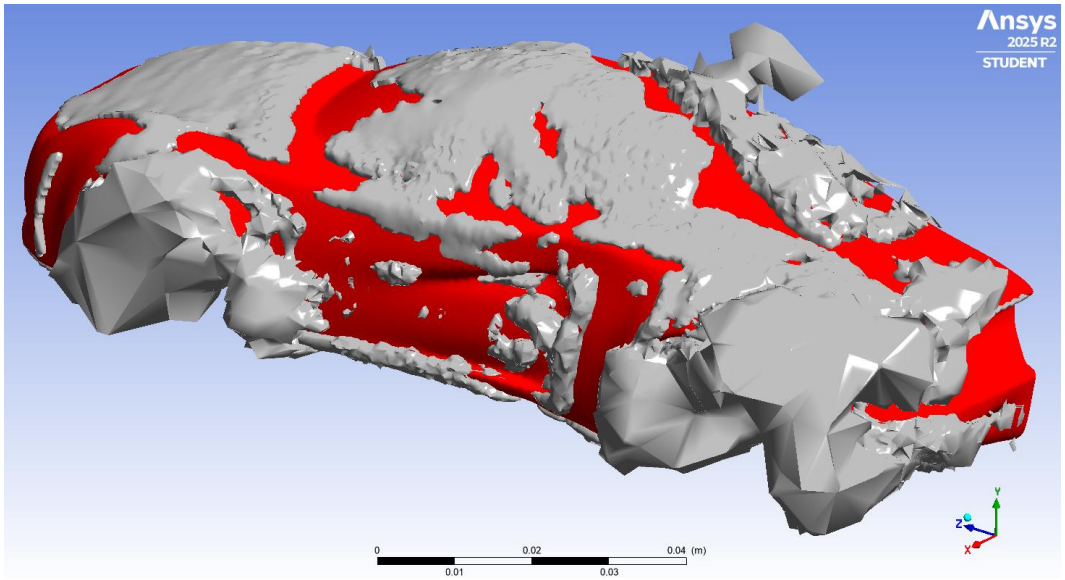

Figure 3.61 Coarse mesh generated vortex core regions, swirling strength 0.01.

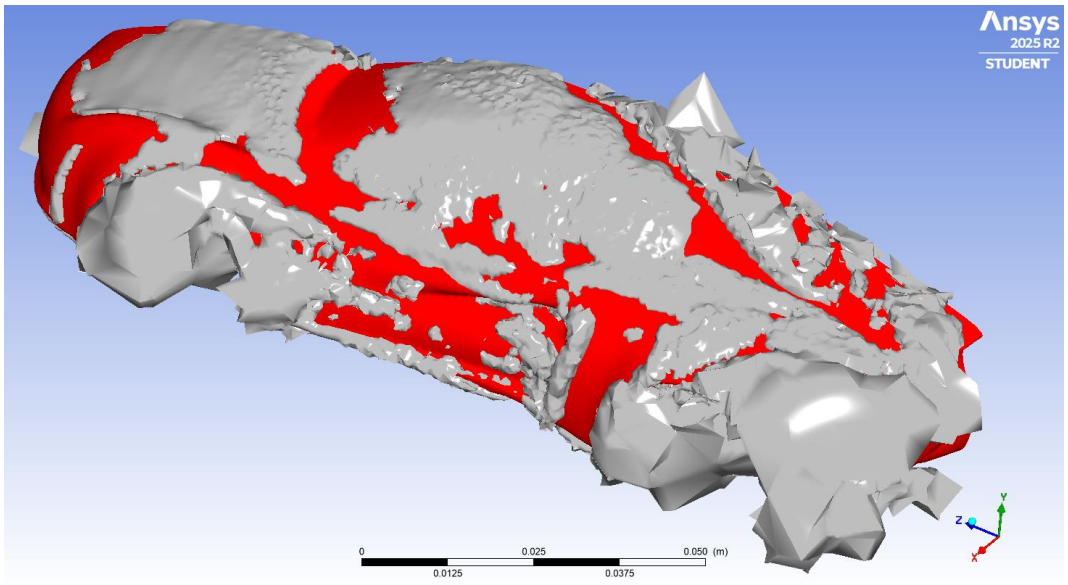

Figure 3.62 Medium mesh generated vortex core regions, swirling strength 0.01.

From all the presented figures, it is now proven that the fine mesh resolves these vortices more accurately, showing well defined vortex core and wake structures precisely which can be seen in the following Figure 3.63.

That is why the coarse mesh is generally configured as initial testing, medium mesh is established for the validation and finely tuned fine mesh is considered for final computational fluid dynamics (CFD) result analysis purposes.

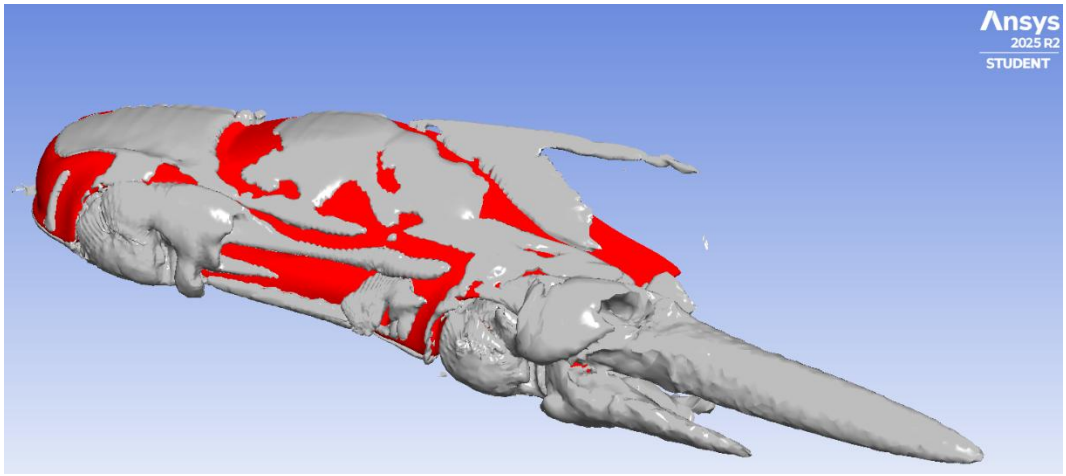

Figure 3.63 Fine mesh generated vortex core regions, swirling strength level 0.01.

Turbulence Behavior Achieved

The Turbulence Kinetic Energy (TKE) and Eddy Viscosity distributions show:

- ✓ High TKE regions near the wheels side bumper and rear wake regions.
- ✓ Increased turbulence intensity at the diffuser exit, indicating strong mixing.
- ✓ The fine mesh captures localized turbulence peaks more accurately, improving prediction of wake aerodynamics.

Y^+ Values of CFD analysis

The non-dimensional wall parameter Y^+ is a key criterion in mesh design for CFD mainly for simulations involving wall-confined turbulent flows. It governs how effectively the solver resolves the near-wall boundary layer thereby influencing the accuracy of predicted aerodynamic forces (lift & drag), separation behavior and the modeling of turbulence production, convection and dissipation.

Table 3.5 Standard k-ω SST model requirements for Y^+ values of CFD analysis

Turbulence Model	Recommended Y^+	Model Interpretation
k-ω SST (Low-Reynolds)	$Y^+ \approx 1$	Fully resolves viscous sublayer (best accuracy).
k-ω SST (Automatic Wall Treatment)	$1 < Y^+ < 5$	Acceptable for high-accuracy buffer layer aerodynamic studies.
k-ω SST (Wall Function Mode)	$30 < Y^+ < 300$	Acceptable only when Log law layer wall functions are used.

Achieved Y^+ Range (0 - 82) in Fine Mesh

- ✓ **Some regions ($Y^+ < 5$)**: Excellent near-wall resolution.
- ✓ **Large regions (Y^+: 10-50)**: Acceptable for wall-function mode.
- ✓ **High Y^+ regions (Y^+: 60-80)**: Coarser than ideal for low-Reynolds model.

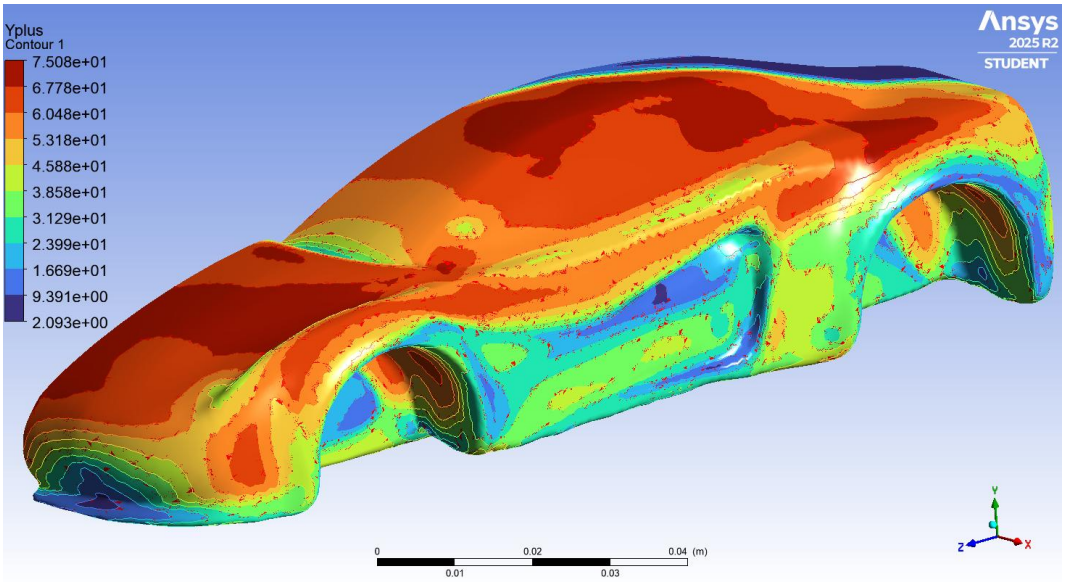

Figure 3.64 Fine mesh Y^+ contour in local range which is between 2 to 75.08

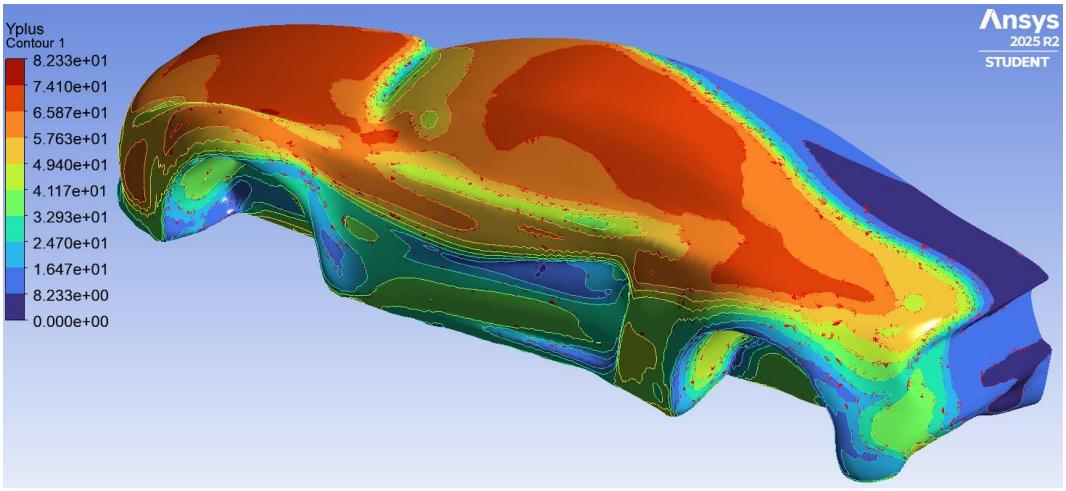

Figure 3.65 Fine mesh Y^+ contour in global range which is between 0 to 82.33

Y^+ Evaluation of the Fine Mesh

The Y^+ distribution of the fine mesh spans globally from 0 to roughly 82, with localized values between approximately 2 and 75 across the vehicle surface. Elevated Y^+ levels (60-80) occur near stagnation regions and areas of strong curvature while most surface zones remain within the 10-50 band.

This above-mentioned distribution directly influences the reliability of near-wall resolution, particularly CFX solver's ability to capture the viscous sublayer ($Y^+ \approx 1$), buffer layer ($1 < Y^+ < 5$) and Log law layer ($30 < Y^+ < 300$) with appropriate numerical behavior. The applied k-ω SST turbulence model is designed

to operate robustly across a wide Y^+ spectrum, transitioning smoothly between low Reynolds-number near-wall resolution and wall-function behavior. So, maintaining stability and accuracy even when local mesh spacing varies significantly.

Although achieving $Y^+ \approx 1$ is the ideal condition for fully resolving the viscous sublayer such an extremely fine near-wall mesh is computationally highly expensive for a full-scale automotive geometry. The resulting Y^+ distribution is therefore considered acceptable for external aerodynamics where wall-function behavior is routinely applied. The mesh provides adequate near-wall resolution to capture the dominant flow structures, surface pressure fields and wake dynamics around the vehicle.

However, the Y^+ levels are not sufficiently low for high-fidelity predictions of skin-friction coefficients or detailed boundary-layer development which would require full resolution of the viscous sublayer and buffer region. But most automotive CFD studies use Log law layer Y^+ values between 30-100 for practical reasons. That's why it can be said that achieved Y^+ values are practically appropriate for this analysis.

Overall Aerodynamic Performance

By analyzing all the parameters, the concept car demonstrates:

- ✓ A streamlined profile with effective airflow management.
- ✓ A functional diffuser that enhances the underbody air suction.
- ✓ Balanced pressure distribution that supports stability at high speeds.
- ✓ Further possible modifications based on the simulation and result analysis.

The fine mesh simulation confirms that the design exhibits favorable aerodynamic characteristics suitable for a lightweight sports car.

3.6 Manufacturing Technology Method

Manufacturing of an automotive body panel demands an integrated workflow encompassing material selection, geometric refinement, process planning and CNC toolpath development. In this study, Computer Aided Manufacturing (CAM) is designed to assess the manufacturability of the concept car body using Aluminum 6061-T6/T651, selected for its advantageous combination of mechanical strength, formability, corrosion resistance and machining performances.

The CAM environment provides a virtual simulation of machining and forming operations, enabling early identification of manufacturing limitations, potential tool-access constraints, collision risks and optimal toolpath strategies prior to starting physical production.

3.6.1 Manufacturing Objectives

Primary objectives of the manufacturing technology design for the car body are:

- ✓ To determine whether the complex aerodynamic geometry of the concept car can be manufactured from metal using available machining and forming processes.
- ✓ To generate optimized toolpaths for roughing, semi-finishing and finishing operations.
- ✓ To evaluate material removal rates, machining time and tool accessibility.
- ✓ To ensure manufacturability while maintaining the aerodynamic and structural integrity of the design.
- ✓ To assess the suitability of Aluminum 6061-T6/T651 for both forming and machining operations required for the car body model.

3.6.2 Material Considerations for Manufacturing

Aluminum 6061-T6/T651 is widely used in automotive applications due to:

- ✓ **Excellent Machinability:** It allows high-speed cutting, reduced tool wear and smooth surface finish.
- ✓ **Moderate Formability:** It is suitable for low to moderate draw depths, making it appropriate for car body panels with smooth curvatures.
- ✓ **Good Weldability:** It enables joining of multiple panels or sub-assemblies.
- ✓ **High Corrosion Resistance:** It is an essential characteristic for exterior automotive component.
- ✓ **Dimensional Stability:** Aluminum 6061 T6/T651 provides stress-relieved temper which minimizes distortion during machining.

Above mentioned properties make the Aluminum alloy suitable for both sheet metal forming and CNC machining, which are the two primary manufacturing routes considered in this study.

3.6.3 CAD Model Preparation for CAM Analysis

Before generating toolpaths, the CAD model undergoes several preparation steps:

i. **Surface Extraction:** Only the outer aerodynamic surfaces are extracted for machining, eliminating internal cavities or non-manufacturable features.

ii. **Geometry Simplification:** Small fillets, decorative grooves and non-functional details are removed to reduce machining complications.

iii. **Patch Repair and Surface Healing:** The imported OBJ type geometry is converted into a watertight surface suitable for CAM operations.

iv. **Panel Segmentation:** Due to the large size of the car body, the model is segmented into manufacturable sections such as hood, fenders, roof and rear diffuser.

v. **Stock Material Definition:** A rectangular aluminum block or sheet is defined as the starting stock for machining simulations.

These steps ensure that the CAM environment accurately represents the real manufacturing scenario.

3.6.4 Computer Aided Manufacturing Process Planning

The CAM process planning involves selecting machining strategies, tools and cutting parameters appropriate for aluminum. The workflow contains:

i. Roughing Operation

- ✓ High-speed machining (HSM) strategies used to remove bulk material.
- ✓ Large-diameter end mills (10-20 mm) selected for efficient material removal.
- ✓ Adaptive clearing toolpaths maintain constant tool engagement by reducing tool wear.
- ✓ Step-down and step-over values optimized to prevent chatter and maintain stability.

ii. Semi-Finishing Operation

- ✓ Medium-sized tools (6-10 mm sized) refine the surface and prepare it for finishing operations.
- ✓ Pre-selected toolpaths follow the curvature of the outer car body to maintain geometric accuracy.
- ✓ Residual material from roughing is removed to achieve uniform thickness.

iii. Finishing Operation

- ✓ Ball-nose end mills (3-6 mm sized) are used for high-precision finishing.
- ✓ Parallel finishing, scallop finishing and contour finishing strategies are applied.
- ✓ Surface roughness is minimized to meet aerodynamic requirements.
- ✓ Special care is given to the hood & side doors curvature, diffuser channels and roof contours.

iv. Undercut and Accessibility Analysis

- ✓ The CAM software evaluates tool accessibility for deep narrow regions.
- ✓ Areas with undercuts (e.g., diffuser curved grooves) may require:
  - Smaller tools
  - Multi-axis machining
  - Re-orientation of the workpiece
- ✓ If machining is not feasible for fabrication, forming or multi-piece assembly is recommended.

3.6.5 Sheet Metal Forming Considerations

Although machining is suitable for prototypes, mass production of car bodies relies on sheet metal forming. The following considerations are evaluated:

- ✓ **Minimum Bend Radius:** Aluminum 6061-T6 requires larger bend radius to avoid cracking in the body model.
- ✓ **Spring back Behavior:** The alloy exhibits moderate spring back; compensation must be applied in die design.
- ✓ **Forming Limit Diagram (FLD):** The car body curvature is checked against forming limits to avoid thinning or tearing.
- ✓ **Multi-Stage Forming:** Complex regions such as the diffuser may require incremental forming or multiple dies.
- ✓ **Heat Treatment:** Forming in T4 temper followed by artificial aging to T6 may be required for deep-draw sections.

3.6.6 Toolpath Simulation and Verification

The Computer Aided Manufacturing (CAM) simulation provides:

- ✓ **Collision Detection:** It ensures that the tool, holder or spindle does not collide with the workpiece.
- ✓ **Material Removal Visualization:** It shows the progressive machining of the car body.
- ✓ **Tool Load Analysis:** It predicts cutting forces and spindle load to avoid tool breakage.
- ✓ **Machining Time Estimation:** It helps evaluate production cost and efficiency.

- ✓ **Surface Quality Prediction:** It identifies areas requiring additional finishing passes.

The simulation confirms that the car body can be manufactured using a combination of CNC machining and sheet metal forming.

3.6.7 Manufacturing Feasibility Assessment

Based on the CAM analysis, the following conclusions can be finalized:

- ✓ The hood, roof and side panels can be manufactured using sheet metal forming with Aluminum 6061-T6.
- ✓ The rear diffuser and aerodynamic curved body parts require CNC machining due to their complex geometry.
- ✓ A hybrid manufacturing approach combining the forming and machining can be an optimal feasible manufacturing option.
- ✓ Multi-piece construction is suggested for large or deeply contoured regions.
- ✓ The selected material demonstrates excellent machinability and acceptable formability for the required operations.

3.6.8 CAM Design Summary

The CAM analysis verifies that the designed concept car body panel can be manufactured from Aluminum 6061-T6/T651 alloy through a combined forming and CNC machining workflow. The simulated toolpaths confirm that the complex aerodynamic geometry can be produced with the required dimensional precision and surface finish. This integrated digital manufacturing approach ensures that the final body panel maintains its structural and aerodynamic performance targets while remaining feasible within practical industrial production constrictions.

4. Developments and Recommendations

This chapter synthesizes the engineering insights gained from the structural, aerodynamic and manufacturing analyses of the concept car body. It highlights the practical implications of the findings, identifies the limitations of the current study, and proposes future developments and recommendations to enhance the design, simulation accuracy and manufacturability of the model. The outcomes of this research demonstrate the feasibility of producing a lightweight, aerodynamically efficient car body using Aluminum 6061-T6/T651 and modern CAM-based manufacturing technologies.

4.1 Limitations of The Analysis

Despite the comprehensive nature of the study, several limitations must be acknowledged:

4.1.1 CFD Limitations

- ✓ The Y^+ distribution of the fine mesh, although acceptable, does not fully resolve the viscous sublayer, limiting the accuracy of skin-friction drag predictions.
- ✓ The simulation assumes steady-state flow which does not capture transient aerodynamic phenomena such as vortex shedding or crosswind effects.
- ✓ The absence of rotating wheels, ground motion and wheel-well flow reduces the practicality of the aerodynamic model.

4.1.2 Structural Limitations

- ✓ The structural analysis does not include crashworthiness, fatigue or vibration studies which are essential for full vehicle structural validation.
- ✓ The car body is treated as a single shell, without internal reinforcements, ribs or mounting structures that would exist in a real vehicle.

4.1.3 Manufacturing Limitations

- ✓ CAM analysis is performed based on idealized machining conditions, without considering tool wear, machine deflection or thermal effects.
- ✓ Sheet metal forming simulations such as FLD & spring back analysis were not performed, limiting the accuracy of formability predictions.
- ✓ Segmentation of the car body into manufacturable panels is conceptual and does not include joining methods such as welding, riveting or any other adhesive type bonding.

4.1.4 Material Limitations

- ✓ Aluminum 6061-T6/T651 which is suitable for machining but it has lower formability compared to 5XXX series alloys which may restrict deep-draw operations.
- ✓ The analysis does not consider alternative materials such as composites.

4.2 Possible Developments

Several developments can enhance the accuracy, manufacturability, and industrial relevance of the study:

4.2.1 Advanced CFD Improvements

- ✓ Implement **transient CFD (URANS or LES)** to capture unsteady aerodynamic effects.
- ✓ Include moving ground, rotating wheels and wheel-well flow for more realistic simulations.
- ✓ Refine the near-wall mesh to achieve $\mathbf{Y^+ \approx 1}$ for high-accuracy boundary-layer resolution.

4.2.2 Enhanced Structural Modelling

- ✓ Introduce multi-layer shell modelling with reinforcements, ribs and realistic thickness variations.
- ✓ Perform modal analysis, fatigue analysis and crash simulations to ensure safety and durability.
- ✓ Incorporate material anisotropy for formed aluminum panels.

4.2.3 Manufacturing Process Development

- ✓ Conduct sheet metal forming simulations to evaluate thinning, wrinkling and spring back.
- ✓ Explore Incremental Sheet Forming (ISF) for complex geometries such as the diffuser.
- ✓ Develop multi-piece panel assemblies with realistic joining techniques.

4.2.4 Material and Design Optimization

- ✓ Investigations of alternative materials such as:
  - Aluminum 5754/5182 for improved formability
  - Carbon-fiber composites for high-performance applications
  - Magnesium alloys for ultra-lightweight structures

- ✓ Apply topology optimization to reduce weight while maintaining stiffness.

4.2.5 Prototype Development

Produce a scaled physical prototype using CNC machining or 3D printing to validate aerodynamic and structural performance experimentally.

4.3 Recommendations

Drawing from the outcomes of this study, the following directions are recommended for subsequent research efforts and for advancing practical deployment within industrial environments:

4.3.1 Aerodynamic Optimizations

- ✓ Refine the mesh to achieve lower Y^+ values for improved drag prediction.
- ✓ Incorporate real-world conditions such as crosswinds and road turbulence.
- ✓ Optimize the diffuser geometry to enhance underbody airflow.

4.3.2 Structural Enhancements

- ✓ Add reinforcement ribs or internal structures to reduce stress concentrations.
- ✓ Evaluate alternative panel thicknesses to balance weight and stiffness.
- ✓ Perform fatigue and crash simulations for safety validation.

4.3.3 Manufacturing Implementations

- ✓ Use of hybrid manufacturing such as sheet forming for large panels and CNC machining for complex aerodynamic features.
- ✓ Develop a panel assembly strategy including welding, adhesive bonding or implementing mechanical fastening.

4.3.4 Future Research

- ✓ Integrate multi-objective optimization combining aerodynamics, weight, simulating cost and manufacturability.
- ✓ Explore AI assisted or integrated design for rapid geometry refinement.
- ✓ Conduct wind tunnel testing to validate the CFD predictions.

5. Conclusion

In this thesis, a comprehensive investigation was performed to present the structural, aerodynamic and manufacturing characteristics of a concept car body by using an integrated FEM-CFD-CAM workflow. The study successfully demonstrated how modern computational tools can be applied to evaluate and optimize a sportscar outer body design from multiple engineering perspectives, ensuring both performance and manufacturability. Through systematic modelling, simulation and several analyses, the research validated the feasibility design of producing a lightweight, aerodynamically efficient car body from Aluminum 6061-T6/T651 alloy by utilizing modern manufacturing technologies.

The **Finite Element Method (FEM)** analysis confirmed that the selected car body material provides adequate toughness and deformation resistance for non-primary automotive body panels. The structural behavior of the thin-shell car body aligned with real-world expectations with stress concentrations occurring primarily at the curvature transitions and at the mounting regions. These findings of external pressure, excessive point and distributed load of denting deformations highlights further the importance of car body geometric refinement and localized reinforcement in future panel design repetitions which will be helpful to manufacture a body panel of a two-seated sports car as per the requirements.

The **Computational Fluid Dynamics (CFD)** analysis provided valuable insights into the aerodynamic performance of the concept car. The mesh independence study conducted using coarse (15 mm), medium (12.5 mm) and fine (5 mm) meshes; verified that the fine mesh produced the most stable outstanding convergence factors and physically consistent flow fields. The performed Grid Convergence Index (GCI) verified that the mesh sensitivity analysis was mesh independent or not. Executed aerodynamic results revealed favorable pressure distributions, effective car underbody suction and well-defined wake structures; all of which contribute to the enhanced high-speed stability.

Although, the Y^+ values of the fine mesh did not fully resolve the viscous sublayer which is $Y^+ \approx 1$ but achieved Y^+ values remained acceptable for external aerodynamics applying the k-ω SST turbulence model. Mostly, automotive CFD studies use Log law layer Y^+ values between 30-100 for practical reasons which is also found same in this performed simulation. That is why it can be said that achieved Y^+ values are practically appropriate for this analysis. So, this study confirms that the car body design exhibits promising aerodynamic characteristics which are suitable for lightweight sports-car applications and possible improvements in the rear side of the car body design specifically in the diffuser and wind shield curvature modifications.

The **CAM based manufacturing** analysis established that the concept car body can be manufactured introducing a hybrid approach combining CNC machining and sheet metal forming altogether. The toolpath simulations validated the feasibility of machining complex aerodynamic surfaces while the material properties of Aluminum 6061-T6/T651 supported its suitability for forming moderately curved panels. The study also identified regions requiring multi-axis machining or multi-piece assembly, reflecting realistic industrial manufacturing constraints. This hybrid manufacturing strategy aligns with current automotive practices where formed panels and machined components are integrated into a unified body structure.

Across all analyses, the research highlighted several **engineering and practical consequences** including the importance of mesh quality in CFD accuracy, the need for reinforcement in structurally sensitive regions and the benefits of combining forming and machining processes for complex geometries. At the same time, the study acknowledged limitations such as the absence of transient aerodynamic modelling, simplified structural assumptions and idealized manufacturing conditions. These limitations provide clear direction for future work, including advanced CFD modelling, detailed forming simulations, crash-fatigue analysis and prototype validation.

Overall, this thesis demonstrates that the selected concept car body design is both aerodynamically efficient and manufacturable, offering a balanced combination of performance, structural integrity along with production feasibility. The integrated computational approach used in this research provides a robust framework for future automotive design studies, enabling engineers to evaluate and optimize vehicle bodies with greater accuracy and reduced development time. All the findings contribute to the broader fields of automotive engineering by demonstrating how digital tools can accelerate novelty, support justifiable material choices and enhance the overall design-to-manufacturing workflow.

List of References/Bibliography

[1] R. Stephen, “Research and development of a body kit for passenger cars to enhance aerodynamic efficiency / Richard Stephen. - Vilniaus universitetas.” Accessed: Dec. 02, 2025. [Online]. Available: https://virtualibiblioteka.vu.lt/discovery/fulldisplay/alma9913125586808452/370LABT_VU:VU

[2] J. Li, X. Zhu, C. Zhang, S. Dang, and G. Chen, “CFD Simulation of Passenger Car Aerodynamics and Body Parameter Optimization,” *FDMP*, vol. 21, no. 9, pp. 2305–2329, 2025, doi: 10.32604/fdmp.2025.067087.

[3] Y. Zhang, R. Zhou, C. Su, Z. Zhang, and X. Zang, “Aerodynamic optimization of car top box design for drag reduction using CFD and Kriging modeling,” *Journal of Engineering Research*, p. S2307187725000665, Jun. 2025, doi: 10.1016/j.jer.2025.06.003.

[4] GPfans.com, “F1 Explained: What is downforce and why is it important?,” GPfans. Accessed: Dec. 04, 2025. [Online]. Available: https://www.gpfans.com/en/f1-news/104261/f1-downforce-explained/

[5] F.-J. Granados-Ortiz, P. Morales-Higueras, and J. Ortega-Casanova, “3D CFD simulation of the interaction between front wheels&brake ducts and optimised five-element F1 race car front wings under regulations,” *Alexandria Engineering Journal*, vol. 69, pp. 677–698, Apr. 2023, doi: 10.1016/j.aej.2023.02.011.

[6] “Causes of aerodynamic drag,” Science Learning Hub. Accessed: Dec. 04, 2025. [Online]. Available: https://www.sciencelearn.org.nz/resources/1346-causes-of-aerodynamic-drag

[7] ASA, “Aerodynamics: Drag - Learn To Fly.” Accessed: Dec. 04, 2025. [Online]. Available: https://learntoflyblog.com/aerodynamics-drag/

[8] K. Kurec, M. Remer, and J. Piechna, “The influence of different aerodynamic setups on enhancing a sports car’s braking,” *International Journal of Mechanical Sciences*, vol. 164, p. 105140, Dec. 2019, doi: 10.1016/j.ijmecsci.2019.105140.

[9] Laurent, “Understanding the Aerodynamic Forces in Flight,” Study flight. Accessed: Dec. 05, 2025. [Online]. Available: https://www.studyflight.com/understanding-the-aerodynamic-forces-in-flight/

[10] M. Mohammadi, S. M. R. Nazemosadat, D. Fazel, and Y. Bazargan Lari, “An integrated approach for structural modeling, modal analysis, and aerodynamic evaluation of an electric vehicle body shell using finite element method and computational fluid dynamics,” *Materials Today Communications*, vol. 45, p. 112331, Apr. 2025, doi: 10.1016/j.mtcomm.2025.112331.

[11] J. Basson, “Analysis of the aerodynamic attributes of motor vehicles,” Oct. 2013. Accessed: Dec. 05, 2025. [Online]. Available: https://www.semanticscholar.org/paper/Analysis-of-the-aerodynamic-attributes-of-motor-Basson/2f2e3463b6e6716ed04f2f12aafd8e776b0f4d67#citing-papers

[12] "Aerodynamic Upgrades," Rapid Racer. Accessed: Dec. 06, 2025. [Online]. Available: https://www.rapid-racer.com/tuning/aerodynamic-upgrades/

[13] "Location and height of front air dam - Fuel Economy, Hypermiling, EcoModding News and Forum - EcoModder.com." Accessed: Dec. 06, 2025. [Online]. Available: https://ecomodder.com/forum/showthread.php/location-height-front-air-dam-38334.html

[14] C. Fu, M. Uddin, and A. C. Robinson, "Turbulence modeling effects on the CFD predictions of flow over a NASCAR Gen 6 racecar," *Journal of Wind Engineering and Industrial Aerodynamics*, vol. 176, pp. 98–111, May 2018, doi: 10.1016/j.jweia.2018.03.016.

[15] The Efficient Engineer, *Understanding the Finite Element Method*, (Apr. 27, 2021). Accessed: Dec. 01, 2025. [Online Video]. Available: https://www.youtube.com/watch?v=GHjopp47vvQ

[16] "ME280A.pdf." Accessed: Dec. 01, 2025. [Online]. Available: https://csml.berkeley.edu/Notes/ME280A.pdf

[17] F. Ozcan and S. Ersoy, "Analysis of the vehicle: applying finite element method of 3D data," *Mathematical Models in Engineering*, vol. 7, no. 4, pp. 63–69, Dec. 2021, doi: 10.21595/mme.2021.22328.

[18] P. Qin, A. Ricci, and B. Blocken, "CFD simulation of aerodynamic forces on the DrivAer car model: Impact of computational parameters," *Journal of Wind Engineering and Industrial Aerodynamics*, vol. 248, p. 105711, May 2024, doi: 10.1016/j.jweia.2024.105711.

[19] T.-L. Le, T.-P. Phan, D. Tran, V.-T. Vu, and L.-H.-T. Do, "A CFD study of the aerodynamic characteristics of a DrivAer fastback model," *Aerospace Science and Technology*, vol. 168, p. 111043, Jan. 2026, doi: 10.1016/j.ast.2025.111043.

[20] "The FEM mesh of the future - mastering complexity, automating the mesh!" Accessed: Dec. 06, 2025. [Online]. Available: https://blog.cadfem.net/en/the-fem-mesh-of-the-future-mastering-complexity-automating-the-mesh

[21] "Car Body Concept_2 | 3D CAD Model Library | GrabCAD." Accessed: Apr. 18, 2026. [Online]. Available: https://grabcad.com/library/car-body-concept_2-1